Modeling of the interplay between single-file diffusion and conversion reaction in mesoporous systems

by

Jing Wang

A dissertation submitted to the graduate faculty

in partial fulfillment of the requirements for the degree of

DOCTOR OF PHILOSOPHY

Major: Applied Mathematics

Program of Study Committee:
Jim Evans, Major Professor
Hailiang Liu
Michael Smiley
Zhijun Wu
Alex Roitershtein

Iowa State University
Ames, Iowa
2013

TABLE OF CONTENTS

Page

Page

ACKNOWLEDGEMENTS

I would like to thank my committee members who were more than generous with their expertise and precious time. A special thanks to Dr. Jim Evans, my committee chairman for his guidance, support, encouraging and most of all patience throughout the course of this research. Thank you Dr. Hailiang Liu, Dr. Michael Smiley, Dr. Zhijun Wu, and Dr. Alex Roitershtein for agreeing to serve on my committee.

In addition, I would also like to thank my friends, colleagues, the department faculty and staff for making my time at Iowa State University a wonderful experience. Special thanks goes to the Department of Mathematics and Ames Laboratory for their continued support.

Finally, thanks to my parents, Guohua Wang and Haiying Wang, for their encouragement and to my husband, Yiping Hao, for his support, respect and love.

This work was performed at the Ames Laboratory under contract number DE-AC02-07CH11358 with the U.S. Department of Energy. The document number assigned to this dissertation is IS-T_____.

ABSTRACT

We analyze the spatiotemporal behavior of species concentrations in a diffusion-mediated conversion reaction which occurs at catalytic sites within linear pores of nanometer diameter. A strict single-file (no passing) constraint occurs in the diffusion within such narrow pores. Both transient and steady-state behavior is precisely characterized by kinetic Monte Carlo simulations of a spatially discrete lattice–gas model for this reaction–diffusion process considering various distributions of catalytic sites. Exact hierarchical master equations can also be developed for this model. Their analysis, after application of mean-field type truncation approximations, produces discrete reaction–diffusion type equations (mf-RDE). For slowly varying concentrations, we further develop coarse-grained continuum hydrodynamic reaction–diffusion equations (h-RDE) incorporating a precise treatment of single-file diffusion (SFD) in this multispecies system. Noting the shortcomings of mf-RDE and h-RDE, we then develop a generalized hydrodynamic (GH) formulation of appropriate gh-RDE which incorporates an unconventional description of chemical diffusion in mixed-component quasi-single-file systems based on a refined picture of tracer diffusion for finite-length pores. The gh-RDE elucidate the non-exponential decay of the steady-state reactant concentration into the pore and the non-mean-field scaling of the reactant penetration depth. Then an extended model of a catalytic conversion reaction within a functionalized nanoporous material is developed to assess the effect of varying the reaction product – pore interior interaction from attractive to repulsive. The analysis is performed utilizing

the generalized hydrodynamic formulation of the reaction-diffusion equations which can reliably capture the complex interplay between reaction and restricted transport for both irreversible and reversible reactions.

CHAPTER 1. GENERAL INDROCUTION

Background

Anomalous transport can be induced by the feature that molecules or particles within the narrow pores of mesoporous catalytic material either cannot pass each other, resulting in so-called single-file diffusion (SFD). Anomalous behavior may persist even if molecules just have difficulty in passing each other. Such mesoporous (or more accurately nanoporous) systems are realized by materials incorporating arrays of linear pores which are sufficiently narrow. This no-passing feature results in anomalous tracer diffusion [1–3]. There have been extensive studies motivated by studies of transport and catalytic reaction in zeolites [4] and other functionalized nanoporous materials, emphasizing the anomalous nature of tracer- or self-diffusion [4,5]. Diffusion-mediated reaction processes have traditionally been modeled with mean-field (MF) reaction-diffusion equations (RDE) [6, 7]. These RDE include a conventional treatment of chemical kinetics that ignores spatial correlations between reactants. This approach has been effectively applied to heterogeneous catalysis on extended surfaces, where reactant species reside at a periodic array of adsorption sites on the nanoscale, and complex spatial concentration patterns can develop on the micron scale [8]. Actually, for such catalytic surface reactions, it has been recognized that mean-field kinetics has limitations due to nonrandom reactant distributions. However, there has been less appreciation of the complexity of diffusion in mixed reactant adlayers.

For the reaction-diffusion phenomena which are of interest here, it is actually

chemical diffusion [9] which controls behavior [10], and for which the connection to tracer diffusion is not well recognized. Another key aspect of these open reaction-diffusion systems is that steady-state behavior is not described by a classic Gibbs thermodynamic ensemble. In fact, a fundamental understanding of these steady-states, which depend on both the reaction kinetics and transport, remains a significant challenge [6,11,12]. One goal here is to use these exact results to assess the consequences of single-file diffusion for the transient behavior in conversion reactions, a relatively unexplored issue. We will also analyze behavior for various distributions of catalytic sites within the pore. In addition, regarding steady-state behavior, we will assess fundamental scaling behavior of quantities related to reactivity as a function of key model parameters.

In the basic model for A→B conversion [13] (see Fig.1), reactants A (products B re-enter if allowed) enter the pore from the surrounding fluid and are converted to products, B, at catalytic sites (c). Reactants and products within the pore are localized to sites of a 1D linear lattice traversing that pore (and outside the pore can be regarded as localized to a 3D lattice). The simplest prescription for diffusion within the pores is that A and B hop to adjacent empty (E) sites at rate **h**. This would correspond to single-file diffusion with a strict no-passing constraint. We can also allow positional exchange of adjacent A and B at rate $\mathbf{P_{ex}}$ **h** to relax the strict single-file constraint, noting that exchange of adjacent particles of the same type has no effect. Conversion reaction at catalytic sites (c) occurs at rate **k**. In addition, we must specify adsorption and desorption processes at the pore openings (as discussed further below).

Advances in synthesis of nanomaterials have led to broad capabilities for multifunctionalization of mesoporous or nanoporous catalysts. Such capabilities allow for not only effective functionalization with catalytic groups, but also the possibility to tune the interaction between reaction products and the interior pore environment [14-16]. This can in turn significantly impact and potentially enhance catalytic reactivity. For example, creation of an unfavorable environment for product species within pores can lead to enhanced product extrusion or inhibited product re-entry. This feature would shift the equilibrium of reversible reactions towards completion.

Accounting for detailed balance requirements, it follows that creating an unfavorable environment for a reaction product within the pore increases the ratio of the rate of product desorption from the pore opening to that for product (re)adsorption. One should note that product readsorption can become significant for substantial conversion of reactant to product in the surrounding fluid. Thus, in our modeling, we can account for the effects of multifunctionalization and for different behavior with increasing conversion during the reaction, by suitable specification of the adsorption and desorption rates at the pore openings. We note that modifying the interior pore environment can change loading of product in the pore even for irreversible reactions. The loading can have a dramatic effect on effective transport for narrow pores, especially in the SFD regime where species cannot pass each other in the pore, and this in turn greatly impacts reactivity.

In these models, a key factor impacting reactivity is the extent to which reactants and products A and B can pass each other. Previous analyses for SFD or highly

restricted passing [10,13,17,18,19-22] reveal that reactivity in these systems can be strongly inhibited as reactant (and thus reaction) is strongly localized near the pore openings [18]. The reason is that except near their ends, the pores tend to be exclusively populated by product which is not readily extruded. Thus, the pore center does not participate in the conversion A→B. Kinetic Monte Carlo (KMC) simulation (which is often computationally expensive) can always be utilized to provide a precise characterization of model behavior. However, in this thesis we focus on the development of analytic formulations. While simple mean-field type reaction-diffusion equations [10,17,19,20] are not adequate in systems with strongly inhibited passing, our studies show that behavior in this regime is captured by a "generalized hydrodynamic" (GH) formulation which accounts for both the effect of restricted passing on chemical diffusion as well as fluctuation effects in adsorption-desorption at pore openings [21].

Thesis organization

The main body of this dissertation is based on three published papers (Chapter 2, 3 and 4), and three additional parts (Chapter 5, 6 and 7).

Chapter 2 reprints the published paper "Catalytic conversion reaction mediated by single-file diffusion in linear nanopore: Hydrodynamic versus stochastic behavior", by D. M. Ackerman, J. Wang, J. H. Wendel, D.-J Liu, M. Pruski, and J. W. Evans in the Journal of Chemical Physics 134, 114107 (2011). David Ackerman performed the kinetic Monte Carlo simulations for the models, and I performed the analytic investigations and related numerical simulations of discrete reaction-diffusion equations.

This paper gives a detailed description and analysis of the simple reaction conversion $A \rightarrow B$ model with single-file constraint. MF approximations are applied into a system of discrete RDE and a classic hydrodynamic treatment is used in to associate continuum RDE. MF-type treatment can capture the fluctuation near the pore openings but overestimate the fluxes within the pore, especially the pore center. Hydrodynamic method captures the correct behavior but fails near the pore openings. A set of more precise KMC results is used as the exact behavior.

Chapter 3 reprints the published paper "Generalized hydrodynamic treatment of the interplay between restricted transport and catalytic reaction in nanoporous materials", by D. Ackerman, J. Wang, and J.W. Evans, in Phys. Rev. Lett. 108, 228301 (2012). David Ackerman performed the kinetic Monte Carlo simulations for the models, and I performed the analytic investigations and related numerical simulations of discrete reaction-diffusion equations. This paper develops a reliable generalized hydrodynamic treatment as noting the shortcomings of MF-type approximation and classic hydrodynamic treatment. The generalized hydrodynamic method successfully captures both fluctuation at the ends of pore and the correct behavior in the pore center.

Chapter 4 reprints the published paper "Controlling reactivity of nanoporous catalyst materials by tuning reaction product-pore interior interactions: Statistical mechanical modeling", by J. Wang, D. M. Ackerman, V. S.-Y. Lin, M. Pruski, and J. W. Evans in the Journal of Chemical Physics 138, 134705 (2013). This paper uses generalized hydrodynamic treatment to deal with the effect of varying the reaction

product-pore interior interaction from attractive to repulsive. Both irreversible and reversible reaction conversions are considered.

Chapter 5 is a discussion on "Higher-order truncation approximation" for the tracer diffusion coefficient D_{tr} with MF-type approximation in semi-infinite pores.

Chapter 6 is a discussion on "Taylor expansion results for tracer diffusion". This is the only analytic way to figure out D_{tr} as in my knowledge.

Chapter 7 is a discussion on "Improved analysis of the steady-state continuum reaction-diffusion equations".

References

[1] A.L. Hodgkin and R.D. Keynes, J. Physiol. (London) **128**, 61 (1955).
[2] T.E. Harris, J. Appl. Prob. **2**, 323 (1965).
[3] P.A. Fedders, Phys. Rev. B, **16**, 1393 (1977).
[4] J. Kärger and D. Freude, Chem. Eng. Technol. 25, 769 (2002).
[5] Reikert, L. In Advances in catalysis; Eley, D. D., Pines, H. Weisz, P. B., Eds.; Academic Press: New York, Vol.21, p 281 (1970).
[6] G. Nicolis and I. Prigogine, *Self-organization in Non-equilibrium Systems* (Wiley, New York, 1977).
[7] A.S. Mikhailov, *Foundations of Synergetics I* (Springer, Berlin, 1990)
[8] R. Imbihl and G. Ertl, Chem. Rev. **95**, 697 (1995).
[9] R. Krishna, J. Phys. Chem. C 113, 19765 (2009).
[10] D.M. Ackerman, J. Wang, J.H. Wendel, D.-J. Liu, M. Pruski, and J.W. Evans, J. Chem. Phys. 134, 114107 (2011).
[11] J. Marro and R. Dickman, "Non-equilibrium Phase Transitions in Lattice-Gas Models" (CUP, Cambridge, 1999).
[12] J.W. Evans, D.-J. Liu, and M. Tammaro, Chaos 12, 131 (2002).
[13] C. Rodenbeck, J. Kärger, and K. Hahn, J. Catal. 157, 656 (1995).
[14] J.A. Melero, R. Van Grieken, and G. Morales, Chem. Rev. 106, 3790 (2006)
[15] E.L. Margelefsky, R.K. Zeiden, and M.E. Davis, Chem. Soc. Rev. 37, 1118 (2008).
[16] J.M. Thomas and R. Raja, Acc. Chem. Res. 41, 708 (2008).
[17] J.G. Tsikoyiannis and J.E. Wei, Chem. Eng. Sci. 46, 233 (1991).
[18] J. Kärger, M. Petzold, H.S. Pfieffer, S. Ernst, and J. Weitkamp, J. Catal. 136, 283 (1992).

[19] M.S. Okino, R.Q. Snurr, H.H. Kung, J.E. Ochs, and M.L. Mavrovouniotis, J. Chem. Phys. 111, 2210 (1999).
[20] S.V. Nedea, A.P.J. Jansen, J.J Lukkien, and P.A.J. Hilbers, Phys. Rev. E 65, 066701 (2002); 66, 066705 (2002); 67, 046707 (2003).
[21] D.M. Ackerman, J. Wang, and J.W. Evans, Phys. Rev. Lett., 108, 228301 (2012).
[22] J. Wang, D.M. Ackerman, K. Kandel, I.I. Slowing, M. Pruski, and J.W. Evans, MRS Symp. Proc. Vol. 1423 (MRS, Pittsburgh, 2012) DOI: 10.1557/opl.2012.229

Figures

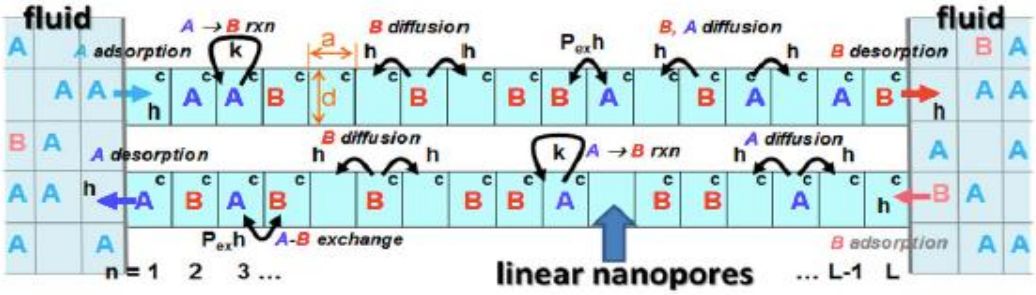

Fig.1**.** Schematic of the A→B conversion reaction model illustrating processes within a single pore (shaded blue), as well as the surrounding fluid. ‘c’ denotes catalytic sites.

CHAPTER 2. CATALYTIC CONVERSION REACTION MEDIATED BY SINGLE-FILE DIFFUSION IN LINEAR NANOPORE: HYDRODYNAMIC VERSUS STOCHASTIC BEHAVIOR

A paper published in the Journal of Chemical Physics

David M. Ackerman, [1,2,*] Jing Wang, [1,3,*] Joseph H. Wendel, [1] Da-Jiang Liu, [1] Marek Pruski, [1] and James W. Evans[1, 3,4]

[1]Ames Laboratory – USDOE, Iowa State University, Ames, Iowa 50011, USA

[2]Department of Chemistry, Iowa State University, Ames, Iowa 50011, USA

[3]Department of Mathematics, Iowa State University, Ames, Iowa 50011, USA

[4]Department of Physics and Astronomy, Iowa State University, Ames Iowa 50011, USA

[*]David Ackerman performed the kinetic Monte Carlo simulations for the models, and I performed the analytic investigations and related numerical simulations of discrete reaction-diffusion equations.

Abstract

We analyze the spatiotemporal behavior of species concentrations in a diffusion-mediated conversion reaction which occurs at catalytic sites within linear pores of nanometer diameter. Diffusion within the pores is subject to a strict single-file (no passing) constraint. Both transient and steady-state behavior is precisely characterized by kinetic Monte Carlo simulations of a spatially discrete lattice–gas model for this reaction–diffusion process considering various distributions of catalytic sites. Exact

hierarchical master equations can also be developed for this model. Their analysis, after application of mean-field type truncation approximations, produces discrete reaction–diffusion type equations (mf-RDE). For slowly varying concentrations, we further develop coarse-grained continuum hydrodynamic reaction–diffusion equations (h-RDE) incorporating a precise treatment of single-file diffusion in this multispecies system. The h-RDE successfully describe nontrivial aspects of transient behavior, in contrast to the mf-RDE, and also correctly capture unreactive steady-state behavior in the pore interior. However, steady-state reactivity, which is localized near the pore ends when those regions are catalytic, is controlled by fluctuations not incorporated into the hydrodynamic treatment. The mf-RDE partly capture these fluctuation effects, but cannot describe scaling behavior of the reactivity.
[doi:10.1063/1.3563638]

I. Introduction

Diffusion-mediated reaction processes have traditionally been modeled with mean-field (MF) reaction-diffusion equations (RDE) [1, 2]. These RDE include a conventional treatment of chemical kinetics which ignores spatial correlations between reactants, and also a simple description of diffusion typically with constant Fickian diffusion coefficients. This approach has been effectively applied to heterogeneous catalysis on extended surfaces, where reactant species reside at a periodic array of adsorption sites on the nanoscale, and complex spatial concentration patterns can develop on the micron scale [3]. Actually, for such catalytic surface reactions, it has

been recognized that mean-field kinetics has limitations due to nonrandom reactant distributions. However, there has been less appreciation of the complexity of diffusion in mixed reactant adlayers. This complexity arises even in simple lattice–gas (LG) reaction models with no interactions between reactants on different adsorption sites (but exclusion of multiple occupancy of sites) [4]. There are further complications in the treatment of diffusion in these mixed systems when one accounts for interactions between reactants [5].

In contrast, the nontrivial nature of diffusion is well-recognized for transport and possible reaction in so-called single-file systems. Such mesoporous (or more accurately nanoporous) systems are realized by materials incorporating arrays of linear pores which are sufficiently narrow that molecules cannot pass each other inside the pores. This no-passing feature results in anomalous tracer diffusion [6–8]. To assess the interplay between such anomalous transport and reaction, there have been several studies of a basic conversion reaction model and its variants [9–15]. In this basic model, the reactant, A, adsorbs at the end of pore, converts to product, B, at catalytic sites within the pore, and both reactants and products can exit the pore.

In an early study considering possibly reversible conversion reactions, Tsikoyiannis and Wei [9] developed hierarchical rate equations for a general class of lattice–gas models. They analyzed behavior for the canonical irreversible reaction model A→ B with all sites catalytic by kinetic Monte Carlo (KMC) simulation and compared results against predictions from first-order mean-field and second-order pair truncation approximations of the hierarchy [9]. The model was revisited by Okino et al. [10] who

refined the pair or doublet truncation approximation and analyzed behavior of the reversible A↔ B as well as irreversible A→ B conversion reaction. Kärger and co-workers [11–13] examined model behavior via KMC simulation and included the possibility of attractive interactions between participating molecules. Finally, Nedea et al. [14, 15], also considered behavior of the canonical irreversible reaction model A→ B without interactions, exploiting both KMC simulation and truncation of hierarchical rate equations. They further considered behavior for different distributions of catalytic sites within the pore, and also analyzed nontrivial limiting behavior for rapid diffusion (but with finite exchange rates at the pore ends). These studies have focused primarily on elucidating steady-state reactivity.

While the anomalous aspects of tracer diffusion in single-file systems are well characterized, the behavior of chemical diffusion, which is of particular relevance for reaction-diffusion phenomena, is less completely characterized. It has been recognized that Onsager's classic theory of transport can be applied to assess chemical diffusion fluxes in multi-species systems with and without single-file constraints [16,17]. Also, some of the above studies of single-file conversion reactions have described the corresponding discrete RDE, but only based on approximate mean-field treatments [9,14]. However, what has not been exploited is the existence of exact results for diffusion fluxes in multi-species lattice-gas models with site exclusion and species-independent hop rates and interactions [18]. One can apply these results to single-file systems. One goal here is to use these exact results to assess the consequences of single-file diffusion for the transient behavior in conversion reactions, a relatively unexplored

issue. We will also analyze behavior for various distributions of catalytic sites within the pore. In addition, regarding steady-state behavior, we will assess fundamental scaling behavior of quantities related to reactivity as a function of key model parameters.

In Sec. II, we specify in detail the single-file conversion reaction model, the associated hierarchical rate equations and mean-field-type RDE (mf-RDE), and discuss basic model properties. Then, in Sec. III, we formulate a treatment for the "hydrodynamic regime" where the evolution of slowly varying species concentrations might be described by continuum hydrodynamic RDE (h-RDE). Both steady-state and transient behavior is described in Sec. IV for a "canonical" conversion reaction model where all sites within the pore are catalytic. Behavior where either the peripheral or the central sites are catalytic is described in Sec. V. Finally, we offer some comments on more general models, and present conclusions in Sec. VI.

II. Reaction-diffusion model: prescription and basic properties

The model considered in this study was developed previously to describe the diffusion-mediated catalytic conversion of a reactant to a product ($A \rightarrow B$) inside linear pores which are sufficiently narrow as to allow only single-file diffusion [9-15]. To treat the spatial aspects of this process, the model incorporates the feature that both reactants and products inside the pore reside at the sites of a linear lattice. The introduction of a discrete spatial structure should not affect the basic aspects of model behavior, at least for concentration profiles varying smoothly over several lattice constants. Such LG modeling also greatly facilitates both analytic investigation and simulation. The key

mechanistic steps in the model are: adsorption of "external" (ext) reactant species A at terminal sites (t) of the pore provided that these sites are unoccupied or empty, E; subsequent diffusion of A within the pore by hopping to nearest-neighbor (NN) empty sites; conversion reaction A $\rightarrow$ B at catalytic sites (c) within the pore. The product, B, also undergoes diffusion by hopping to NN empty sites, and both the reactant and product undergo desorption from terminal sites (t) of the pore. Thus, to summarize, the mechanistic steps of the reaction are:

$$A(ext) + E_t \rightarrow A_t \text{ (adsorption)};\ \ A_n + E_{n+1} \leftrightarrow E_n + A_{n+1} \text{ (diffusion)};\ \text{ and}$$

$$A_t \rightarrow A(ext) + E_t \text{ (desorption)}$$

$$A_c \rightarrow B_c \text{ (reaction)};\ \ B_n + E_{n+1} \leftrightarrow E_n + B_{n+1} \text{ (diffusion)};\ \text{ and}$$

$$B_t \rightarrow B(ext) + E_t \text{ (desorption)},$$

where we label the sites in the pore by n=1, 2,…, L (for pore length L). Thus, the terminal sites t are n=1 and n=L. The catalytic sites may constitute all sites or various subsets of sites within the pore, as described below. Total reactivity (i.e., the total production rate of B), R^B_{tot}, is simply proportional to the total amount of A within the catalytic regions of the pore. The system geometry and these mechanistic steps are also illustrated in Fig.1.

Rates for the various processes described above will be denoted by $W^A_{ads} = W_{ads}$ for adsorption of A, W^K_{des} for desorption of species K = A or B; W^K_{diff} for hopping of species K to NN empty sites, and W_{rx} for A $\rightarrow$ B conversion. An exact analytical description of such stochastic Markov processes is provided by the master equation for the evolution of probabilities of various configurations for the entire system [19]. Often

these are written in hierarchical form. Here, we use $\langle K_n \rangle$ to denote the probability or ensemble averaged concentration for species K at site n, $\langle K_n E_{n+1} \rangle$ for the probability that K is at site n and for site n+1 to be empty (E), etc.. Then, the lowest order-equations describe the probabilities that individual sites are occupied by various species. When all sites are catalytic, one has that

$$d/dt \langle A_1 \rangle = W_{ads}\langle E_1 \rangle - W^{A}_{des}\langle A_1 \rangle - W_{rx}\langle A_1 \rangle - J_A^{1>2}, \quad (1a)$$

$$d/dt \langle B_1 \rangle = - W^{B}_{des}\langle B_1 \rangle + W_{rx}\langle A_1 \rangle - J_B^{1>2}, \quad (1b)$$

$$d/dt \langle A_n \rangle = -W_{rx}\langle A_n \rangle - J_A^{n>n+1} + J_A^{n-1>n}, \text{ for } 1<n<L, \text{ and} \quad (1c)$$

$$d/dt \langle B_n \rangle = +W_{rx}\langle A_n \rangle - J_B^{n>n+1} + J_B^{n-1>n}, \text{ for } 1<n<L, \quad (1d)$$

and similar equations for the terminal site n=L to those for n=1. In these equations,

$$J_K^{n>n+1} = W^{K}_{diff} [\langle K_n E_{n+1} \rangle - \langle E_n K_{n+1} \rangle], \quad (2)$$

denotes the net diffusive flux of K = A or B from n to n+1 (i.e., the difference between the flux from n to n+1 and that from n+1 to n). The total reactivity is given by $R^{B}_{tot} = W_{rx} \sum_{n=c}\langle A_n \rangle$, where the sum is over all catalytic sites (i.e., over the entire pore in the above example).

These equations (1) are coupled to probabilities for various configurations of pairs of sites. Equations for pair probabilities couple to those for various triples, etc., thus generating a hierarchy. Pair, triplet, etc., probabilities are not trivially related to single-site probabilities due to the presence of spatial correlations. In these models, correlations derive from the interplay of adsorption-desorption and diffusion with reaction. Implementing a simple mean-field (MF) factorization approximation, $\langle K_n E_{n+1} \rangle$

$\approx \langle K_n\rangle\langle E_{n+1}\rangle$, etc., produces a closed set of discrete mf-RDE's for single site concentrations, $\langle A_n\rangle$ and $\langle B_n\rangle$ noting that $\langle A_n\rangle + \langle B_n\rangle + \langle E_n\rangle = 1$.

A more accurate pair approximation retains pair quantities like $\langle K_n E_{n+1}\rangle$, but factorizes triplet quantities, e.g., $\langle K_n M_{n+1} N_{n+2}\rangle \approx \langle K_n M_{n+1}\rangle\langle M_{n+1} N_{n+2}\rangle / \langle M_{n+1}\rangle$, with K, M, N = A, B, or E. This generates a closed set of equations for single site quantities, $\langle A_n\rangle$ and $\langle B_n\rangle$, together with the pair quantities, $\langle A_n A_{n+1}\rangle$, $\langle A_n B_{n+1}\rangle$, $\langle B_n A_{n+1}\rangle$, and $\langle B_n B_{n+1}\rangle$. See, for example, [9,10,14]. Note that there exist various exact relations determined by conservation of probability, i.e., $\langle A_n B_{n+1}\rangle + \langle A_n A_{n+1}\rangle + \langle A_n E_{n+1}\rangle = \langle A_n\rangle$, allowing one to determine $\langle A_n E_{n+1}\rangle$ from the set of the six selected quantities above. Higher-order approximations are also possible retaining probabilities of configurations of strings of n>2 sites, although the gain in accuracy with increasing order, n, may be slow [20].

A precise determination of model behavior is obtained by standard KMC simulation implementing processes with probabilities proportional to their rates. More specialized simulation algorithms may be applied to assess behavior in limiting regimes [15].

Following previous studies [10,12,14,15], to reduce the number of parameters in the model and also to induce some special features of model behavior, we will primarily consider the case where desorption rates and diffusion rates for both species are equal, i.e., $W^K_{des} = W_{des}$ and $W^K_{diff} = W_{diff}$, for K = A and B. There is an important consequence of this rate choice. Suppose one does not discriminate between the identity of particles, but only considers whether sites are empty, E, or filled, X=A+B (i.e., if one

just considers the total concentration at various sites). Then, the dynamics corresponds to a pure adsorption-desorption-diffusion process for particles X with no reaction. Correspondingly, from Eqs. (1), one obtains the exact equations

$$d/dt \langle X_1 \rangle = W_{ads}\langle E_1 \rangle - W_{des}\langle X_1 \rangle - J_X^{1>2}, \quad (3a)$$

$$d/dt \langle X_n \rangle = - J_X^{n>n+1} + J_X^{n-1>n}, \text{ for } 1<n<L, \quad (3b)$$

$$d/dt \langle X_L \rangle = W_{ads}\langle E_L \rangle - W_{des}\langle X_L \rangle + J_X^{L-1>L}, \quad (3c)$$

$$\text{where } J_K^{n>n+1} = W_{diff} [\langle X_n E_{n+1} \rangle - \langle E_n X_{n+1} \rangle] = W_{diff} [\langle X_n \rangle - \langle X_{n+1} \rangle]. \quad (4)$$

The exact relation corresponding to the last equality in Eq. (4) expressing $J_K^{n>n+1}$ in terms of single-site quantities amounts to an exact reduction of a many (X) particle problem to a single-particle problem. This feature was first noted by Kutner for an infinite lattice [21]. Extension of this reduction to semi-infinite and finite lattices has also been recognized previously [14,22]. Thus, the evolution of $\langle X_n \rangle$ is described exactly by standard discrete diffusion Eq. (3b), augmented by adsorption and desorption terms at the end sites in equations (3a) and (3c). The equations are closed noting that $\langle E_n \rangle = 1 - \langle X_n \rangle$.

It is thus straightforward to visualize the evolution of the total concentration starting from an empty pore. The total concentration will first build up near the ends of the pore, then spread by diffusion to the interior, and finally achieve a spatially uniform steady-state. Since there is no reaction in the dynamics of particles X, the steady-state corresponds to a conventional grand canonical equilibrium state with activity $z = W_{ads}/W_{des}$ [23]. Furthermore, since there are no interactions between particles X in this model, they are randomly distributed (i.e., there are no spatial correlations) in this trivial

equilibrium state. The equilibrium concentration at each site satisfies $\langle X_n \rangle_{eq} = X_{eq} = z/(1+z) = W_{ads}/(W_{ads}+W_{des})$ (cf. [9,15]). As an aside, we note that while the equilibrium steady-state is free of spatial correlations just considering the distribution of filled sites, X, such correlations do develop during filling of the pore. Remarkably, an exact closed set of equations can be obtained for pair probabilities, $\langle X_n X_{n+m} \rangle$, or associated correlations, as these decouple from triplet correlations [24]. Likewise, an exact closed set of equations can be obtained for the triplet correlations which decouple from the quartet correlations, etc. The nature of this decoupling is analogous to that described for Eq. (4).

In our analyses below, we will choose $W_{ads} + W_{des} = 1$ which sets the time-scale. We will present results only for: (i) $W_{ads} = 0.2$, $W_{des} = 0.8$ [low loading]; (ii) $W_{ads} = 0.8$ (or 0.9), $W_{des} = 0.2$ (or 0.1) [high loading]. Single-file effects are stronger for high loading. Parameters W_{rx} and W_{diff} will either have suitably-selected fixed values when comparing predictions of various treatments, or will be systematically varied in scaling studies. Note that well-defined limiting behavior is found in the regimes where: (a) $W_{ads}+W_{des}$ (with fixed $z = W_{ads}/W_{des}$) far exceeds W_{rx} and W_{diff} [12], so that reaction is not limited by adsorption and desorption at the ends at the pore; (b) W_{diff} far exceeds all other parameters. In contrast to typical reaction-diffusion systems where concentrations become uniform in this limit, nontrivial behavior is found in this single-file system [15]; (c) W_{diff} is far smaller than other parameters, so then only the terminal sites have a non-zero population of A in the steady-state [25].

III. Hydrodynamic regime and reaction-diffusion equations

In discrete LG reaction-diffusion systems, it is common to consider behavior in the "hydrodynamic regime" of substantial diffusion (on the time scale of other adsorption-desorption and reaction processes) and slowly varying particle concentrations (on the length scale of lattice constants) [4,5,26]. Within this framework, one might describe behavior by continuum hydrodynamic reaction-diffusion equations (h-RDE) after coarse-graining the discrete spatial variable to a continuous variable. Specifically, for linear lattices, one sets x = na, where n is the lattice site label and "a" is the lattice constant. (As an aside, it is often convenient to set a=1 in the following.) Then, species concentrations per unit length become functions of a continuous variable $K(x=na) \approx a^{-1} <K_n>$, where we leave implicit the t-dependence. To develop h-RDE, one needs an appropriate description of collective or chemical diffusion in this multi-species lattice-gas system [4,5,16,17,26] incorporating the single-file nature of diffusion.

Before addressing this major challenge, we comment on the much simpler task of describing the behavior of the coarse-grained total particle concentration per unit length, $X(x=na) \approx a^{-1} <X_n>$, in the hydrodynamic regime. As noted in Sec.II, the dynamics of this concentration profile is described by a reaction-free discrete diffusion equation. If J_X denotes the corresponding diffusion flux, then in the hydrodynamic regime, one has that

$$\partial/\partial t\, X(x) = -\partial/\partial x\, J_X \text{ with } J_X = -D_X\, \partial/\partial x\, X(x) \text{ and } D_X = a^2 W_{diff} . \qquad (5)$$

The feature that the chemical diffusion coefficient, D_X, is independent of concentration is well known for this single-component problem [21]. Thus, the single-file nature of the system does not reveal itself when considering chemical diffusion for a

single species X. Eq. (5) is augmented with the appropriate Robin boundary conditions $\pm J_X = aW_{ads}(X_m - X) - aW_{des}X$ at the pore ends, a relation derived from a steady-state form of Eq. (1a). Here, $X_m = 1/a$ is the maximum concentration per unit length.

For the case where all sites are catalytic, the h-RDE in our conversion reaction model for individual species concentrations, A(x) for A, and B(x) for B (leaving implicit the t-dependence), have the form

$$\partial/\partial t\, A(x) = -W_{rx}\, A(x) - \partial/\partial x\, J_A \text{ and } \partial/\partial t\, B(x) = +W_{rx}\, A(x) - \partial/\partial x\, J_B. \qquad (6)$$

where X(x) = A(x)+B(x). If sites within the pore are catalytic only in specific (e.g., peripheral) regions, then the reaction terms appear only for those locations. Description of the diffusion fluxes, J_A and J_B, for species A and B, respectively, is non-trivial in mixed lattice-gases even in the absence of interactions beyond site exclusion. The appropriate Robin boundary conditions for Eq. (6) at the pore ends have the form $\pm J_A = aW_{ads}(X_m - X) - aW_{des}A$, and $\pm J_B = -aW_{des}B$.

Onsager's transport theory ensures that the diffusive flux of A has the form [4,5,16,17,26]

$$J_A = - D_{A,A}\, \partial/\partial x\, A(x) - D_{A,B}\, \partial/\partial x\, B(x), \qquad (7)$$

where in general the diffusion coefficients $D_{A,K}$ depend on species concentrations. Thus, the flux J_A is induced by gradients in both <A> and <B>. A similar expression applies for the flux, J_B, of B. The four diffusion coefficients, $D_{K,K'}$, with K, K′ = A or B, can be conveniently collected into a 2x2 diffusion tensor $\underline{\underline{D}}$. Onsager's theory [16,17,26] further shows that this tensor involves both a thermodynamic "inverse compressibility" factor and a kinetic "conductivity" factor [27].

A. Exact hydrodynamic diffusion fluxes

As indicated above, there is a general appreciation that in principle the components of $\underline{\underline{D}}$ can be determined using the statistical mechanical formulation of Onsager theory. However, what has not been exploited is the existence of an exact result for the case of a multi-species lattice-gas with no interactions beyond site exclusion and for equal hop rates, W_{diff} [4,18,26]. For one-dimensional (1D) systems with single-file diffusion, one has the simple and intuitive exact form

$$J_A = -D_X [A(x)X(x)^{-1}] \partial/\partial x\, X(x), \;\; J_B = -D_X [B(x)X(x)^{-1}] \partial/\partial x\, X(x). \qquad (8)$$

In obtaining Eq. (8) from more general results [18,26], we have exploited the feature that the tracer diffusion coefficient vanishes for 1D single-file systems. See Appendix A.

There is an important consequence of the form (8) of the diffusion fluxes for the steady-states of the h-RDE. From Eq. (8), it is clear that fluxes J_A and J_B vanish for states with uniform total concentration, $X(x)$ = constant, irrespective of whether there are gradients in individual species concentrations. This reflects the lack of intermixing in single-file systems. Since the steady-state of the reaction model is characterized by constant $X(x) = a^{-1} X_{eq} = a^{-1} W_{ads}/(W_{ads}+W_{des})$, J_A and J_B must vanish for long times. Consequently, in this regime, concentrations interior to the pore change only due to reaction. As a result, any A is converted to B in regions with catalytic sites, so that $<A>=0$ and $<B> = X_{eq}$ in the steady-state in such regions. For example, if all sites are catalytic, then the steady-state is completely unreactive in the hydrodynamic picture. In

the actual model with all sites catalytic, reactivity does actually persist near pore ends in the steady state, but only due to fluctuations absent in the hydrodynamic treatment.

In the transient regime, as noted above, the evolution of $<X_n>$ or $X(x)$ is simply described by the nonreactive diffusion problem. A gradient develops as particles diffuse into the pore, and thus the diffusion fluxes J_A and J_B in Eq. (8) are nonzero and always in the direction towards the center of the pore. We will show that the correct description of diffusion in hydrodynamic RDE does capture key aspects of transient behavior. For such comparisons with KMC simulation results, we utilize discrete hydrodynamic RDE which incorporate a discrete version of Eq. (8) as described in Appendix B.

B. Mean-field diffusion fluxes

In contrast to the above hydrodynamic treatment, a mean-field (MF) treatment of chemical diffusion fluxes yields the distinct form

$$J_A(MF) = -D_X [1 - B(x)X_m^{-1}] \partial/\partial x\, A(x) -D_X [A(x)X_m^{-1}] \partial/\partial x\, B(x), \qquad (9)$$

and an analogous expression applies for J_B^{MF}. Again $X_m=1/a$ is the maximum concentration per unit length. This previously utilized result [16,17,28] can be obtained from Onsager theory accounting for the known thermodynamics of a non-interacting lattice-gas, but also incorporating a crude approximation for species conductivity [27]. However, it is instructive to note that an alternative simple kinetic derivation of the MF result (9) is also possible [14,29]: one simply applies the MF factorization to $J_A^{n>n+1}$ and $J_B^{n>n+1}$ in Eqs. (1c,d) and recasts the results in terms of continuous derivatives for slowly varying concentrations.

Clearly, this MF form of the diffusion fluxes which applies for any lattice dimension fails to capture the single-file nature of diffusion, and thus also fails to capture aspects of the correct hydrodynamic behavior. For example, the form (9) allows nonzero diffusion fluxes for constant X, and this can produce artificially enhanced intermixing of A and B. Specifically, one has that

$$J_K(\mathrm{MF}) \to -D_X(1-X_{eq})\,\partial/\partial x\, K(x),$$

$$\text{when } X \to a^{-1} X_{eq} \text{ (steady-state) for K = A or B.} \qquad (10)$$

The MF form also allows diffusion of species away from the center of the pore. Severe failure can be anticipated in the regime of large W_{diff} where the MF formulation predicts complete intermixing [14,15], but the actual single-file nature of diffusion prohibits such behavior.

For comparison with results of KMC simulation for both transient and steady-state behavior, we will implement the mf-RDE associated with the MF truncation approximation to Eq. (1). These constitute the natural discrete version of Eq. (9). See Appendix B. In addition, we will implement discrete mf-RDE associated with the pair approximation which might be regarded as providing a refined treatment of diffusion. (As an aside, it is nontrivial to extract continuum h-RDE for the pair-approximation [30].) We shall see that both the MF and pair approximations do capture some aspects of fluctuation effects near the end of the pore in contrast to the hydrodynamic treatment.

IV. Canonical model: all sites catalytic

A. Steady-state behavior

Fig. 2 shows a "typical" example of the evolution of concentration profiles towards the steady-state for the parameter choice W_{ads}=0.2, W_{des}=0.8, W_{rx}=1, W_{diff}=1, and pore length L=30. Precise results of KMC simulations in Fig.2a are compared against those from various approximate analytic formulations in Fig.2b-d. The mean-field and pair approximation are quite effective in capturing behavior near the pore end as noted previously [9,10,14]. These approximations and the hydrodynamic treatment all describe effectively exactly evolution in the interior of the pore where there is just one species (B). Note that the A-concentration profile reaches a non-trivial steady-state form (with significant population only on the four sites closest to the pore end) long before the steady-state of the entire system is reached (for which $<X_n>$=0.2). This can be anticipated since all that is required for development of steady-state $<A_n>$ is sufficient diffusion into the pore end so that $<X_n>$ is close to its steady state value at sites near the pore end. Filling of the interior of the pore by species B occurs on a slower time scale. Simulation with the same rate parameters but for longer pores produces essentially identical steady-state $<A_n>$ distribution, but just take longer for the interior of the pore to fill with B.

As noted above, hydrodynamic analysis predicts that in the steady-state, the central region will contain just B and no A, so that $<B_n> = W_{ads}/(W_{ads}+W_{des}) \approx X_{eq}$ and $<A_n> \approx 0$. Only the end sites have significant A population in our discrete formulation. Thus, the nonzero population of A near the pore ends observed in simulations can be associated with fluctuation effects not included in the hydrodynamic formulation. Since

the reactivity of the system is determined by the population of A in the pore, these fluctuations are entirely responsible for the steady-state reactivity.

This observation motivates more detailed analysis of the dependence of this steady-state $<A_n>$ concentration profile on model parameters. Steady-state profiles appear to have an exponential form,

$$<A_n> \approx c\cdot r^n = c\cdot\exp(-\lambda n) = c\cdot\exp(-n/L_{p1}), \text{ at least for larger } n < L/2. \quad (11)$$

In Eq. (11), $\lambda = -\ln r$ is the decay rate, and $L_{p1}=1/\lambda$ is a measure of the penetration depth of A into the pore. In our analysis of KMC data below, we do find deviations from simple exponential decay for smaller n, most clearly in cases where L_{p1} is large (so decay is slow). The behavior (11) also implies that the production rate, R_B^{tot}, should converge exponentially to a finite value with increasing pore length. We note that another natural measure a penetration depth, L_p, at least in the regime where L_p is large is $L_{p2} = \sum_{n<L/2} <A_n>/<A_1>$. Yet another alternative is $L_{p3} = -1/\ln(1- 1/L_{p2})$, which would correspond exactly to L_{p1} for perfect exponential decay where $<A_n> = <A_1> r^{n-1}$. See Table I.

First, we examine the dependence on reaction rate, W_{rx}, of steady-state penetration depth L_p (considering all of L_{p1}, L_{p2}, and L_{p3}). We set $W_{diff} =1$ and vary W_{rx} from 1 to 10^{-3} for a system of size L=100. The lower the reaction rate, the greater the extent of penetration of A into the pore, and the greater L_p. Fig.3a-b show concentration profiles for W_{ads}=0.8 and W_{des}=0.2 for various W_{rx}. Analysis of this data and analogous data for W_{ads}=0.2 and W_{des}=0.8 to extract L_p versus W_{rx} is shown in Fig.3c-d. One finds that L_p increases with decreasing W_{rx} much more slowly than $(W_{rx})^{-1/2}$. Instead, we

suggest that $L_p \sim (W_{rx})^{-1/4}$, as $W_{rx} \to 0$, corresponding to asymptotically linear behavior in Fig.c-d for large abscissa. This behavior might be anticipated from the postulate that L_p should reflect the root-mean-square displacement for single-file diffusion on a time-scale corresponding to the reaction time, $\tau_{rx} = 1/W_{rx}$. This implies that $(L_p)^4 \sim \tau_{rx}$ and thus that $L_p \sim (W_{rx})^{-1/4}$. This result for L_p immediately yields scaling of the total reactivity per pore as $R^B_{tot} \sim W_{rx} L_p \sim (W_{rx})^{3/4}$.

Second, we examine the dependence on diffusion rate, W_{diff}, of steady-state behavior. For a conventional reaction-diffusion system, increase of hopping rates ultimately produces spatial uniformity of species concentrations due to "efficient stirring" corresponding to $L_p \to \infty$. One also achieves randomization of configurations in the absence of interactions [4,30]. A special feature of the single-file system being considered here [14,15] is the existence of nontrivial spatially non-uniform limiting behavior as $W_{diff} \to \infty$ (but retaining finite W_{ads}, W_{des}, and W_{rx}) [31]. One obtains a well-defined limiting concentration profile with finite penetration depth, $L_p(W_{diff} \to \infty) < \infty$, in this regime. More detailed analysis of steady-state concentration profiles for increasing W_{diff} suggests that $L_{p1} \sim L_{p1}(W_{diff} \to \infty) + c(W_{diff})^{-1/4}$. See Fig.4. Limiting values of $L_{p1}(W_{diff} \to \infty)$ was obtained from a tailored simulation algorithm (cf. [15]). Separate analysis indicates that L_{p2} and L_{p3} are fairly insensitive to W_{diff}.

Next, we consider the predictions of MF-type analytic treatments regarding the above behavior. The simplest MF approximation exhibits precise exponential decay for long pores. This behavior, noted previously [14], is a result of the feature that $\langle E_n \rangle = 1 - \langle X_n \rangle$ is constant, which in turn allows reduction of the steady-state form of Eq. (1c) to a

linear coupled set of equations. Setting $\varepsilon = W_{rx}/W_{diff}$ and $X_{eq} = W_{ads}/(W_{ads}+W_{des})$, then seeking a solution to these linear equations of the form $\langle A_n \rangle \propto r^n$ yields for r, the quadratic equation (cf. [14])

$$(1-X_{eq})(r + r^{-1} -2) = \varepsilon. \qquad (12)$$

Consequently, one has that $\delta = 1-r \sim (1-X_{eq})^{-1/2} \varepsilon^{1/2}$, for small ε, so that (cf. [14])

$$L_{p1}(MF) \sim \delta^{-1} \sim (1-X_{eq})^{1/2} (W_{rx})^{-1/2}(W_{diff})^{1/2}, \text{ for } W_{rx} \to 0 \text{ or } W_{diff} \to \infty. \qquad (13)$$

The result (13) can be obtained more directly from the continuum MF formulation [32]. This result reveals a fundamental failure of the MF treatment to describe asymptotic behavior of L_p. The failure to describe scaling as $W_{rx} \to 0$ or $W_{diff} \to \infty$ reflects an inability to capture single-file aspects of diffusion. Since concentration profiles become spatially uniform within the MF approximation as $W_{diff} \to \infty$, this enables simple direct analysis of MF behavior, e.g., showing that MF reactivity converges such as 1/L rather than exponentially as $L \to \infty$. See Appendix C.

It is instructive to assess the predictions of the higher-order pair approximation for the behavior of the penetration length, L_p. The complex nonlinear form of pair equations [14] excludes exact exponential decay. However, there should be asymptotic exponential decay $\langle A_n \rangle \sim \exp(-n/L_{p1})$ for large $n < L/2$. In the steady-state, one has the relations $\langle A_n \rangle + \langle B_n \rangle = X_{eq}$ and $\langle B_n B_{n+1} \rangle + \langle B_n A_{n+1} \rangle + \langle A_n B_{n+1} \rangle + \langle A_n A_{n+1} \rangle = (X_{eq})^2$. Since one expects that $\langle A_n A_{n+1} \rangle$ decreases more quickly than $\langle A_n \rangle$, $\langle A_n B_{n+1} \rangle$, or $\langle B_{n-1} A_n \rangle$ for increasing n, it follows that one can just analyze equations for the latter quantities. Anticipating solutions of the form $\langle A_n \rangle \approx c \cdot r^n$, $\langle A_n B_{n+1} \rangle \approx c \cdot \beta \cdot r^n$, and

$\langle B_{n-1}A_n\rangle \approx c\cdot\gamma\cdot r^n$ and substituting into the rate equations for the pair approximation yields three coupled equations

$$(1-\beta)(r-1) + (1-\gamma)(r^{-1}-1) = \varepsilon, \quad (1-\gamma)(\gamma^{-1}X_{eq})(r^{-1}+1) - (1-X_{eq}) - (1-\beta) = \varepsilon,$$

$$\text{and } (1-\beta)(\beta^{-1}X_{eq})(r+1) - (1-X_{eq}) - (1-\gamma) = \varepsilon. \qquad (14)$$

Seeking solutions for small ε and $\delta = 1-r$ with $\beta \approx X_{eq} + B\delta$ and $\gamma \approx X_{eq} + C\delta$ yields $C = -B = X_{eq}(1-X_{eq})(2+X_{eq})^{-1}$ [33] and

$$L_{p1}(\text{pair}) \sim \delta^{-1} \sim (2-X_{eq})^{1/2}(2+X_{eq})^{-1/2}L_p(\text{MF}) \text{ , for large } L_{p1}. \qquad (15)$$

Thus, L_{p1}(pair) is smaller than L_{p1}(MF) and closer to the exact L_{p1}, but still has the incorrect asymptotic functional form as $W_{rx} \to 0$ or $W_{diff} \to \infty$.

B. Transient behavior

In this subsection, we characterize the evolution of concentration profiles during filling of a very long (semi-infinite) pore with an emphasis on scaling behavior for increasing time, t. Recall that the total concentration satisfies a standard discrete diffusion equation which reduces to the conventional continuum equation in the hydrodynamic regime. Thus, it follows that this profile has the "classic" scaling form

$$\langle X_n(t)\rangle \approx \langle X(t=\infty)\rangle\, F(n/(W_{diff}\, t)^{1/2}), \text{ for } n<L/2, \text{ where } F(y) = \text{erfc}(y/2), \qquad (16)$$

and where erfc is the complementary error function [34]. Thus, concentration profiles collapse onto a single curve for increasing t after rescaling the n-axis by $(W_{diff}\, t)^{1/2}$. However, when considering the individual species A and B, the system is dominated by B for increasing time due to reaction (when keeping all parameters fixed). After rescaling the spatial variable, one obtains $\langle B_n\rangle \sim \langle X_n\rangle$ and $\langle A_n\rangle \sim 0$. To achieve non-

trivial scaling profiles with significant populations of both species inside the pore, it is natural to reduce the reaction rate as time is increased so that $W_{rx}t$ remains constant. More precisely, we seek scaling solutions for the individual species concentrations of the form

$$<A_n(t)> \approx <X(t=\infty)> F^A(n/(W_{diff}\, t)^{1/2}, W_{rx}t) \text{ and} \quad (17a)$$

$$<B_n(t)> \approx <X(t=\infty)> F^B(n/(W_{diff}\, t)^{1/2}, W_{rx}t), \quad (17b)$$

for $n<L/2$, where $F^A + F^B = F$. Support for the existence of such solutions comes from substitution of these forms into the hydrodynamic reaction-diffusion equations of Sec.III. One then obtains a closed coupled pair of partial differential equations for the scaling functions $F^{A,B}(y, u)$. The specific form of the equations depends on the choice of diffusion fluxes (e.g., hydrodynamic versus MF), as do the solutions $F^{A,B}$. See Appendix D.

From the earlier discussion of hydrodynamic versus fluctuation effects, one might anticipate the following: (i) The MF and pair approximations should capture exact KMC behavior better for shorter times when most particles are relatively close to the pore opening. In this regime, behavior is more influenced by fluctuations. (ii) The hydrodynamic treatment should provide a better description of exact KMC behavior for longer times where the concentration profiles vary smoothly over many lattice constants. Indeed, this is the case as shown in Fig.5. For the selected parameters, the peak $<A_n>$-concentration of around 0.08 in the MF and pair approximations for smaller times (larger W_{rx}) matches KMC results, but these approximations retain this value for longer times. In contrast, the peak in hydrodynamic treatment increases to about 0.13-0.14 for longer

times (smaller W_{rx}) in good agreement with long-time KMC results. This peak is far above the converged MF and pair approximation value of 0.08.

V. Peripheral or central catalytic sites

A. Peripheral catalytic sites

Here, we consider situations where contiguous strings of sites at each end of the pore are catalytic, but sites in the central region are not. One can imagine this type of distribution might result where catalytic sites are created by grafting after formation of a meso- or nano-porous material and where diffusion into the pores is inhibited. (An alternative co-condensation process for mesoporous silica materials tends to produce a more uniform distribution of catalytic sites [35].) An example of the results of KMC simulations for evolution to the steady-state is shown in Fig.6. The parameter choices is $W_{ads} = 0.8$, $W_{des} = 0.2$, $W_{rx} = 0.017$, and $W_{diff} = 10$ for a pore of length L=100 with 20 catalytic sites at each end.

Characterization of behavior in this system is most appropriately divided into two regimes (provided that the reaction rate is not too large). In the first transient regime of "pore filling", a significant amount of A may avoid reaction in the peripheral catalytic regions and diffuse into the central non-catalytic region, i.e., A will successfully run the gauntlet passing catalytic sites without conversion. After the pore has filled so that the total concentration $\langle X_n \rangle \sim X_{eq}$ is roughly constant, one expects a peak in the concentration of A (i.e., a "blob" of A) in the center of the pore, and strongly decreasing A concentrations approaching and entering the peripheral regions from the center of the

pore. Indeed, in a hydrodynamic treatment, one achieves a stationary state with a frozen blob of A in the central non-catalytic region of the pore, and the peripheral catalytic regions occupied only by B and completely devoid of A. (Note that this hydrodynamic steady-state is not unique, the specific form of the frozen A-distribution in the central region will depend on the initial conditions.) However, this is not a true steady-state of the stochastic model, although it might be regarded as a metastable state.

Fluctuations at the end of the pore ensure that the A-concentration profile always has a local maximum at this location which does not diminish for long times (contrasting the hydrodynamic description). In fact, this part of the concentration profile is very similar to that for pore with all sites reactive (and with the same rate parameters).

However, more dramatically, in the second late-stage regime, fluctuation effects mean that the blob of A formed during the transient regime in the central non-catalytic region is not frozen. The entire blob can undergo anomalous diffusion, and is thus guaranteed to reach the peripheral catalytic regions. As a result, eventually essentially all of the A in this blob will be converted to B leading to the true steady-state with the central non-catalytic region, and indeed most of the interior of the pore, devoid of A. Indeed, the true steady-state for this case is very similar to that for the case where all sites are catalytic (with the same rate parameters). The reason is that for the case with all sites catalytic, it is only the end of the pore where one has conversion $A \rightarrow B$ in the steady state.

Fig.7 compares the predictions of the hydrodynamic treatment and other approximations with exact KMC simulations for a finite time selected to correspond to

the end of the first transient regime in the KMC results. The parameter choices is W_{ads} = 0.8, W_{des} =0.2, W_{rx} =0.017, and W_{diff} =10. Specifically, we choose the time t = 420 where the A-concentration at the center of the pore has roughly reached its maximum. In Fig.7, the concentration profile of the central A-blob in the KMC simulations is reasonably described by the hydrodynamic treatment. Small discrepancies presumably result from the feature that we have chosen a fairly small system, so fluctuation effects are still significant. In contrast, the MF and pair approximations fail to predict a significant peak in the concentration of A in central region. This is a consequence of the tendency of these approximations to allow artificially enhanced mixing of A and B. The pair approximation prediction is slightly closer to KMC behavior, reflecting the somewhat improved description of diffusion relative to MF.

In Fig.8, we show a series of snapshots from KMC simulations for fluctuation-dominated evolution in the late-stage regime. These fluctuations lead to diminution and removal of the significant A-concentration in the central non-reactive region of the pore. The diffusion of the A-blob within the non-catalytic region is clear, as well as its ultimate complete annihilation after several “collisions” with the peripheral catalytic region.

B. Central catalytic sites

Here, we consider situations where a contiguous string of sites in the center of the pore is catalytic, but sites in the peripheral regions are not. This geometry of catalytic sites has been considered in previous studies [14]. Toward the end of the first transient

stage of pore filling, a central catalytic region with reactant A largely converted to product B has been created, with non-catalytic regions on both sides primarily occupied by reactant A. Then, in the second late-stage regime, the central catalytic region remains essentially exclusively populated by B, but the concentration of product B in the non-catalytic end regions increases and that of reactant A decreases to achieve the final steady-state form. The details of this fluctuation-dominated process are described below. It should be noted that there is very low reactivity in the steady-state for this system (compared with a pore with all sites catalytic and the same parameters) since there is little population by A of the central catalytic region.

Fig.9 compares evolution in exact KMC simulations with the predictions of the hydrodynamic treatment and also the MF and pair approximations for a finite time selected to correspond roughly to the end of the first transient regime. In the hydrodynamic treatment, since diffusion fluxes are always towards the center of the pore, it is impossible to populate the non-catalytic end regions with B. Thus for long times in this treatment one has $\langle A_n \rangle \approx X_{eq}$ and $\langle B_n \rangle = 0$ in the non-catalytic end regions, and $\langle A_n \rangle \approx 0$ and $\langle B_n \rangle \approx X_{eq}$ in the central catalytic region. This is a steady-state in the hydrodynamic treatment, which might be described as a metastable state for the stochastic model. In fact, this simple hydrodynamic picture describes quite well the KMC results, deviations being due to fluctuations. In contrast, the MF and pair approximations predict a B-population in the non-catalytic end regions which is far too high. This is again a consequence of the tendency of these approximations to allow artificially enhanced mixing of A and B. The pair approximation prediction is slightly

closer to KMC behavior, again reflecting the somewhat improved description of diffusion relative to MF.

Fig. 10 shows KMC results for more complete evolution to the reactive steady-state. This occurs quite quickly for X_{eq}=0.1 (left frame). But for the case with X_{eq}=0.9 (right frame), this evolution is much slower. In either case, one finds the development of quasi-linear concentration profiles in non-catalytic end regions. Note that the MF treatment predicts linear concentration profiles in the non-catalytic end regions. This result follows from Eq. (10) noting that the steady-state J_K(MF) must be constant in these regions, which yields the relation $\partial/\partial x\ K(x)$ = constant for K = A or B. Further insight into this behavior comes from the analysis immediately following.

In Fig.11, we show a series of snapshots from KMC simulations for fluctuation-dominated evolution in the late-stage regime for a case similar to Fig.9 where X_{eq}=0.9. These fluctuations lead to the development of a significant B-population in the peripheral non-catalytic regions of the pore (while the central catalytic region remains essentially exclusively populated by B). The simplest case is where the reaction rate W_{rx} is fairly large. Then, in any single realization of the reaction system, there is relatively little intermixing of the A and B species, i.e., the peripheral regions are essentially all A and the central region is essentially all B. (There is strictly no intermixing in the limit $W_{rx}\to\infty$.) Thus, evolution in this regime simply involves the interface between A- and B-regions undergoing an (anomalous) random walk within the non-catalytic end regions, where this random walk is effectively subject to reflecting boundary conditions. When the interface and thus A species attempts to move into the central catalytic region, those

A are quickly converted to B, so the interface effectively cannot pass into the catalytic region and eventually meanders back into the non-catalytic region. When the interface and thus the B species reach the end of the pore, they can desorb and are replaced by adsorbing A species, so that the interface eventually wanders back toward the center of the pore. Thus, the quasi-linear steady-state concentrations in non-catalytic region shown in Fig.9, and also in previous studies [14], correspond to an ergodic-like time-average over the interface position.

VI. Generalizations and conclusions

There are many instructive generalizations of the above model and analyses. Here, we briefly comment on a few of these. It is natural to consider other distributions of catalytic sites not necessarily involving contiguous strings of such site. Simple examples would be periodic or spatially homogeneous random distributions. For a conventional reaction-diffusion system (without single-file diffusion), a coarse-grained continuum description of the form (6) would simply reduce the reaction rate by a factor proportional to the local density of catalytic sites. However, in single-file systems with steady-state reactivity localized at the end of the pore, this procedure might not be effective unless the penetration depth is very large.

Other natural generalizations include the introduction of unequal hop rates for reactant and product species in the absence of interactions between species. Then, the behavior of the non-equilibrium steady-state will be more complex, but key features induced by single-file diffusion persist [36]. One could also introduce interactions

between these species where all rates must be chosen to satisfy detailed-balance [13]. For simplicity, one might choose the strength of the interactions and also the adsorption-desorption rates to be species-independent (cf. [13]). Then, just focusing on whether sites are occupied by particles X=A+B, the steady-state is a conventional grand canonical equilibrium state with a uniform total particle density away from the pore ends. In the hydrodynamic regime, the chemical diffusion fluxes must still vanish in this steady-state as a consequence of the single-file nature of diffusion [36]. Thus, just as for our simpler model, one can conclude that catalytic regions inside the pore will be unreactive (as all reactant A will be converted to product), and that steady-state reactivity will be controlled by fluctuations [36].

Yet another class of generalizations of the above process include sequential conversion reactions $A \to B \to C \to \ldots$ or parallel conversion reactions $A \to B$, $A \to C$, etc., at catalytic sites. For simplicity, consider the special choice of rates, $W^K_{des} = W_{des}$ and $W^K_{diff} = W_{diff}$, for all species types, K. Again, if one does not discriminate between the identity of particles, but only considers whether sites are empty, E, or filled, X=A+B+…, then evolution of X is described by a standard discrete diffusion equation. Furthermore, significantly, the exact hydrodynamic treatment of diffusion for the two-species case readily generalizes to treat this more complex case (cf. [37]). Thus, effective analysis of transient behavior should be possible with appropriate h-RDE, and again we expect steady-state reactivity to be controlled by fluctuation effects [36].

In summary, the transient and steady-state behavior of single-file conversion reaction systems displays some general features. Transient evolution of concentration

profiles is effectively described by hydrodynamic RDE which properly incorporate the single-file nature of diffusion. However, steady-state reactivity is controlled by fluctuation effects not incorporated in the hydrodynamic treatment. MF-type treatments can capture some aspects of this steady-state behavior, but not scaling properties for extreme choices of reaction and diffusion rates.

Acknowledgements

This work was supported by the Division of Chemical Sciences (Basic Energy Sciences), U.S. Department of Energy (USDOE) through the Ames Laboratory PCTC, Chemical Physics, and Catalysis projects, and also a SULI project. Ames Laboratory is operated for the USDOE by Iowa State University under Contract No. DE-AC02-07CH11358.

Appendix A: Exact hydrodynamic diffusion fluxes

Consider a two-component lattice-gas where species A and B have equal hop rates, W_{diff}, to NN empty sites, and there are no interactions beyond site exclusion. Set $D_X = a^2 W_{diff}$. Then, for hyper-cubic lattice of any dimension, the diffusion flux for species A in the hydrodynamic regime of slowly varying concentrations has the exact form [4,18,26]

$$\underline{J}_A = -D_X X^{-1}[A + B F_{tr}(X)] \nabla A - D_X X^{-1} A [1 - F_{tr}(X)] \nabla B$$

$$= -D_X [A X^{-1}] \nabla X - D_X F_{tr}(X) X^{-1} [B \nabla A - A \nabla B], \qquad (18)$$

with an analogous expression for J_B. Here, A, B and X=A+B represent concentrations per unit length, and ∇ denotes the spatial gradient. The quantity F_{tr} represents the tracer diffusion coefficient for a tagged particle with hop rate of unity within a dense single-component lattice-gas on the hyper-cubic lattice of concentration X. Generalizations have been explored for the case of unequal hop rates of A and B [4,38].

For an infinite 1D lattice, J_A is a scalar, $\nabla = \partial/\partial x$, and $F_{tr} = 0$, recovering the result (8). F_{tr} vanishes since diffusion is anomalous in 1D, the root-mean-square displacement of the tagged particle increasing like $t^{1/4}$ rather than $t^{1/2}$ [6-8]. It is instructive to note that the MF form of the diffusion fluxes (9) is recovered by choosing $F_{tr} = (1- X/X_m)$. This offers the possibility of developing a hybrid expression for the diffusion fluxes capturing both aspects of the MF description near the pore ends and the hydrodynamic description in the pore interior [36].

Appendix B: Discrete forms of diffusion fluxes

For comparison of KMC results sometimes for relatively short pores with predictions based on a hydrodynamic treatment of diffusion, we naturally incorporate an appropriate discrete version, $J_K^{n>n+1}$, of the hydrodynamic diffusion fluxes (8) into the discrete RDE's (1). We have utilized discrete forms

$$J_K^{n>n+1} = -W_{diff}\, P_K^{n,n+1}\, \Delta\langle X_n\rangle \text{ with } \Delta\langle X_n\rangle = \langle X_{n+1}\rangle - \langle X_n\rangle \text{ for K=A or B,} \quad (19)$$

with $P_K^{n,n+1} = 1$ if $\langle X_n\rangle\langle X_{n+1}\rangle = 0$. For $\langle X_n\rangle\langle X_{n+1}\rangle \neq 0$, one standard choice would set

$$P_K^{n,n+1} = \tfrac{1}{2}\,(\langle K_n\rangle/\langle X_n\rangle + \langle K_{n+1}\rangle/\langle X_{n+1}\rangle). \quad (20)$$

However, other reasonable choices have the form $P_K^{n,n+1} = \langle K_{n,n+1}\rangle / \langle X_{n,n+1}\rangle$ where $\langle K_{n,n+1}\rangle = \frac{1}{2}(\langle K_n\rangle + \langle K_{n+1}\rangle)$, or $2\langle K_n\rangle\langle K_{n+1}\rangle/(\langle K_n\rangle + \langle K_{n+1}\rangle)]$, or $\sqrt{\langle K_n\rangle}\sqrt{\langle K_{n+1}\rangle}$. Analysis of evolution typically finds only small differences between results from these different choices.

One case requiring special treatment is where just the central sites are catalytic. Then, there is a sharp boundary between a central region with finite population of B and peripheral regions devoid of B (in a continuum treatment). Choice (20) produces a substantial B-flux from the site just outside to that just inside the catalytic region, producing an unphysical negative B-concentration for the former. The same behavior occurs to varying degrees in the other choices. However, in our analysis, we eliminate this problem by setting to zero the B-flux between these two sites (and identifying the A-flux with the total particle flux).

As an aside, for the continuum MF diffusion flux (9), a standard numerical PDE treatment would implement various discretizations, e.g., analogous to (20). However, our analysis starting with the discrete master equations and applying a factorization approximation suggests the natural form

$$J_A^{n>n+1}(\mathrm{MF}) = -W_{\mathrm{diff}}\,[(1-\langle B_n\rangle)\Delta\langle A_n\rangle + \langle A_n\rangle\Delta\langle B_n\rangle]. \qquad (21)$$

Appendix C: Mean-field behavior as $W_{\mathrm{diff}} \to \infty$

The MF prediction for $W_{\mathrm{diff}} \to \infty$ of spatially uniform concentration profiles enables simple analysis of the MF steady-state. Summing all of the equations for $\langle A_n\rangle$ implies

$$0 = d/dt\ (\sum_n \langle A_n \rangle)$$

$$= W_{ads}(\langle E_1 \rangle + \langle E_L \rangle) - W_{des}(\langle A_1 \rangle + \langle A_L \rangle)$$

$$- W_{rx}\ (\sum_n \langle A_n \rangle) + (\sum_n J_A^{n>n+1} = 0), \quad (22)$$

where $\sum_n J_A^{n>n+1}=0$ by symmetry. Consequently, using spatial homogeneity yields

$$\langle A_n \rangle|_{MF} = 2W_{ads}\, E_{eq}/(2W_{des} + LW_{rx}) \sim 1/L \text{ where } E_{eq} = W_{des}/(W_{ads}+W_{des}). \quad (23)$$

and $\langle A_n \rangle|_{MF} + \langle B_n \rangle|_{MF} = X_{eq}=1-E_{eq}$. Thus, the MF total reactivity, $R_{tot}^{MF} = W_{rx}L\langle A_n \rangle|_{MF}$, converges like 1/L, as $L\rightarrow\infty$, rather than displaying the correct exponential convergence.

Appendix D: Scaling forms for pore filling

For the total concentration X(x,t), substitution of the form $X(x,t) \approx F(x/(D_x t)^{1/2})$ into the standard diffusion equation yields

$$-\tfrac{1}{2}\, yF'(y) = F''(y), \quad (24)$$

which is satisfied by the "classic" erfc solution. Next, consider the scaling forms $A(x,t) \approx F^A(x/(D_x t)^{1/2}, W_{rx}t)$ and $B(x,t) \approx F^B(x/(D_x t)^{1/2}, W_{rx}t)$ for the concentrations of A and B. Substitution into the hydrodynamic RDE yields

$$-\tfrac{1}{2}\, y\, F^A{}_1(y,u) + uF^A{}_2(y,u) = - uF^A(y,u) + K(F^A, F^B), \quad (25a)$$

$$-\tfrac{1}{2}\, y\, F^B{}_1(y,u) + uF^B{}_2(y,u) = + uF^B(y,u) + K(F^B, F^A), \quad (25b)$$

where the subscripts 1(2) denote partial differentiation with respect to the first (second) variable y (u). The "diffusion terms" K have the form

$$K(F^A, F^B) = [1-F^B]F^A{}_{11} + F^A F^B{}_{11}\ (MF), \quad (26a)$$

$$K(F^A, F^B) = F^A{}_1 F^B{}_1/F - F^A\ (F)^{-2}\ (F_1)^2 + F^A\ (F)^{-1}\ F_{11}\ (\text{exact hydrodynamic}). \quad (26b)$$

References

[1] G. Nicolis and I. Prigogine, *Self-organization in Non-equilibrium Systems* (Wiley, New York, 1977).
[2] A.S. Mikhailov, *Foundations of Synergetics I* (Springer, Berlin, 1990)
[3] R. Imbihl and G. Ertl, Chem. Rev. **95**, 697 (1995).
[4] J.W. Evans, D.-J. Liu, and M. Tammaro, Chaos **12**, 131 (2002).
[5] D.-J. Liu and J.W. Evans, Surf. Sci. **603**, 1706 (2009) (Ertl Nobel issue).
[6] A.L. Hodgkin and R.D. Keynes, J. Physiol. (London) **128**, 61 (1955).
[7] T.E. Harris, J. Appl. Prob. **2**, 323 (1965).
[8] P.A. Fedders, Phys. Rev. B, **16**, 1393 (1977).
[9] J.G. Tsikoyiannis and J.E. Wei, Chem. Eng. Sci, **46**, 233 (1991).
[10] M.S. Okino, R.Q. Snurr, H.H. Kung, J.E. Ochs, and M.L. Mavrovouniotis, J. Chem. Phys. **111**, 2210 (1999).
[11] J. Kärger, M. Petzold, H. Pfieffer, S. Ernst, and J. Weitkamp, J. Catal. **136**, 283 (1992).
[12] C. Rodenbeck, J. Kärger, and K. Hahn, J. Catal. **157**, 656 (1995).
[13] C. Rodenbeck, J. Kärger, and K. Hahn, Phys. Rev. E **55**, 5697 (1997).
[14] S.V Nedea, A.P.J. Jansen, J.J. Lukkien, and P.A.J. Hilbers, Phys. Rev. E **65**, 066701 (2002); **66**, 066705 (2002).
[15] S.V Nedea, A.P.J. Jansen, J.J. Lukkien, and P.A.J. Hilbers, Phys. Rev. E **67**, 046707 (2003).
[16] R. Krishna, T.J.H. Vlugt, and B. Smit, Chem. Eng. Sci.**54**, 1751 (1999).
[17] D. Paschek and R. Krishna, Phys. Chem. Chem. Phys. **3**, 3185 (2001).
[18] J. Quastel, Commun. Pure Appl. Math. **45**, 623 (1992).
[19] N.G. Van Kampen, *Stochastic Processes in Physics and Chemistry* (North Holland, Amsterdam, 1981).
[20] J.W. Evans, Rev. Mod. Phys. **65**, 1281 (1993).
[21] R. Kutner, Phys. Lett. **81A**, 239 (1981)
[22] J.W. Evans, Phys. Rev. B **41**, 2158 (1990).
[23] T.L. Hill, *Introduction to Statistical Thermodynamics* (Addison-Wesley, Reading, 1960).
[24] J.W. Evans and D.K. Hoffman, Phys. Rev. B **30**, 2704 (1984).
[25] For W_{diff} <<1, the steady-state $\langle A_n \rangle \approx 0$ except for n=1 and L. Solving (1a) yields $\langle A_1 \rangle = p_A \langle X_1 \rangle$ with $p_A = W_{des}/(W_{des}+W_{rx})$, and $\langle B_1 \rangle = p_B \langle X_1 \rangle$ with $p_A + p_B = 1$.
[26] H. Spohn, *Large Scale Dynamics in Interacting Particle Systems* (Springer, Berlin, 1991).
[27] Onsager theory writes $J_K = - \sum_M \sigma_{K,M} \partial/x \, \mu_M$ where μ_M is the chemical potential for species M, and $\sigma_{K,M}$ are components of the conductivity tensor. Without interactions, one has that $\mu_K = (k_B T) \ln[\langle K \rangle (1-\langle X \rangle)^{-1}]$. The MF approximation sets $\sigma_{K,M} \propto (k_B T)^{-1} \langle K \rangle (1-\langle X \rangle) \delta_{K,M}$.
[28] V.P. Zhdanov, Surf. Sci. **194**, 1 (1988).
[29] J.W. Evans, J. Chem. Phys. **97**, 572 (1992).

[30] See X. Guo, Y. De Decker, and J.W. Evans, Phys. Rev. E **82**, 021121 (2010). h-RDE have been extracted for pair approximations in simple single-species reaction diffusion models. However, for this two species model, there are additional challenges related to the asymptotic convergence of continuum quantities $a^{-1} \langle A_n B_{n+1} \rangle \sim [AB](x)$ and $a^{-1} \langle B_n A_{n+1} \rangle \sim [BA](x)$.
[31] There is partial randomization of configurations as $W_{diff} \to \infty$ [15]: configurations with the same number of particles and sequence of particle types have equal probability.
[32] In the steady state, one has $W_{rx}\, A(x) = -\partial/\partial x\, J_A = D_X(1-X_{eq})\, \partial^2/\partial x^2\, A(x)$ from (6) and (10), solution of which immediately reveals the exponentially decaying solutions.
[33] The result C>0 and B<0 is consistent with the expectation that $\langle A_n B_{n+1} \rangle$ exceeds $\langle B_{n-1} A_n \rangle$ given a higher B concentration further into the pore.
[34] J. Crank, *Mathematics of Diffusion* (Oxford University Press, Oxford, 1956).
[35] S. Huh, J.W. Wiench, J.-C. Yoo, M. Pruski, and V.S.-Y. Lin, Chem. Mater. **15**, 4247 (2003).
[36] D.-J. Liu, J. Wang, D.M. Ackerman, M. Pruski, H.-T. Chen, V.S.-Y. Lin, and J.W. Evans, ACS Catalysis, submitted (2011). (Victor S.-Y. Lin Memorial Issue).
[37] M. Tammaro and J.W. Evans, J. Chem. Phys. **108**, 7805 (1998).
[38] K.W. Kehr, K. Binder, and S.M. Reulein, Phys. Rev. B **39**, 4891 (1989).

Tables

Table I. Tabulation of L_p-values from KMC simulations, and the MF and pair-approximations, for the cases analyzed in Fig.3.

	W_{ads} = 0.8 and W_{des} = 0.2					W_{ads} =0.2 and W_{des} = 0.8			
W_{rx}	1	0.1	0.01	0.001		1	0.1	0.01	0.001
L_{p1}(KMC)	0.41	0.69	1.00	2.56		0.88	2.13	5.56	16.7
L_{p2}(KMC)	1.10	1.47	2.64	5.21		1.47	2.92	6.77	15.2
L_{p3}(KMC)	0.42	0.88	2.10	4.69		0.87	2.39	6.25	14.7
$L_{p1,3}$(MF)	0.520	1.44	4.48	14.1		0.937	2.84	8.95	28.29
L_{p2}(MF)	1.17	2.00	5.00	14.7		1.53	3.37	9.46	27.78
L_{p1}(pair)	0.432	1.23	2.92	9.26		0.882	2.59	8.11	27.89
L_{p2}(pair)	1.11	1.79	3.47	9.77		1.48	3.12	8.61	27.84
L_{p3}(pair)	0.433	1.23	2.94	9.26		0.882	2.59	8.10	27.33

Figures

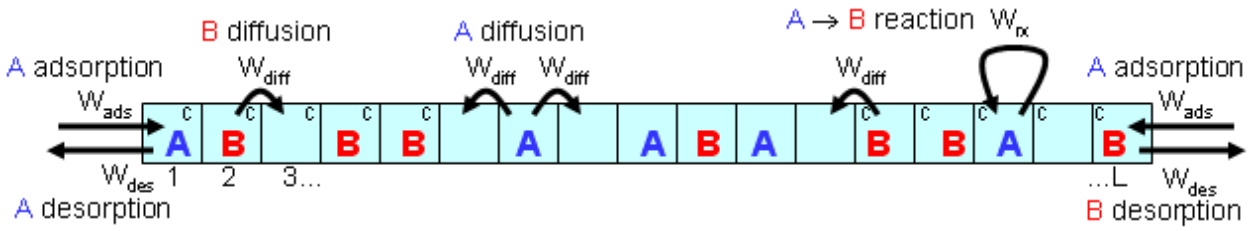

Fig.1. Schematic of catalytic conversion reaction A→B in a single-file system. Catalytic sites (c) are located near the pore ends in this illustration. The configuration shown represents the transient regime. See Sec.IV.

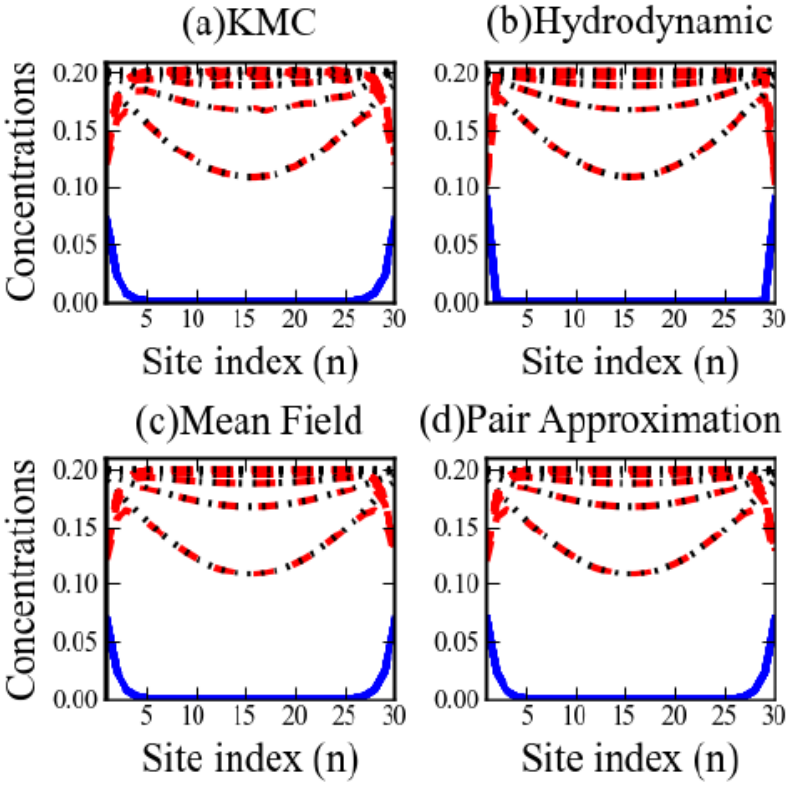

Fig.2. Evolution of concentration profiles to the steady-state in a pore with all sites reactive: A (blue solid lines); B (red dashed lines); X=A+B (black dotted lines). This format is used in subsequent figures. Parameters are $W_{ads} = 0.2$, $W_{des} = 0.8$, $W_{rx} = 1$, $W_{diff} = 1$, and $L = 30$. Time increments are $\Delta t = 100$. (a) KMC results averaged over 2.5×10^5 simulations; (b) hydrodynamic, (c) MF, and (d) pair approximation results. The B-concentration increases with time.

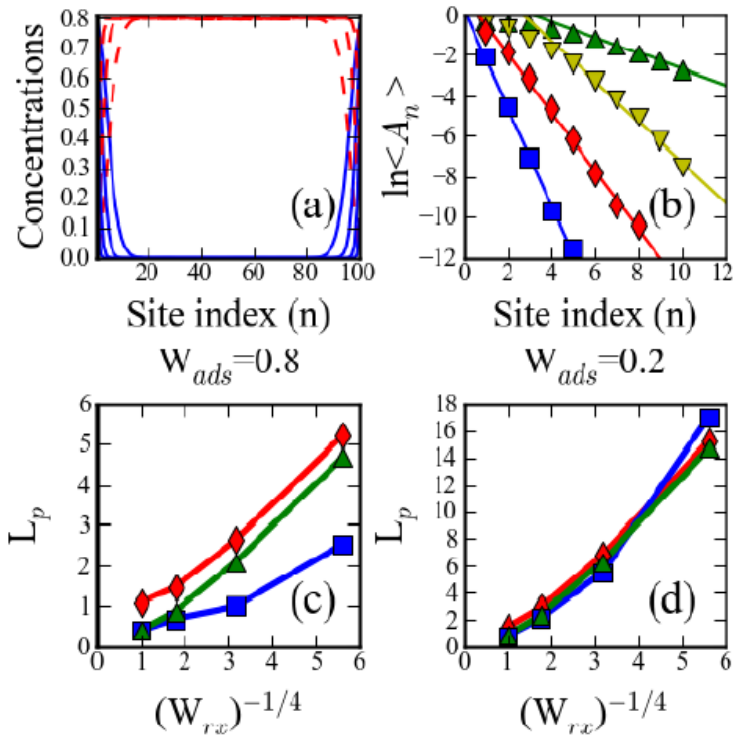

Fig.3. Steady-state behavior for a mesopore with all sites catalytic. (a) Concentration profiles for W_{ads}=0.8, W_{des}=0.2, and W_{diff}=1, with L=100 for W_{rx}=1, 0.1, 0.01, and 0.001; (b) ln $<A_n>$ versus n<<L/2 for the data in (a); data for smaller W_{rx} has greater penetration in (a) and smaller slopes in (b); L_p versus $(W_{rx})^{-1/4}$ with W_{diff}=1 for: (c) W_{ads}=0.8, W_{des}=0.2; and for (d) W_{ads}=0.2, W_{des}=0.8. Squares, diamonds, and triangles denote L_{p1}, L_{p2}, and L_{p3}, respectively.

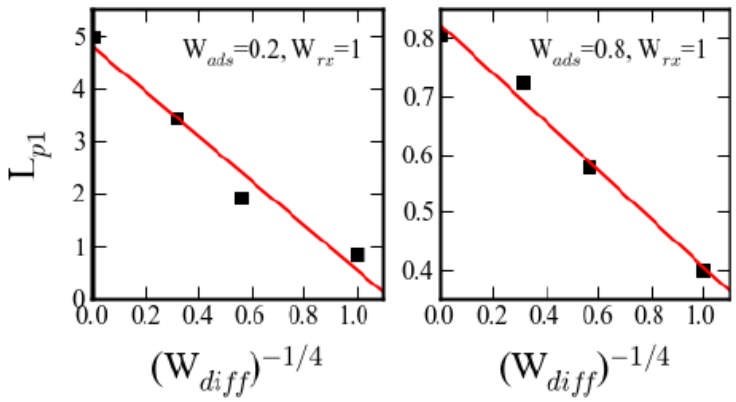

Fig.4. Dependence of L_{p1} on W_{diff} (but retaining fixed finite W_{ads}, W_{des}, and W_{rx}) demonstrating the nature of the convergence to $L_{p1}(W_{diff} \rightarrow \infty)$ as $W_{diff} \rightarrow \infty$.

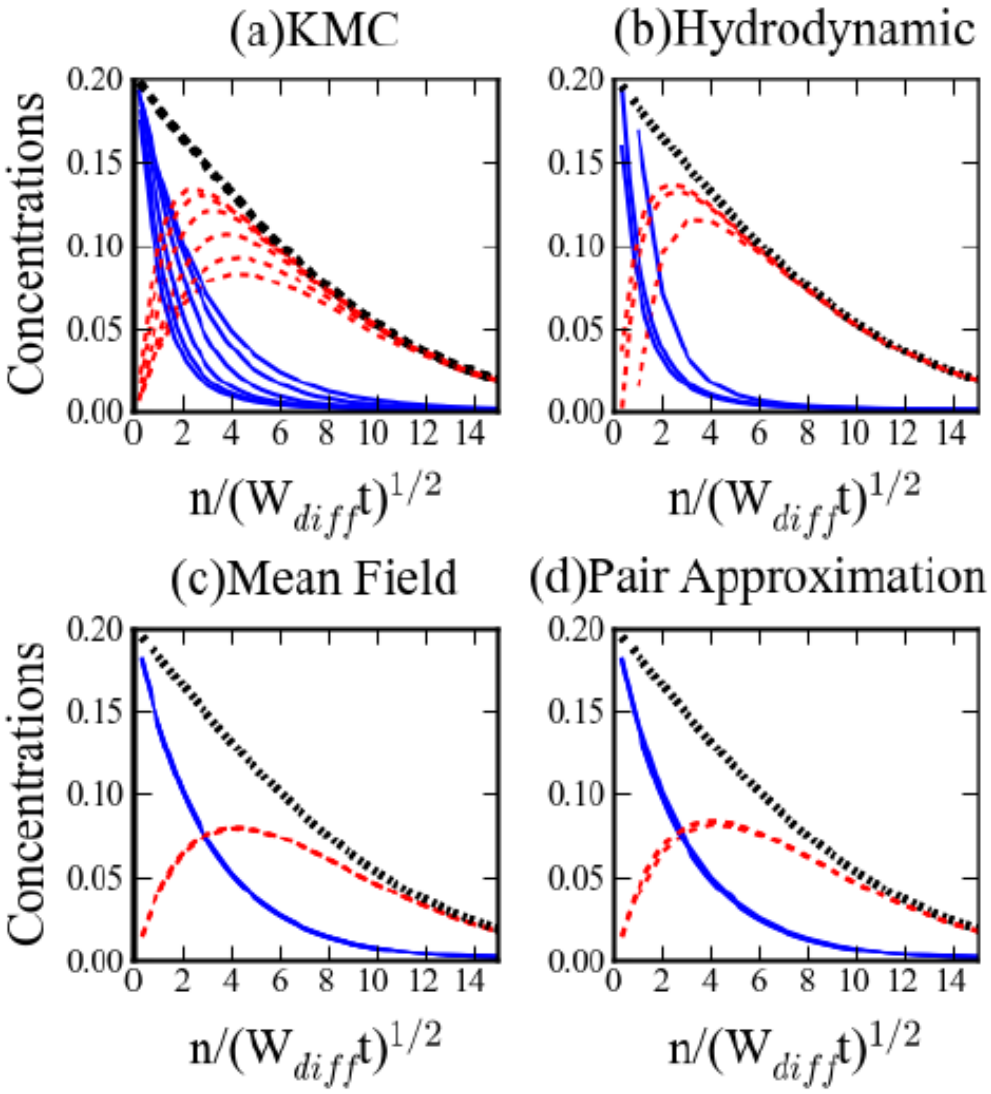

Fig.5. Diffusion into an initially empty semi-infinite pore with all sites catalytic. Parameters: W_{ads}=0.2, W_{des}=0.8, W_{diff} = 1, and W_{rx} t = 4 (ensuring comparable amounts of A and B in the pore). Rescaled concentration profiles for: (a) KMC simulation; (b) hydrodynamic; (c) MF; and (d) pair approximations. KMC results are shown for W_{rx} = 0.1, 0.01,… and 0.000001 (6 cases), where convergence to the limiting profile shapes is very slow. Convergence is fast for the MF and pair approximations (by W_{rx}~0.01), and moderate for the hydrodynamic treatment (by W_{rx}~0.001 where data is shown for W_{rx} = 0.1, 0.01, and 0.001).

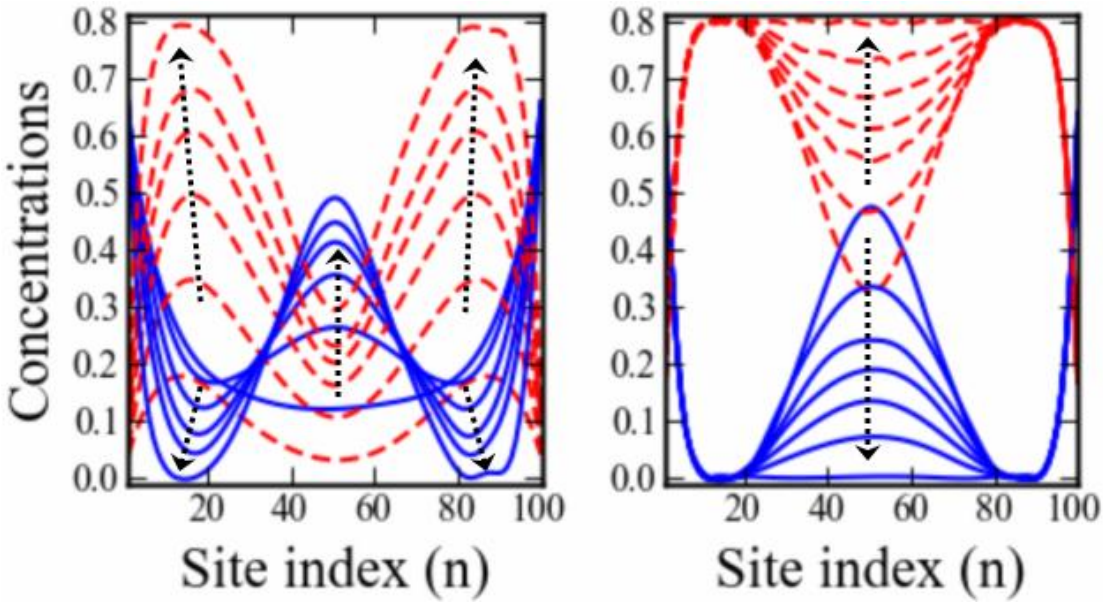

Fig.6. KMC results for the complete evolution of species concentrations for a pore of length L=100 with 20 sites at each end catalytic. Parameters are W_{ads} = 0.8, W_{des} =0.2, W_{rx} =0.017, and W_{diff} =10. The left frame shows the transient pore-filling regime for time increments of 60 up to t=600 where the peak $<A_{50}>$ is growing significantly to reach a maximum. The following "metastable regime" has little change over ~10^3 time units. The right frame shows slow late-stage evolution for times t = 1000, 5000, 10000, 14000, 20000, and 100000 where $<A_{50}>$ decreases below its maximum. The steady-state (with $<A_n>\approx 0$ in the central region) is reached after ~10^5 time units. Black dotted arrows indicate evolution with increasing time.

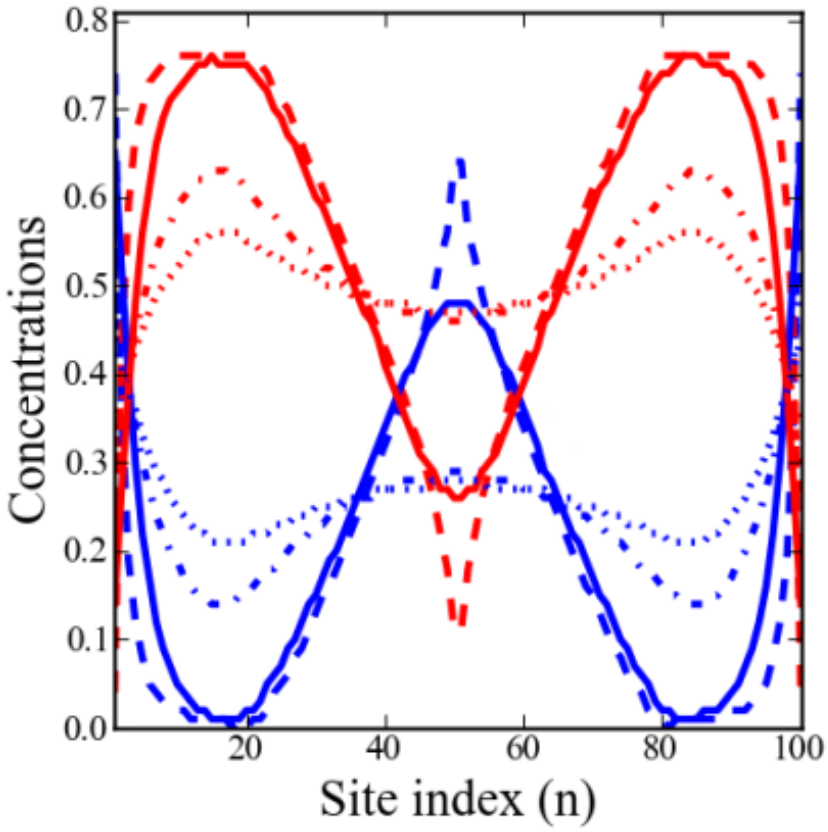

Fig. 7. Behavior roughly at the end of the transient regime t = 420 for a pore of length L=100 with 20 peripheral sites catalytic at each end. The parameter choices is W_{ads} = 0.8, W_{des} =0.2, W_{rx} =0.017, and W_{diff} =10. Reactant A in the pore center has "run the gauntlet" through the peripheral catalytic regions. Results from: KMC (solid); hydrodynamic (dashed); pair (dot-dashed); MF (dotted).

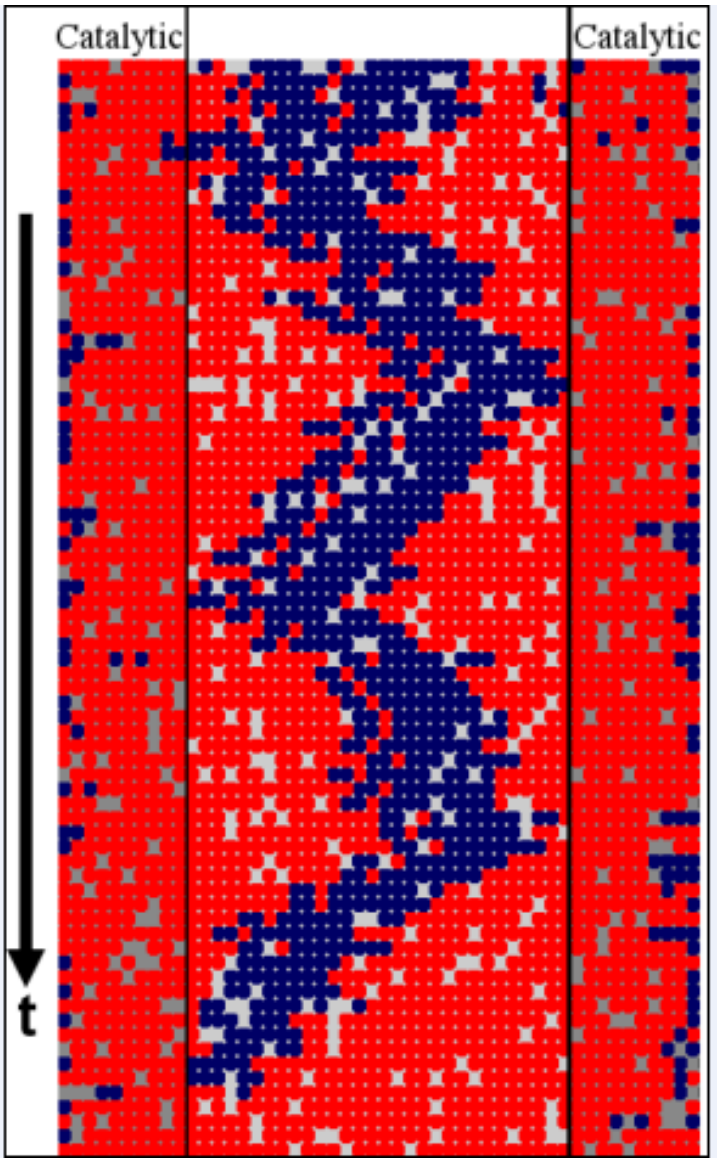

Fig. 8. Later-stage evolution in a pore of length L=50 with 10 catalytic sites (grey) on each end catalytic. Dark blue circles are reactant A. Lighter red circles are product B. Sequence of images separated by 42 time units from a single KMC simulation run. Parameters: W_{ads}=0.1, W_{des}=0.9, W_{rx}=0.08, and W_{diff}=100. The central A-blob diffuses to the peripheral catalytic regions ultimately being converted to product. Higher X_{eq}=0.9 makes the A-blob more visible.

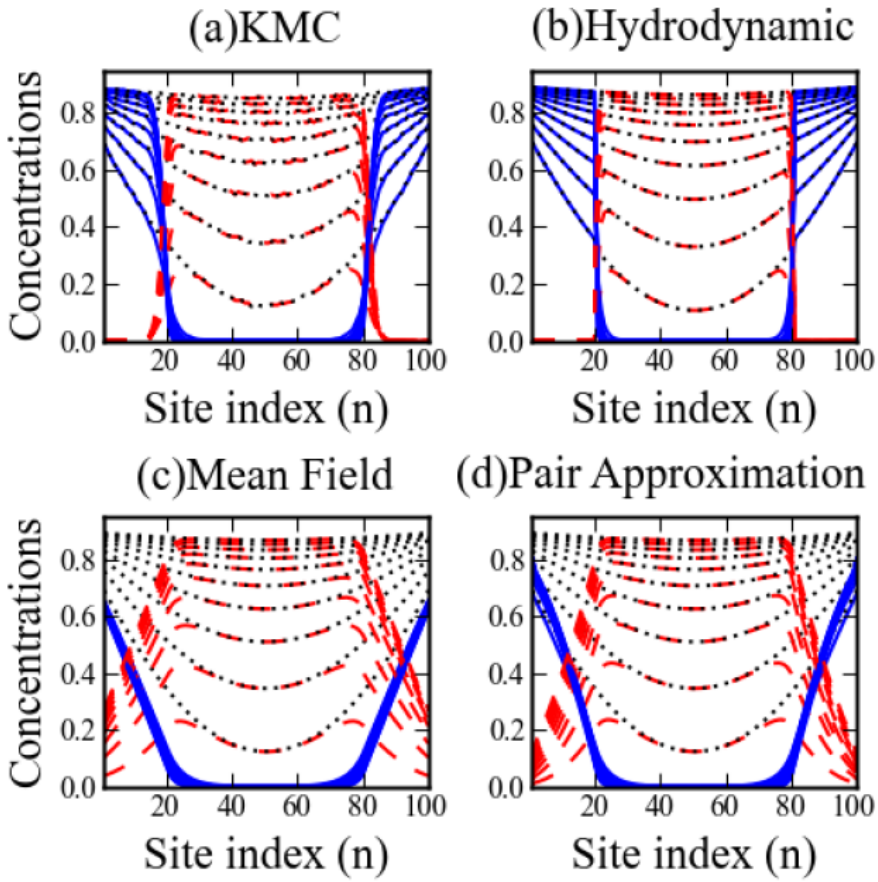

Fig.9. KMC of concentration profile evolution for the central 60 sites catalytic in a pore of length L=100. Parameters are W_{rx} = 0.33, W_{diff} = 10, and for (a) W_{ads} = 0.1, W_{des} = 0.9; (b) W_{ads} = 0.9, W_{ads} = 0.1. Time increments are 50 and the final time is t=500.

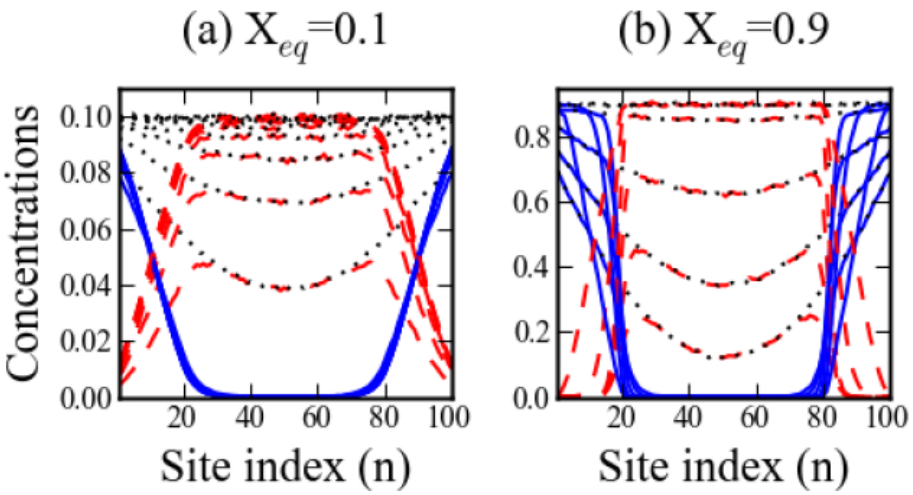

Fig. 10. KMC results for the complete evolution of species concentrations for the central 60 sites catalytic in a pore of length L=100 with W_{rx} = 0.33, W_{diff} = 10 for two cases. (a) W_{ads} = 0.1, W_{des} = 0.9 (so X_{eq}=0.1) with time-evolution in increments of 100, so the steady-state is achieved quickly by t ~700; (b) W_{ads} = 0.9, W_{ads} = 0.1 (so X_{eq}=0.9) and profiles are shown at times t=50, 100, 200, 500, 1500, 15000. Thus in (b), the steady-state is achieved slowly, where $<A_n>$ again finally achieves a quasi-linear steady-state variation in the end non-catalytic regions.

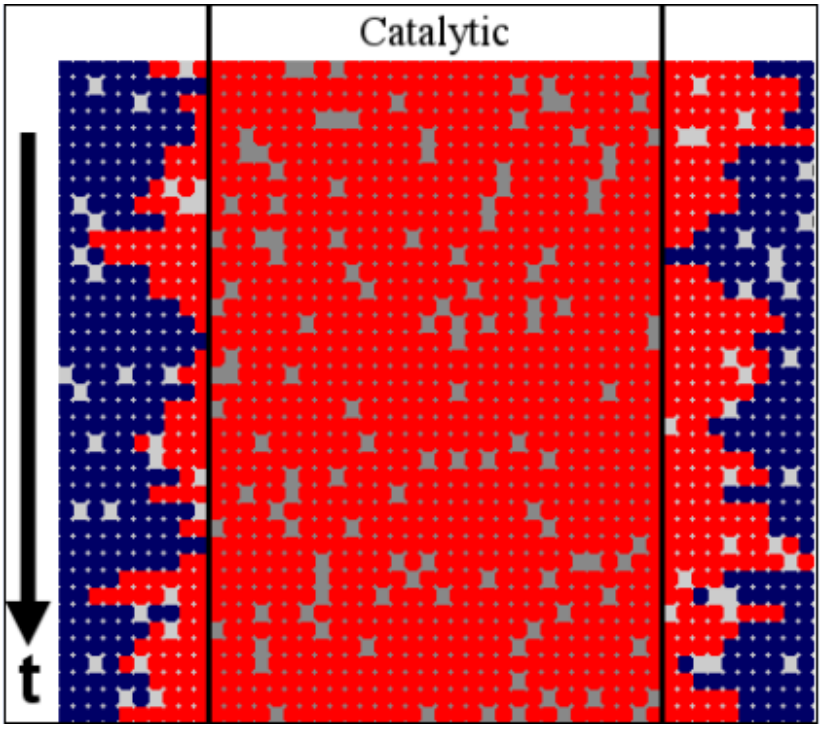

Fig. 11. Later-stage evolution in a pore of length L=50 with the 30 central catalytic sites (grey). Dark blue circles are reactant A. Lighter red circles are product B. Sequence of images separated by 300 time units from a single KMC simulation run. Parameters: W_{ads} = 0.9, W_{des} = 0.1, W_{rx} = 0.6, and W_{diff} = 3. The interface between A- and B-dominated regions diffuses within the non-catalytic end regions. Higher X_{eq}=0.9 makes the interface more visible.

CHAPTER 3. GENERALIZED HYDRODYNAMIC TREATMENT OF THE INTERPLAY BETWEEN RESTRICTED TRANSPORT AND CATALYTIC REACTION IN NANOPOROUS MATERIALS

A paper published in Physical Review Letters

David M. Ackerman, [1,2,*] Jing Wang, [1,3,*] and James W. Evans[1, 3,4]

[1]Ames Laboratory – USDOE, and Department of [2]Chemistry, [3]Mathematics, and [4]Physics and Astronomy, Iowa State University, Ames Iowa 50011, USA

[*]David Ackerman performed the kinetic Monte Carlo simulations for the models, and I performed the analytic investigations and related numerical simulations of discrete reaction-diffusion equations.

Abstract

Behavior of catalytic reactions in narrow pores is controlled by a delicate interplay between fluctuations in adsorption-desorption at pore openings, restricted diffusion, and reaction. This behavior is captured by a generalized hydrodynamic formulation of appropriate reaction-diffusion equations (RDE). These RDE incorporate an unconventional description of chemical diffusion in mixed-component quasi-single-file systems based on a refined picture of tracer diffusion for finite-length pores. The RDE elucidate the nonexponential decay of the steady-state reactant concentration into the pore and the non-mean-field scaling of the reactant penetration depth.

Text

Anomalous tracer diffusion of a "tagged" particle in a single-file system, where particles within narrow pores cannot pass each other, was proven in the 1960's for hard-core interactions [1] and later for general interactions [2]. Often motivated by early investigations of biological transport across membranes [3,4], numerous studies have considered single-file tracer diffusion in finite open [5], periodic [6,7], or closed [8] "pores", and in other systems [9]. This type of inhibited transport has also been recognized to impact reactivity for catalysis in zeolites and other functionalized nanoporous materials [10-15]. For the latter reaction-diffusion phenomena which are of interest here, it is actually chemical diffusion [16] which controls behavior [15], and for which the connection to tracer diffusion is not well recognized. Another key aspect of these open reaction-diffusion systems is that steady-state behavior is not described by a classic Gibbs thermodynamic ensemble. In fact, a fundamental understanding of these steady-states, which depend on both the reaction kinetics and transport, remains a significant challenge [17-19].

Our specific focus is on first-order conversion reactions, $A \rightarrow B$, occurring inside a parallel array of linear nanopores of a catalytically functionalized material such as mesoporous silica. Reactants, A, enter the pore openings, diffuse to catalytic sites, convert to a product, B, with microscopic rate k, and both reactants and products can diffuse out of the pore [11-15]. Furthermore, we assume that these pores are sufficiently narrow that passing of reactant and product species is inhibited or even excluded. It was recognized that reactivity can be strongly inhibited for single-file diffusion (SFD)

relative to unhindered passing [12]. The reason is that except near their ends, the pores tend to be exclusively populated by product which is not readily extruded. Thus, the pore center does not participate in the conversion A→B.

Some studies have suggested that this type of behavior, even for inhibited transport, can be captured by mean-field-type treatments of reaction-diffusion [13] which predict an exponential decay of reactant concentration into the pore with penetration depth scaling like $L_p \sim k^{\zeta}$ with $\zeta = -½$ [14,15]. However, we will find fundamental shortcomings in these mean-field treatments, noting that exact behavior for SFD even exhibits different scaling of L_p with $\zeta \neq -½$. A deterministic hydrodynamic treatment [20] accounting for SFD [15] can describe reaction-diffusion behavior in the regime of slowly varying concentration profiles (for long pores) even for SFD, but this treatment completely fails to describe steady-state reactivity [15]. The reason for this failure is that steady-state behavior is controlled by the stochastic nature of adsorption and desorption of species at the pore openings. Thus, to correctly capture behavior, in this Letter, we pursue a generalized hydrodynamic formalism. This formalism requires an appropriate description of chemical diffusion in mixed-component systems, including the case of SFD, based on a relationship between chemical and tracer diffusion deriving from interacting particle systems theory. However, it also requires a refined picture of tracer diffusion for finite-length pores.

In our model for A→B conversion (Fig.1), we consider a catalytic material composed of an array of similar parallel linear nanopores. Species within any pore are localized at a linear array of cells (or sites) labeled n=1 - L traversing the pore. The cell

width “a” is chosen as a~1 nm comparable to species size. To describe the surrounding fluid, we can extend the 1D lattice inside the pores to a 3D lattice outside. But the fluid is assumed well stirred, so that cells of the 3D lattice are randomly occupied with specified probabilities, $<A_{out}>$ and $<B_{out}>$, corresponding to the suitably normalized external reactant and product concentrations, respectively. The total concentration, $<X_{out}> = <A_{out}> + <B_{out}> = \chi$, say, is fixed, whereas $<B_{out}>$ slowly increases from an initial value of zero during extended reaction. This slow time-scale is controlled by the fluid volume and far exceeds that for relaxation of the concentration profile within the pore.

In the simplest prescription corresponding to SFD within the pores, A and B hop to adjacent empty (E) cells at rate h per direction. We can also allow positional exchange of adjacent A and B at rate $h_{ex} = h P_{ex}$ to relax the strict SFD constraint, noting that exchange of adjacent particles of the same type has no effect. The passing propensity, P_{ex}, will increase with pore diameter d from $P_{ex} = 0$ below a SFD-threshold to $P_{ex} \sim 1$ for unhindered passing. Other mechanistic steps in the model are: **(i)** Impingement of external species at terminal cells n=1 and n=L of the pore at rate $i_A = h <A_{out}>$ ($i_B = h <B_{out}>$) for the reactant A (product B), successful adsorption occurring if these end cells are unoccupied or empty (E), **(ii)** Attempted desorption of both A and B from terminal cells of the pore at rate h, success occurring with probability $<E_{out}> = 1 - <X_{out}>$ for the neighboring fluid site to be unoccupied (E_{out}), and **(iii)** Conversion $A \rightarrow B$ at rate k at catalytic cells.

For the above rate choice, which follows previous studies [11-15], the "species blind" dynamics for particles X = A or B corresponds to a non-reactive diffusion process. In the steady-state, cells within the pore are randomly occupied by particles X with probability $<X_{out}> = \chi$ [14]. We will assess typical concentration profiles within a pore, corresponding to averaging over many pores. Both time evolution and steady-state behavior (see Fig.2 for examples for the initial stages of reaction with $<B_{out}> \approx 0$) can be assessed precisely by Kinetic Monte Carlo (KMC) simulation.

An exact description of our discrete reaction-diffusion model is provided by hierarchical master equations for the evolution of probabilities of various configurations of subsets of cells within the pore [11,13-15]. Let $<C_n>$ denote the probability that species C = A or B is at cell n, $<C_nE_{n+1}>$ that C is at cell n and that cell n+1 is empty (E), etc. Then, the total conversion rate is $R_{tot} = k \sum_{n=c}<A_n>$ with the sum extending over all catalytic cells. Below we consider only the case of all cells catalytic (c). Then, the lowest-order equations in the hierarchy are [14,15]

$$d/dt <A_n> = -k <A_n> - \nabla J_A^{n>n+1},$$

$$d/dt <B_n> = +k <A_n> - \nabla J_B^{n>n+1}, \text{ for } 1<n<L. \qquad (1)$$

Separate equations for terminal cells reflect adsorption-desorption boundary conditions (BC's), e.g., $d/dt <A_1> = h(<A_{out}><E_1> - <E_{out}><A_1>) - k<A_1> - J_A^{1>2}$. In (1), we have defined the discrete derivative, $\nabla K_n = K_n - K_{n-1}$. The *net flux*, $J_A^{n>n+1}$, of A from site n to n+1 is given by

$$J_A^{n>n+1} = h[<A_nE_{n+1}> - <E_nA_{n+1}>] + h_{ex}[<A_nB_{n+1}> - <B_nA_{n+1}>]. \qquad (2)$$

The first term gives the contribution from hopping to adjacent empty cells, and the second from exchange. The expression for the net flux, $J_B^{n>n+1}$, of B is analogous. In the special case of unhindered transport where P_{ex} =1 so h_{ex} = h, (2) reduces exactly to $J_A^{n>n+1} = -h \nabla \langle A_n \rangle$ [15,21].

Equations (1) couple to pair probabilities in (2). Pair probability evolution couples to that of triples, etc., producing a hierarchy. Multisite probabilities are not simply related to single-cell probabilities due to spatial correlations. The lowest-order site-approximation, $\langle C_n E_{n+1} \rangle \approx \langle C_n \rangle \langle E_{n+1} \rangle$, etc., produces a closed set of discrete reaction-diffusion equations (RDE) for single-cell concentrations. A pair approximation factorizes triples in terms of pair and single-cell quantities generating a closed set of equations for these [13-15]. The triplet approximation factorizes quartets in terms of triplets, etc. [22]. However, these and all higher-order mean-field (MF) like truncation approximations suffer fundamental shortcomings. While accuracy increases with the order of the approximation, convergence to exact behavior can be slow. See Fig.2(a).

An alternative coarse-grained description considers concentrations per unit length, $C(x=na, t) \approx a^{-1} \langle C_n \rangle$, for C = A or B, smoothly varying with position x, which satisfy the continuum RDE

$$\partial/\partial t\, A(x, t) = -k\, A(x, t) - \partial/\partial x\, J_A, \qquad \partial/\partial t\, B(x, t) = +k\, A(x, t) - \partial/\partial x\, J_B. \qquad (3)$$

BC's for (3) at the pore ends reflect the adsorption-desorption dynamics [15]. Description of the diffusion fluxes, J_A and J_B, is critical. Setting $X(x,t)=A(x,t)+B(x,t)$, we exploit a little-used result from interacting particle systems theory for mixtures of particles with identical dynamics [23]

$$J_A = -D(A/X)\partial X/\partial x - D_{tr}[(B/X)\partial A/\partial x - (A/X)\partial B/\partial x]$$

$$\rightarrow -D_{tr}\,\partial A/\partial x \text{ for uniform } X=a^{-1}\chi, \qquad (4)$$

The form of J_B is analogous. Here $D = a^2h$ is the chemical diffusion coefficient for particles X, and $D_{tr} = D\,F_{tr}$ is a tracer diffusion coefficient. The site-approximation described above implies the mean-field form $F_{tr} = 1 - \chi$ [14,15] after simple coarse-graining of the discrete RDE. This choice overestimates fluxes for SFD. A classic analysis of SFD for infinite systems [1] finds that $F_{tr} = 0$. The associated "hydrodynamic" RDE can describe the evolution of slowly varying profiles during filling of long pores [15]. However, this formulation which sets the diffusion fluxes to zero and neglects fluctuations near pore openings completely fails to describe steady-state profiles [15] as show in Fig.2 (a). A refined treatment setting $F_{tr} \sim 1/L$, motivated by studies of finite-sized SFD systems [3,4,6,7], does not resolve this basic shortcoming.

Thus, our strategy is to develop a "generalized hydrodynamic" form for F_{tr} which captures the mesoscale fluctuations near pore openings being enhanced in these regions. A discrete form of (4) incorporating this F_{tr} then provides fluxes in (1) which are integrated to determine steady-state behavior. One strategy to determine this $F_{tr}(n)$ at cell n [24] for a pore with uniform $<X_n>=\chi$ is based analysis of the "exit time", $t_n(\chi)$, for a tagged particle starting at this cell to reach a pore opening in the sense that its root-mean-square (rms) displacement grows to match the distance from the nearest pore opening. Specifically, we set $F_{tr}(n) = t_n(0+)/t_n(\chi)$ since diffusivity is inversely proportional to the time for the rms displacement to reach some specified value. This recovers the correct limiting value $F_{tr}(n)\rightarrow 1$ as $\chi\rightarrow 0+$. Results for $F_{tr}(n)$ in Fig.3 (a) for

SFD in finite pores reveal a central plateau of magnitude ~1/L (consistent with [3-7]), but with significantly larger values near pore openings. Use of this variable $F_{tr}(n)$ in appropriate RDE to determine steady-state profiles yields excellent agreement with precise results from KMC simulation for SFD with L=100, in marked contrast to other treatments. See Fig.4 for profiles with $<B_{out}> \approx 0$ (the initial stages of the reaction), and results in Table I for the penetration depth L_p, naturally defined as $L_p = \sum_{1\le n\le L/2} <A_n>/<A_1>$.

Next, we turn to the fundamental issue of the form of the concentration profiles and the scaling of the penetration depth L_p for SFD in a semi-infinite pore with $1\le n<\infty$. Clearly now $F_{tr}(n)\to 0$, as $n\to\infty$, but how? Deep inside the pore where classic SFD should apply, the rms displacement increases like $t^{1/4}$ [1], so one expects that $t_n(\chi>0) \sim n^4$. In contrast, $t_n(0+) \sim n^2$ for conventional diffusion. This suggests that $F_{tr}(n) \sim 1/n^2$ as $n\to\infty$. Simulation results indicate that this behavior is achieved quickly for high total concentration χ=0.8, but more slowly for low χ=0.2 which displays an intermediate regime better described by $F_{tr}(n) \sim 1/n$ scaling. Data in both cases is fit well for all n by the form $F_{tr}(n) = F_{tr}(1)(1-\alpha+\beta+\gamma)/(1-\alpha\cdot n^{1/2}+\beta\cdot n+\gamma\cdot n^2)$. See Fig.3 (b).

Insight into the consequences of this decay of $F_{tr}(n)$ comes from analysis of the steady-state solutions of the continuum RDE for a semi-infinite pore $x\ge 0$ using (4) with the form $F_{tr}(x) \sim 1/x^p$. One finds solutions which for small k and large L_p have the dominant form

$$A(x) \sim \exp[-(x/L_p)^q] \text{ where } q=(2+p)/2,$$
$$\text{and } L_p \sim (k/D)^{\zeta} \text{ with } \zeta = -1/(2+p). \qquad (5)$$

Thus, the true asymptotic scaling exponent is $\zeta = -1/4$ (p=2), but behavior mimicking $\zeta \approx -1/3$ (p=1) might be seen for lower χ, both contrasting MF behavior $\zeta = -1/2$ (p=0) [14,15]. These predictions are confirmed by numerical analysis of discrete generalized hydrodynamic RDE's exploiting the capability of this deterministic treatment to obtain much more precise ζ-values than possible by KMC. See Fig.5. Concentration profiles also exhibit the predicted non-exponential decay, a feature which is already indicated in the nonlinear form of the log-linear plots in Fig.4 (the downward bend corresponding to an effective exponent q>1 due to p>0).

We now mention various extensions of the above analysis. All results were presented for initial stages of reaction where $<B_{out}> \approx 0$. However, analysis is readily extended to treat arbitrary fraction of conversion $f = <B_{out}>/<X_{out}>$ and we find an exact linear variation with f of the total conversion rate $R_{tot}(f) = R_{tot}(0)(1-f)$ by virtue of the linearity of the RDE's and BC's. Dropping the SFD constraint, we have also analyzed $F_{tr}(n)$ which still decreases with increasing n but now retains a substantial nonzero L-independent value in the pore center corresponding to tracer diffusion with exchange in an infinite pore. The corresponding generalized hydrodynamic treatment readily recovers behavior shown in Fig.2 (b). The greatest challenge in developing a predictive analytic treatment is for complete or near SFD, as other cases have more MF-like behavior. One can also readily extend the analysis to treat reversible reaction $A \leftrightarrow B$ using the same $F_{tr}(n)$ as determined above.

Finally, we consider more general diffusional dynamics with unequal coefficients, D_A and D_B, for A and B, respectively. Analysis for SFD reveals behavior

entirely analogous to the case of equal hop rates with penetration of reactant into the pore, but the pore center populated only by product. Again, MF treatments overestimate diffusion fluxes and fail to describe steady-state behavior. The key is to describe chemical diffusion for the mixed system (cf. [19,25]). We apply Onsager theory to determine the hydrodynamic form (corresponding to zero tracer diffusion) of $J_A = -A(A/ D_A+B/ D_B)^{-1}\partial X/\partial x$ for SFD, and J_B is analogous. Since the total flux, $J_{X=} J_{A+} J_B$, must vanish in the steady-state, this implies that X is constant, so J_A vanishes which in turn implies that A must be absent from the pore interior due to conversion to B. This failure of the hydrodynamic description to describe reactant penetration must again be overcome by accounting for fluctuation effects at the pore openings.

In summary, the location dependence of tracer diffusion near the openings of narrow pores is shown to control non-MF scaling of reactant penetration depth and thus reactivity for conversion reactions. Generalized hydrodynamic RDE's provide a powerful tool with which to analyze this behavior.

This work is supported by the U.S. Department of Energy, Office of Basic Energy Sciences, Division of Chemical Sciences, Geosciences, and Biosciences through the Ames Laboratory. The Ames Laboratory is operated for the U.S. Department of Energy by Iowa State University under Contract No. DE-AC02-07CH11358.

Note added in proof.—Recently, Dr. P.H. Nelson alerted us to [26], which also performs the same type of alternative analysis of D_{tr} as described in [24].

References

[1] T.E. Harris, J. Appl. Prob. 2, 323 (1965).
[2] M. Kollman Phys. Rev. Lett. 90, 180602 (2003).
[3] A.L. Hodgkin and R.D. Keynes, J. Physiol. 128, 61 (1955).
[4] E.J. Harris, "Transport and accumulation in biological systems" (AP, New York, 1960).
[5] J.E. Santos and G.M. Schutz, Phys. Rev. E 64, 036107 (2001).
[6] H. van Beijeren, K.W. Kehr, and R. Kutner, Phys. Rev. B 28, 5711 (1983).
[7] A. Taloni and F. Marchesoni, Phys. Rev. E 74, 051119 (2006).
[8] L. Lizana and T. Ambjornsson, Phys. Rev. Lett. 100, 200601 (2008).
[9] E. Barkai and R. Silbey, Phys. Rev. Lett. 102, 050602 (2009).
[10] "Catalysis and adsorption in zeolites", G. Ohlman, H. Pfeifer, G. Fricke, Ed.s (Elsevier, Amsterdam, 1991).
[11] J.G. Tsikoyiannis and J.E. Wei, Chem. Eng. Sci 46, 233 (1991).
[12] C. Rodenbeck, J. Karger, and K. Hahn, J. Catal. 157, 656 (1995).
[13] M.S. Okino, R.Q. Snurr, H.H. Kung, J.E. Ochs, and M.L. Mavrovouniotis, J. Chem. Phys. 111, 2210 (1999).
[14] S.V. Nedea, A.P.J. Jansen, J.J. Lukkien, and P.A.J. Hilbers, Phys. Rev. E 65, 066701 (2002)
[15] D.M. Ackerman, J. Wang, J.H. Wendel, D.-J. Liu, M. Pruski, and J.W. Evans, J. Chem. Phys. 134, 114107 (2011).
[16] R. Krishna, J. Phys. Chem. C 113, 19765 (2009).
[17] G. Nicolis and I. Prigogine, "Self-organization in non-equilibrium systems" (Wiley, New York, 1977).
[18] J. Marro and R. Dickman, "Non-equilibrium Phase Transitions in Lattice-Gas Models" (CUP, Cambridge, 1999).
[19] J.W. Evans, D.-J. Liu, and M. Tammaro, Chaos 12, 131 (2002).
[20] H. Spohn, "Large scale dynamics of interacting particles" (Springer, Berlin, 1991).
[21] R. Kutner, Phys. Lett. 81A, 239 (1981).
[22] J.W. Evans, Rev. Mod. Phys. 75, 1281 (1993).
[23] J. Quastel, Commun. Pure Appl. Math. 45, 623 (1992).
[24] We have implemented an alternative strategy obtaining consistent results for $F_{tr}(n)$ by creating steady-states with varying $\langle A_n \rangle$, but constant $\langle X_n \rangle = \chi$, and obtaining varying D_{tr} from simulation results for a discrete version of the ratio $-J_A/\partial A/\partial x$.
[25] K.W. Kehr, K. Binder, and S.M. Reulein, Phys. Rev. B 39, 4891 (1989).
[26] P. H. Nelson and S. M. Auerbach, Chem. Eng. J. 74, 43 (1999).

Tables

Table I. Comparison of reactant penetration depths, L_p (in units of 'a'), with h=1 and L=100, for KMC, generalized hydrodynamic (GHydro) and mean-field site-approximation (MF) analyses.

χ=0.2	k=1	k=0.1	k=0.01	k=0.001	χ=0.8	k=1	k=0.1	k=0.01	k=0.001
KMC	1.47	2.92	6.77	15.2	KMC	1.10	1.47	2.64	5.21
GHydro	1.49	3.10	7.19	15.8	GHydro	1.06	1.43	2.61	5.15
MF	1.53	3.37	9.46	27.8	MF	1.17	2.00	5.00	14.7

Figures

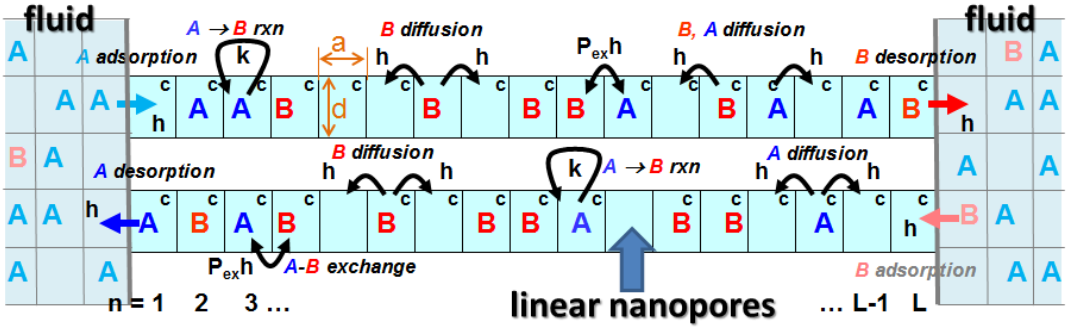

Fig.1 (Color online). Schematic of the key steps in our A→B catalytic conversion reaction model. "c" denotes catalytic cells where reaction occurs at rate k. Behavior is shown in two adjacent pores which should be regarded as part of a larger array of pores.

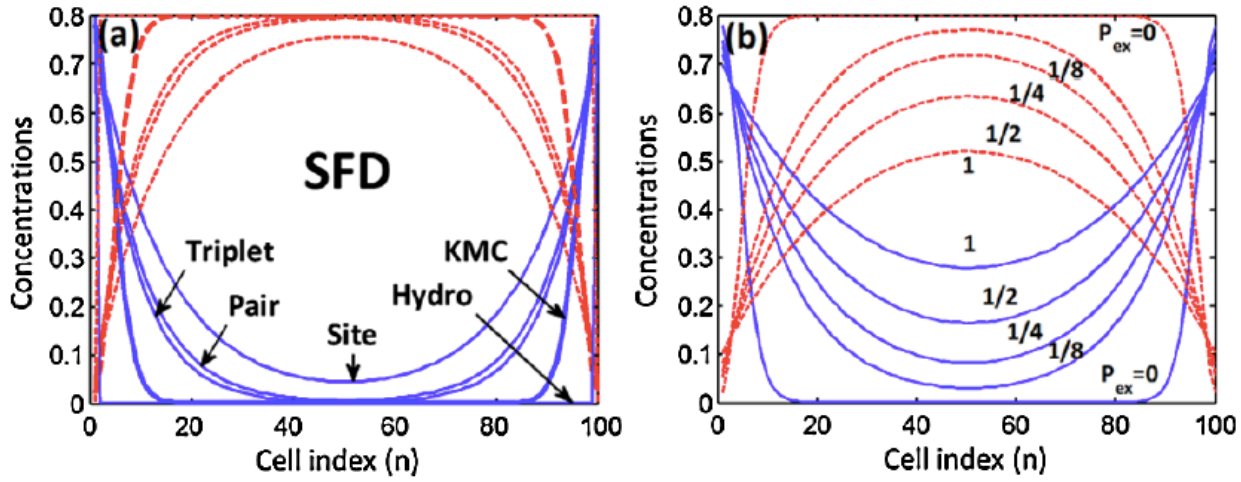

Fig.2 (Color online). Steady-state concentration profiles (A=solid, blue; B=red, dashed) for pore length L=100, k= 0.001, h=1, and χ=0.8: (a) predictions of site, pair, triplet approximations and the standard hydrodynamic treatment (hydro) versus precise KMC results for SFD (P_{ex}=0); (b) KMC results for restricted passing with various $P_{ex}\geq 0$.

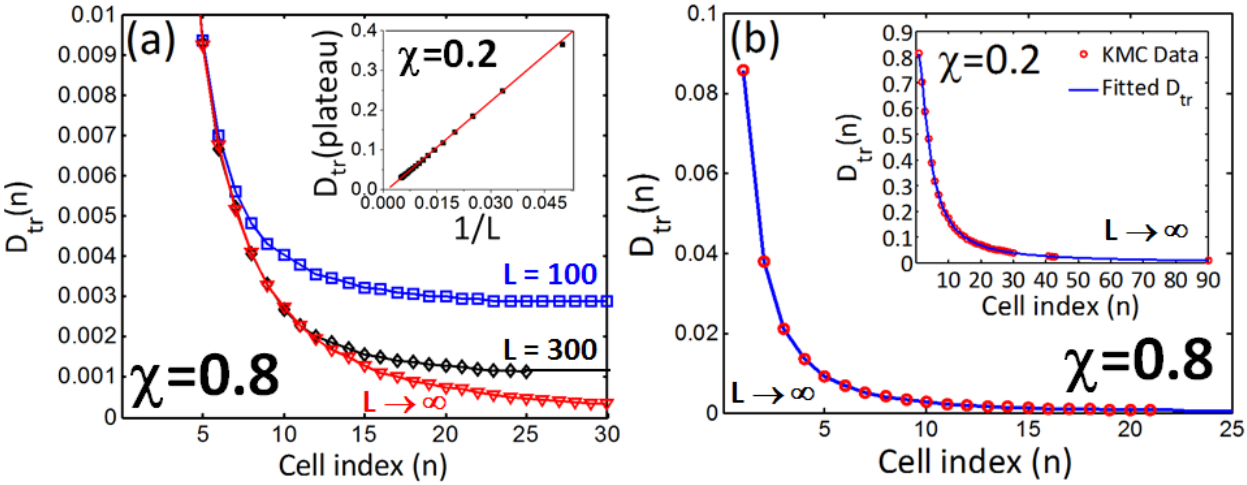

Fig.3 (Color online). KMC results for $D_{tr}(n) = F_{tr}(n)$ for a=h=1: (a) n-dependence for various pore lengths L for χ=0.8 (inset shows L-dependence of central plateau value of D_{tr} for χ=0.2); (b) fitting of the decay of $D_{tr}(n)$ with n for semi-infinite pore. Using the form in text, we choose α=0, β=1.543, γ=0.944 for χ=0.8 (inset: α=0.753, β=0.371, γ=0.0064 for χ=0.2).

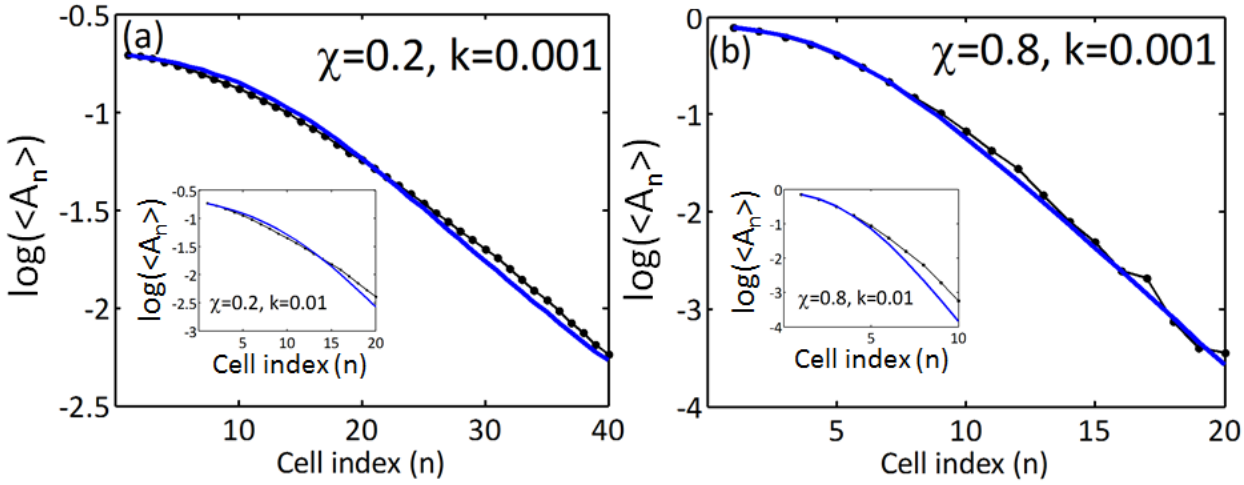

Fig.4 (Color online). Comparison of results for steady-state concentration values for L=100, k=0.001 (inset: k=0.01), and h=1 from KMC (symbols + line) with generalized hydrodynamic RDE predictions (thicker blue curves): (a) χ=0.2; (b) χ=0.8 (log is base 10).

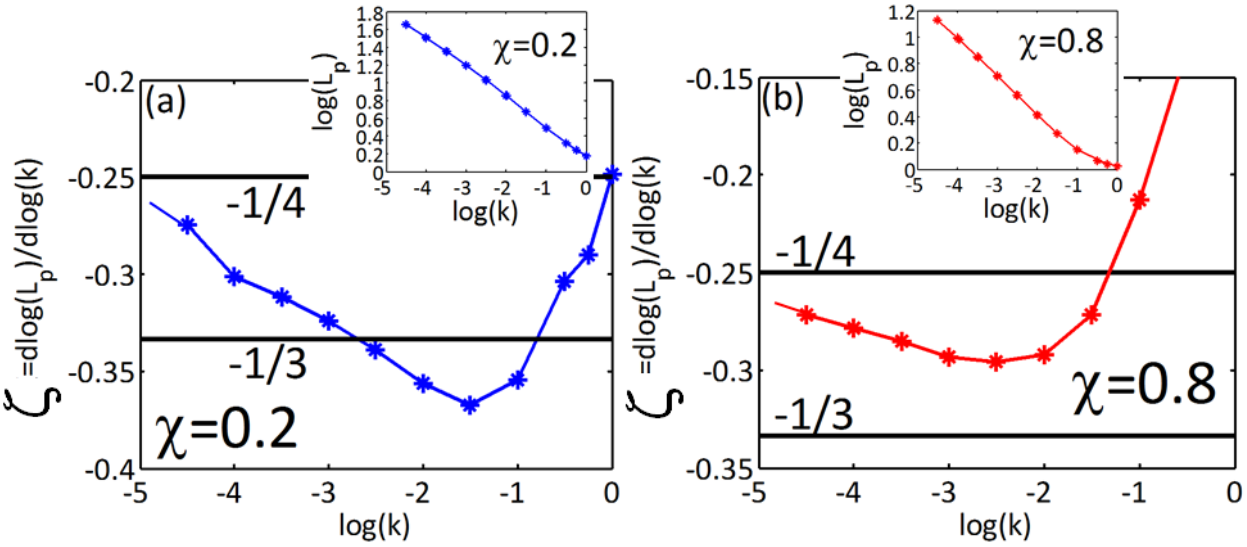

Fig.5 (Color online). Predictions of generalized hydrodynamic RDE for the effective scaling exponent $\zeta = d\log(L_p)/d\log(k)$ for a semi-infinite pore: (a) χ=0.2; (b) χ=0.8. Upper insets: L_p versus k.

CHAPTER 4. CONTROLLING REACTIVITY OF NANOPOROUS CATALYST MATERIALS BY TUNING REACTION PRODUCT-PORE INTERIOR INTERACTIONS: STATISTICAL MECHANICAL MODELING

A paper published in the Journal of Chemical Physics

Jing Wang[1,2], David M. Ackerman[1,3],Victor S.-Y. Lin[1,3,a)], Marek Pruski[1,3], and James W. Evans[1,2,4,]

[1]Ames Laboratory – USDOE, and Department of [2]Mathematics, [3]Chemistry,and [4]Physics and Astronomy, Iowa State University, Ames Iowa 50011, USA

[a)]Victor S.-Y. Lin, Professor of Chemistry and Director of the IPRT Center for Catalysis at Iowa State University, and Director of the Division of Chemical and Biological Sciences at Ames Laboratory – USDOE, passed away on May 4, 2010.

Abstract

Statistical mechanical modeling is performed of a catalytic conversion reaction within a functionalized nanoporous material to assess the effect of varying the reaction product – pore interior interaction from attractive to repulsive. A strong enhancement in reactivity is observed not just due to the shift in reaction equilibrium towards completion, but also due to enhanced transport within the pore resulting from reduced loading. The latter effect is strongest for highly restricted transport (single-file diffusion), and applies even for irreversible reactions. The analysis is performed utilizing a generalized hydrodynamic formulation of the reaction-diffusion equations which can reliably capture the complex interplay between reaction and restricted transport.

I. Introduction

Advances in synthesis of nanomaterials have led to broad capabilities for multifunctionalization of mesoporous or nanoporous catalysts. Such capabilities allow for not only effective functionalization with catalytic groups, but also the possibility to tune the interaction between reaction products and the interior pore environment [1-3]. This can in turn significantly impact and potentially enhance catalytic reactivity. For example, creation of an unfavorable environment for product species within pores can lead to enhanced product extrusion or inhibited product re-entry. This feature would shift the equilibrium of reversible reactions towards completion. Other possible scenarios are discussed below.

One class of examples of the above type is provided by dehydration reactions such as esterification (acid + alchohol $\leftrightarrow$ ester + water) in mesoporous silica nanoparticles (MSN). Multifunctionalization of MSN to include hydrophobic groups, as well as catalytic groups, has been observed to significantly enhance reactivity in several such systems [4-6]. This effect has been explained as a result of functionalization converting an intrinsically hydrophilic interior pore surface of MSN into a hydrophobic environment thereby "expelling" the product water and shifting the equilibrium of the reversible esterification reaction. The greatest enhancement to date has been achieved through solvent-mediated control of the configuration of hydrophobic 3-(pentafluorophenyl) propyl groups which are induced to lie prone on silica surface

thereby minimizing the interaction of the product water with the hydrophilic MSN surface groups [6,7].

In fact, there are several possible scenarios wherein functionalization to tune product-pore interactions can influence both the thermodynamics and the kinetics of transport and reaction, and thereby impact reactivity in meso- or nanoporous reaction systems. First, we discuss thermodynamic factors. Accounting for detailed balance requirements, it follows that creating an unfavorable environment for a reaction product within the pore increases the ratio of the rate of product desorption from the pore opening to that for product (re)adsorption. One should note that product readsorption can become significant for substantial conversion of reactant to product in the surrounding fluid. However, even constraining rates to satisfy detailed balance, there are still many distinct possibilities for rate behavior: (i) the product desorption rate could be tied to the rate of diffusion within the pore, and thus the rate of readsorption would be inhibited for stronger interior pore-product repulsion; (ii) the product readsorption rate could be tied to the rate of external diffusion, and thus the rate of desorption would be enhanced for stronger interior pore-product repulsion; (iii) more general cases where both rates change. Any of these cases will result in a shift of equilibrium for reversible reactions.

Second, we discuss other kinetic factors that can impact reactivity, but which are unrelated to shift of equilibrium for reversible reactions. Although not dictated by thermodynamic considerations, diffusive transport within the pore can also be modified by multifunctionalization. An unfavorable environment could enhance diffusion removing localized regions of strong binding and thereby “smoothing” interaction with

the pore walls. Another possible scenario is that modifying the interior pore environment can change loading of product in the pore even for irreversible reactions. The loading can have a dramatic effect on effective transport for narrow pores, especially in the single-file diffusion (SFD) regime where species cannot pass each other in the pore, and this in turn greatly impacts reactivity. To test this latter effect, we will naturally consider the special case of irreversible reactions.

Our focus in this contribution is on exploring the effects of multifunctionalization for simple first-order catalytic conversion reactions (A to B) in mesoporous or nanoporous materials such as MSN consisting of parallel arrays of effectively identical linear nanopores. A key factor impacting reactivity is the extent to which reactants and products A and B can pass each other. Previous analyses for SFD or restricted passing [8-15] reveal that reaction is strongly localized near the pore openings [9]. While simple mean-field type reaction-diffusion equations [8,11-13] are not adequate, recent studies have shown that behavior in this regime is captured by a "generalized hydrodynamic" (GH) formulation which accounts for both the effect of restricted passing on chemical diffusion as well as fluctuation effects in adsorption-desorption at pore openings [14]. Here, we adopt the latter rather than computationally more expensive Kinetic Monte Carlo (KMC) simulation which could also provide a precise characterization of model behavior.

In Sec. II, we describe our model for conversion reaction in linear nanopores, the associated exact master equations, and associated generalized hydrodynamic reaction-diffusion equations (RDE). In Sec.III, we present results for both irreversible and

reversible conversion reactions focusing on reactivity (i.e., turn-over frequency) per pore as a function of the fraction of reactant converted to product, and contrasting behavior for pores where product entry in enhanced versus inhibited. Our conclusions are presented in Sec.IV.

II. Spatially-discrete model for catalytic conversion inside linear nanopores

A. Spatially discrete stochastic reaction-diffusion model prescription

Our model for catalytic conversion describes nanoporous materials which consist of a parallel array of linear pores by partitioning the continuous-space pores into adjacent cells labeled n = 1 to L [8-14]. The cell width "a" is selected to be comparable to the species size ~1 nm. Species within pores are regarded as localized to specific cells, and diffusive transport is treated as hopping or exchange between adjacent cells. To describe the surrounding fluid, we extend the 1D lattice of cells inside the pores to a 3D lattice outside. See Fig. 1. We specify "external" reactant and product concentrations in the surrounding fluid at each stage of the reaction as $\langle A_{out} \rangle$ and $\langle B_{out} \rangle$, for a fixed total concentration $\langle X_{out} \rangle = \langle A_{out} \rangle + \langle B_{out} \rangle$. These correspond to the probabilities that sites or cells on the 3D lattice are occupied by various species, where fluid cell occupation is assumed random due to efficient stirring. Then, $\langle A_{out} \rangle$ will decrease from an initial value of $\langle X_{out} \rangle$, and $\langle B_{out} \rangle$ will increase from zero with increasing fraction, $F = \langle B_{out} \rangle / \langle X_{out} \rangle$ ($= 1 - \langle A_{out} \rangle / \langle X_{out} \rangle$), of the initial reactant converted to product [14,15].

Following most previous stochastic modeling of reaction-diffusion processes in linear nanopores [8-15], the simplest prescription for diffusion dynamics within the

pores is that A and B hop to adjacent empty (E) sites at rate h, corresponding to a diffusion rate of $D_0 = a^2h$ for isolated particles. This simple prescription would correspond to single-file diffusion with a strict no-passing constraint. For a more general treatment of diffusional dynamics, we also allow positional exchange of adjacent A and B at rate P_{ex} h, thereby relaxing the strict single-file constraint. (Note that exchange of adjacent particles of the same type has no effect.) The passing propensity, P_{ex}, will increase with the effective pore diameter, d, from $P_{ex} = 0$ for d below a threshold for SFD, to $P_{ex} = 1$ for large d and unhindered passing.

In addition to hopping or exchange within the pore, the other mechanistic steps in the model (see Fig. 1) are as follows: (i) Adsorption of external reactant A (product B) to terminal pore sites n=1 and n=L at rate h (αh), provided that these end sites are unoccupied or empty (E). We emphasize that the factor α will account for the effects of multifunctionalization modifying the interior pore-reaction product interaction. (ii) Desorption of both the reactant, A, and product, B, from terminal sites of the pore at rate h provided that the fluid site just outside the pore is unoccupied (E_{out}). The probability for this fluid site to be unoccupied is given by $\langle E_{out} \rangle = 1 - \langle X_{out} \rangle$. (iii) Conversion A $\rightarrow$ B at catalytic (c) sites within the pore at rate k, as well as the reverse reaction B$\rightarrow$A at rate k′. Our model can treat general distributions of catalytic sites, but here we shall assume that all sites are catalytic. (iv) One could also consider exchange in and out of the pore. One choice is to ignore such processes. Another plausibly more realistic choice is to specify that A (B) just outside exchanges with B (A) inside at n = 1 or L at rate P_{ex}h (αP_{ex}h). Both choices (and others) are consistent with detailed balance. We expect that

the choice will not greatly effect of reactivity (except in the special regime of both high P_{ex} and high loading).

It should be emphasized that there is a natural "separation of time scales" for "local" relaxation (in time) of concentration profiles within the pore, and for "global" equilibration of the entire system including the fluid. Relaxation of concentration profiles to a local steady state form determined by the current values of $<A_{out}>$ and $<B_{out}>$ should be effectively instantaneous on the time scale of global equilibration of the entire system (which in experiments is on the order of hours). Thus, the main challenge is to solve the non-trivial statistical mechanical local steady-state problem to determine reactant and product concentration profiles, and thus the reactivity, as a function of the fractional conversion, $F=<B_{out}>/<X_{out}>$, of reactant to product. It should also be noted that the global equilibrium values of $<A_{out}>$ and $<B_{out}>$, and thus of $F = F_{eq}$, are determined not just by the equilibrium constant $K_c = k/k'$ for the conversion reaction within the pores, but also by the parameter α. This issue is addressed immediately below.

For the above model, it is clear that the "color-blind" dynamics for particles X = A+B (i.e., A or B) is described by a non-reactive diffusion process where particles hop within the pore and desorb at rate h. At a specified fractional conversion, F, particles adsorb at an effective rate $h_{ads} = h_{ads}(F) = e_{ads}(F)\, h$ with $e_{ads} = e_{ads}(F) = (1-F) + \alpha F$, where the first (second) term is the weighted contribution from A (B) adsorption. In the local steady state for fixed F, all sites within the pore are randomly occupied by particles, X,

with equal probability $\langle X_{in}\rangle = \langle X_{in}(F)\rangle$, say. Then, balancing the adsorption flux, J_{ads}, and desorption flux, J_{des}, for particles X where

$$J_{ads} = h_{ads}(F)\langle X_{out}\rangle(1-\langle X_{in}\rangle) \text{ and } J_{des} = h(1-\langle X_{out}\rangle)\langle X_{in}\rangle \text{ yields} \quad (1)$$

$$\langle X_{in}\rangle = e_{ads}\langle X_{out}\rangle/[1+(e_{ads}-1)\langle X_{out}\rangle]$$

$$= [1+(\alpha-1)F]\langle X_{out}\rangle/[1 + (\alpha-1)F\langle X_{out}\rangle]. \quad (2)$$

We recall that $\langle X_{out}\rangle$ remains constant at its initial value. As expected, (2) demonstrates that $\langle X_{in}\rangle$ exceeds $\langle X_{out}\rangle$ for $\alpha>1$ (enhanced product reentry), and that $\langle X_{out}\rangle$ exceeds $\langle X_{in}\rangle$ for $\alpha<1$ (inhibited reentry).

A simple analysis of individual species concentrations in the local steady state is not possible since these concentrations exhibit non-trivial spatial profiles within the pore. However, in the final global equilibrium state, concentrations of both species within the pore, $\langle A_{in}\rangle_{eq}$ and $\langle B_{in}\rangle_{eq}$, are spatially uniform, and satisfy $\langle B_{in}\rangle_{eq}/\langle A_{in}\rangle_{eq} = K_c$. Then, separately balancing the adsorption and desorption fluxes for species A and for species B yields

$$\langle A_{out}\rangle_{eq}(1-\langle X_{in}\rangle_{eq}) = \langle A_{in}\rangle_{eq}(1-\langle X_{out}\rangle) \text{ and}$$

$$\alpha\langle B_{out}\rangle_{eq}(1-\langle X_{in}\rangle_{eq}) = \langle B_{in}\rangle_{eq}(1-\langle X_{out}\rangle), \quad (3)$$

so that

$$\langle B_{out}\rangle_{eq}/\langle A_{out}\rangle_{eq} = \alpha^{-1}\langle B_{in}\rangle_{eq}/\langle A_{in}\rangle_{eq} = K_c/\alpha, \text{ and}$$

$$F_{eq} = K_c/(K_c + \alpha). \quad (4)$$

The latter result characterizes the shift in equilibrium for our model associated with tuning of the reaction product-pore interior interaction via multifunctionalization.

We thus find that $<X_{in}>$ changes from its initial value of $<X_{out}>$ at the onset of the reaction (F=0) to

$$<X_{in}>_{eq} = \alpha(1+K_c)<X_{out}>/[\alpha(1+K_c<X_{out}>)+K_c(1-<X_{out}>)], \qquad (5)$$

when $F=F_{eq}$, at completion of the reaction. This result (5) recovers the requirement that $<X_{in}>_{eq} =0$ for blocked product reentry $\alpha=0$. It also shows that for enhanced reentry with, e.g., $\alpha=5$ and $<X_{out}>=0.8$ (the case considered below), one has $<X_{in}>_{eq}/<X_{out}> = (1+K_c)/(1+0.84K_c) >1$.

B. Exact master equations and discrete reaction-diffusion equations

An exact description of our discrete reaction-diffusion model is provided by the master equations for the evolution of probabilities of various configurations within the pore. Often these are written in hierarchical form [8,11-15]. Here, we use $<C_n>$ to denote the probability or ensemble averaged concentration for species C = A or B at site n (or for this site to be empty when C = E), $<C_nE_{n+1}>$ for the probability that C is at site n and for site n+1 to be empty (E), etc. Then, the lowest-order equations in the hierarchy describe the evolution of single-site occupancies.

For A to B conversion in the case where all sites are catalytic, one has that

$$d/dt <A_n> = -k<A_n> + k'<B_n> - \nabla J_A^{n>n+1} \text{ and} \qquad (6a)$$

$$d/dt <B_n> = +k<A_n> -k'<B_n> - \nabla J_B^{n>n+1} \text{ for } 1<n<L, \qquad (6b)$$

where we have defined the discrete derivative, $\nabla G_n = G_n - G_{n-1}$. The *net* diffusion flux, $J_A^{n>n+1}$, of A from site n to n+1 due to both hopping and exchange is given by

$$J_A^{n>n+1} = h\,[<A_nE_{n+1}> - <E_nA_{n+1}>] + P_{ex}\,h\,[<A_nB_{n+1}> - <B_nA_{n+1}>]. \qquad (7)$$

The expression for the net flux, $J_B^{n>n+1}$, of B is analogous. Separate equations for terminal sites reflect adsorption-desorption boundary conditions (BC's). In the presence of in-out exchange with rates as specified in Sec. IIA, one has that

$$d/dt \langle A_1\rangle = h\langle A_{out}\rangle \langle E_1\rangle - h\langle E_{out}\rangle \langle A_1\rangle + P_{ex}\, h \langle A_{out}\rangle\langle B_1\rangle$$
$$- P_{ex}\, \alpha h \langle B_{out}\rangle\langle A_1\rangle - k\langle A_1\rangle + k'\langle B_1\rangle - J_A^{1>2}, \text{ and} \quad (8a)$$

$$d/dt \langle B_1\rangle = \alpha h\langle B_{out}\rangle \langle E_1\rangle - h\langle E_{out}\rangle \langle B_1\rangle + P_{ex}\, \alpha h \langle B_{out}\rangle\langle A_1\rangle$$
$$- P_{ex}\, h \langle A_{out}\rangle\langle B_1\rangle + k\langle A_1\rangle - k'\langle B_1\rangle - J_B^{1>2}, \quad (8b)$$

with analogous equations for concentrations at site n=L. If some sites are not catalytic, then the reaction terms are absent for such sites. Defining $\langle \Delta A_n\rangle = \langle A_n\rangle - K_c^{-1}\langle B_n\rangle$ as the "excess" reactant concentration, the net overall rate of production of B per pore is given by

$$R^B_{rxn} = \sum_{n=c} (k\langle A_n\rangle - k'\langle B_n\rangle) = k \sum_{n=c} \langle \Delta A_n\rangle \quad (9)$$

summing over all catalytic sites, c.

Equations (6a) and (6b) couple to various pair probabilities in (7). Pair probability evolution is coupled to triples, etc., producing a hierarchy. Pair and multisite probabilities are not simply related to single-site probabilities due to spatial correlations. A simple mean-field (MF) factorization approximation, $\langle C_n E_{n+1}\rangle \approx \langle C_n\rangle\langle E_{n+1}\rangle$, etc., produces a closed set of discrete reaction-diffusion equations (RDE) for single-site concentrations. However, this approximation, and even higher-order pair, triplet, etc., approximations, fundamentally fail to capture model behavior, at least for low reactivity $k/h \ll 1$ when $P_{ex} \ll 1$ [13-15]. Thus, below we discuss an alternative "generalized hydrodynamic" approach which does reliably describe model behavior. As an aside, in

the special case P_{ex} =1 (unhindered passing of A and B), (7) reduces exactly to $J_A^{n>n+1}$ = h [$<A_n>$ - $<A_{n+1}>$] = -h ∇ $<A_n>$, and similarly for $J_B^{n>n+1}$ [14-16]. This yields an exact set of discrete RDE matching the MF approximation.

C. Generalized hydrodynamic reaction-diffusion equations

For smoothly varying concentrations within the pore, it is natural to consider a coarse-grained description of the spatially-discrete reaction-diffusion model which regards the species concentrations per unit length, $C(x=na) \approx a^{-1} <C_n>$, as functions of a continuous spatial variable x (leaving the t-dependence implicit), and denote the total concentration by $X(x) = A(x) + B(x)$. The continuum RDE for our A to B conversion reaction model with all sites catalytic then have the form

$$\partial/\partial t\, A(x) = -k\, A(x) + k'\, B(x) - \partial/\partial x\, J_A, \text{ and}$$

$$\partial/\partial t\, B(x) = +k\, A(x) - k'\, B(x) - \partial/\partial x\, J_B. \qquad (10)$$

If only portions of the pore are catalytic, then reaction terms appear just for those locations. BC's for (10) at the pore ends reflect the adsorption-desorption dynamics, i.e., one balances the diffusion fluxes at the end of the pore with the net adsorption-desorption rate for each species. Description of the diffusion fluxes, J_A and J_B, is non-trivial.

Analysis from the theory of interacting particle systems [17,18] for the hydrodynamic regime of slowly varying concentrations suggests the general form [13,14,17,18]

$$J_A = -D_0[1- X^{-1}(1-F_{tr})B]\, \partial A/\partial x - D_0\, X^{-1}(1-F_{tr})A\, \partial B/\partial x. \qquad (11)$$

In this expression, one has $D_0 = a^2h$ and F_{tr} is related to a tracer diffusion coefficient for particles within the pore by $D_{tr} = D_0F_{tr}$. In applying the form (11), we utilize the feature that the diffusive dynamics for both A and B within the pore is identical. An analogous expression applies for J_B. Here, it suffices to consider the local steady-state regime with uniform total concentration, $X = <X_{in}> = <X_{in}(F)>$, corresponding to a counter-diffusion mode [19] where $\partial A/\partial x = -\partial B/\partial x$. Then, (11) and the analogous expression for J_B simply reduce to [13,19]

$$J_A = -D_{tr}\, \partial A/\partial x \text{ and } J_B = -D_{tr}\, \partial B/\partial x. \qquad (12)$$

In the MF treatment, $X^{-1}(1-F_{tr})$ in (11) is replaced by $1-P_{ex}$ which corresponds to the assignment $F_{tr} = F_{tr}(MF) = 1- (1-P_{ex})X$. However, this MF choice overestimates diffusion fluxes within the pore, and thus overestimates overall reactivity, especially for the quasi-SFD regime, $P_{ex}<<1$ and $F_{tr}(MF) \approx 1 - X$ [12,13]. A contrasting deterministic hydrodynamic (DH) formulation of F_{tr}, applicable for large systems (very long pores) with slowly varying concentrations and negligible fluctuation effects, follows from a precise analysis of tracer diffusion for effectively infinite systems. One finds that the corresponding $F_{tr} = F_{tr}(DH) = F_{tr}(X, P_{ex})$ has the form shown in Fig.2. Simple limiting behavior includes:

$$F_{tr}(DH) \to 1, \text{ as } P_{ex} \to 1;\ F_{tr}(DH) \to P_{ex}, \text{ as } X \to 1; \text{ and}$$

$$F_{tr}(DH) \to 0, \text{ as } P_{ex} \to 0 \text{ (for } X>0). \qquad (13)$$

The latter behavior for $P_{ex} =0$ is in marked contrast to the MF form, and reflects the anomalous nature of SFD wherein the mean-square displacement of a tagged particle increases sub-linearly [20]. To account for the finite length of pores, we have considered

a refinement of the DH choice where $F_{tr} \sim 1/L$ for SFD when $P_{ex} = 0$ [21]. This modified choice was motivated by analyses of transport through channels across membranes of finite width [22]. However, choosing either $F_{tr} = 0$ or $F_{tr} \sim 1/L$ for SFD underestimates diffusion fluxes at least near pore openings, and thus underestimates underestimates the overall reactivity [21].

To address the shortcomings of the MF and DH approaches described above, we will utilize a generalized hydrodynamic (GH) treatment [23] which incorporates a position-dependent $F_{tr}(x=na) = F_{tr}(GH)$. This $F_{tr}(x=na)$ is enhanced near pore openings above the deterministic hydrodynamic value of $F_{tr}(DH)$ [14]. This enhancement of $F_{tr}(DH)$ reflects the influence of stochastic adsorption-desorption processes which facilitate transport in and out of the pore near these pore openings [14]. Results are shown in Fig.3 where $F_{tr}(x)$ approaches $F_{tr}(DH)$ for x or n corresponding to the central region of the pore. The algorithm which we use to determine this location-dependent $F_{tr}(GH)$ is described in Ref. [14] and also in the Appendix. Roughly speaking, we set $F_{tr}(x=na) = t_0(x=na)/ t_X(x=na)$ where t_X is time for a tagged particle starting at a specific location, x=na, in a pore with concentration X of other particles to reach the closest pore opening. This choice is based on the classic result that diffusivity scales like the mean-square displacement divided by time. See Ref. [19] for an alternative formulation. Thus, it is immediately clear that $F_{tr}(x) \rightarrow 1$, as $X \rightarrow 0$ (as required). Introducing these variable $F_{tr}(x=na) = F_{tr}(n)$ into a discrete form of (10) and (11) [24] recovers almost exactly the results of precise KMC simulations of model behavior, but much more efficiently [14]. This formalism will be used to generate results in Secs. III A and III B.

III. Catalytic reaction kinetics: reactivity versus conversion

In this section, we present simulation results for the reactivity (i.e., the turn-over frequency) per pore as a function of fractional conversion of reactant to product. We also provide more detailed information on concentration profiles within the pores. In all cases below, we consider a pore of length L=100 a in which all cells are catalytic. The hop rate is set to unity h=1, which determines the time scale. The rate of the forward reaction A→B chosen as k=0.001. The initial reactant concentration, and thus the total concentration in the exterior fluid, is set to $<X_{out}> = 0.8$. This high $<X_{out}>$ results in a high loadings inside the pore, and thus strong SFD effects in the absence of exchange diffusion when $P_{ex} = 0$. We will consider and compare behavior for three cases: (i) significantly enhanced product reentry with $\alpha=5$ (mimicking hydrophilic pores for dehydration reactions); (ii) neutral product reentry with $\alpha=1$; (iii) blocked product reentry with $\alpha=0$ (mimicking strongly hydrophobic pores for dehydration reactions).

A. Irreversible reaction

For irreversible reaction, A→B, where k′=0, Fig.4(a) shows the local steady state concentration profiles for $<A_n>$ and $<B_n>$ versus n at the onset of the reaction (F=0) for various passing probabilities ranging from SFD ($P_{ex} = 0$) to completely unhindered passing ($P_{ex} = 1$). Behavior for F = 0 is independent of α due to the lack of product in the exterior fluid. Note the strongly enhanced penetration of reactant into the pore with increasing passing propensity, P_{ex}. This results in a strong increase in reactivity, R^B_{net}, as

discussed further below. Fig.4(b)-4(d) show the concentration profiles for A→B when F = 0.625 for α = 5, 1, and 0, respectively. Here the α-dependence on behavior is seen clearly not just in the increased values of $<X_{in}>$ for larger α, but also in the increased dominance of product over reactant within the pore.

Our main focus here is on a comprehensive characterization of the variation of reactivity during the "extended reaction". Of particular significance is our demonstration of a dramatic difference between behavior for enhanced versus blocked product reentry to the pore. In Fig.5, we show the reactivity, R^B_{rxn}, as a function of the fraction, F, of reactant outside the pore converted to product for the irreversible reaction A→B. The key observation is the contrasting strong decrease of R^B_{rxn} with increasing F for enhanced product reentry (α=5) versus the slow decrease of R^B_{tot} (or even an initial slight increase with P_{ex}=0) for blocked product reentry (α=0). Thus, blocking reentry greatly enhances the effective reactivity of the system. The neutral case where reentry is neither enhanced or inhibited (α=1) exhibits intermediate behavior with a linear decrease of $R^B_{rxn}(F) = (1-F)\, R^B_{rxn}(0)$ versus F, as explained below.

The enhanced reactivity upon converting from enhanced reentry (α>1) to blocked reentry (α=0) reflects the reduction in pore loading $<X_{in}>$. For example, when $<X_{out}>$ = 0.8 and F=1/2, one has $<X_{in}>$ = 0.92 for α=0 versus $<X_{in}>$ = 0.67 for α=5. Lower $<X_{in}>$ (or higher $<E_{in}>$) impacts the rate of adsorption of reactant A via hopping into the pores,

$$R_A^{ads}(hop) = h<A_{out}><E_{in}> = h<X_{out}><E_{out}>(1-F)/[1+(\alpha-1)F<X_{out}>] \,. \qquad (14)$$

Thus, R_A^{ads}(hop) increases with decreasing α, for F>0, which naturally boosts reactivity. Note, however, that the rate of exchange adsorption of reactant for $P_{ex}>0$ may decrease for lower $<X_{in}>$. More significantly, lower $<X_{in}>$ greatly increases the tracer diffusion coefficient F_{tr}(GH) which strongly increases penetration of reactant into the pore, and thus also boosts reactivity. This strong increase in reactivity in changing from enhanced to blocked product readsorption is purely kinetic in origin rather than thermodynamic (noting that the reaction is irreversible).

Finally, we provide some further comments on reaction kinetics. First, for the neutral case $\alpha=1$, we describe the origin of the linear decrease of $R^B_{net}(F) \propto (1-F)$ with F. This behavior is a consequence of two features. One is the homogeneous F-independent linear form of the steady-state master equations, $0 = -k<A_n> - \nabla J_A^{n>n+1}$, noting that $F_{tr}(GH) = F_{tr}(n)$ is independent of F when $\alpha=1$. The other relates to the feature that the BC terms for $<A_n>$ when n=1 or n=L adopt an inhomogeneous linear form with driving term proportional to 1-F [25]. This implies that all $<A_n> \propto (1-F)$ and thus one has $R^B_{rxn}(F) = (1-F)\, R^B_{rxn}(0)$. A detailed derivation of the analogous result for the more general reversible case is provided in Sec. III B.

Second, we note that if $\alpha\neq1$, R_A^{ads}(hop) in (14) exhibits a non-linear decrease with F, and also the position-dependent tracer diffusion coefficient adopts a non-trivial non-linear dependence of F. As a result, it is not possible to provide a simple analytic expression for the nonlinear dependence of $R^B_{rxn}(F)$ on F when $\alpha\neq1$.

Third, we emphasize that our results for the F-dependence of $R^B_{rxn}(F)$ encode complete information about the reaction kinetics through the equation

$$d/dt \langle A_{out} \rangle = \varepsilon R^B_{rxn}(F), \text{ where } F = 1 - \langle A_{out} \rangle / \langle X_{out} \rangle. \quad (15)$$

Here, the constant ε equals the number of pores in the system divided by the total number of 3D lattice sites associated with the fluid. Thus, for no product reentry $\alpha=0$ where $R^B_{rxn}(F) \approx R^B_{rxn}(0)$ is roughly independent of F (up to $F \approx ¾$), one has a sustained fast linear decrease in time t of $\langle A_{out} \rangle \approx \langle X_{out} \rangle [1 - \varepsilon R^B_{rxn}(0) \langle X_{out} \rangle^{-1} t]$. For $\alpha=1$ where $R^B_{rxn}(F) \propto (1-F)$, one has exponential decay $\langle A_{out} \rangle \approx \langle X_{out} \rangle \exp[-\varepsilon R^B_{rxn}(0) \langle X_{out} \rangle^{-1} t]$. For $\alpha>1$, one has slower decay. All cases exhibit the same α-independent initial decay rate.

B. Reversible reaction

Next, consider the reversible reaction, A↔B, with k=0.001 as above, but now $k'=0.0005$ is non-zero corresponding to a finite equilibrium constant $K_c = 2$. Fig.6(a) shows the local steady state concentration profiles for $\langle A_n \rangle$ and $\langle B_n \rangle$ versus n at the onset of the reaction (F=0) for various passing probabilities P_{ex}. Behavior for F = 0 is independent of α as for reversible reaction, and penetration of "excess" reactant, $\langle \Delta A_n \rangle = \langle A_n \rangle - K_c^{-1} \langle B_n \rangle$, into the pore is strongly enhanced with increasing passing propensity, P_{ex}. Fig.6(b)-6(d) show the concentration profiles for A↔B when $F/F_{eq} = 0.625$ for $\alpha = 5$, 1, and 0, respectively. Here, the reduction in excess reactant with increasing α is evident.

In Fig.7, we show the reactivity, R^B_{rxn}, versus F for the reversible reaction. The contrast between the strong decrease of R^B_{rxn} with increasing F for enhanced product

reentry (α=5) versus the slow decrease or even slight increase of R^B_{tot} for blocked product reentry (α=0) is even greater than for irreversible reaction. This is due to opposite shifts in the global equilibrium for enhanced versus blocked reentry. The neutral case (α=1) exhibits intermediate behavior with a linear decrease of $R^B_{rxn}(F) = (1-F/F_{eq})\, R^B_{rxn}(0)$ versus F, as explained below.

The enhanced reactivity upon converting from enhanced reentry (α>1) to blocked reentry (α=0) partly reflects kinetic effects due to the reduction in pore loading $<X_{in}>$. R_A^{ads}(hop) is still given by (14) and increases with decreasing α, thus boosting reactivity. More significant is that lower $<X_{in}>$ greatly increases the tracer diffusion coefficient F_{tr}(GH) which boosts reactant penetration of excess reactant and thus reactivity. However, a synergistic factor is the strong shift in equilibrium with varying α, noting that blocked reentry allows completion of the reversible reaction to F=1!

Finally, we provide some further comments on reaction kinetics. First, for the neutral case α=1, we describe the origin of the linear decrease $R^B_{net}(F) \propto (1-F/F_{eq})$ where $F_{eq} = K_c/(K_c+1)$. To this end, it is instructive to consider steady-state equations for $<\Delta A_n> = <A_n> - K_c^{-1}<B_n>$. Subtracting K_c^{-1} times (6b) from (6a) yields the homogeneous F-independent equations

$$0 = -k(1+K_c^{-1}) <\Delta A_n> - \nabla J_{\Delta A}^{n>n+1} \qquad (16)$$

where $J_{\Delta A}^{n>n+1} = -h\, F_{tr}\, \nabla(<\Delta A_n>)$.

For the BC at n=1, subtracting K_c^{-1} times (8b) from (8a) yields

$$0 = h<E_{out}> <\Delta A_{out}> - [h<E_{out}> + k(1+K_c^{-1})] <\Delta A_1>$$

$$+ (1+K_c^{-1})\, R_A^{ads\text{-}des}(ex) - J_{\Delta A}^{1>2}. \qquad (17)$$

where $<\Delta A_{out}> = <X_{out}>(1- F/F_{eq})$ and $R_A^{ads\text{-}des}(ex)$ denotes the net rate of exchange of reactant A into the pore at n=1. Using that $<A_1> + <B_1> = <X_{out}>$ for α=1, one can also write

$$(1+K_c^{-1})\, R_A^{ads\text{-}des}(ex) = P_{ex}\, h<X_{out}>^2(1- F/F_{eq}) - P_{ex}\, h<X_{out}><\Delta A_1>. \qquad (18)$$

Thus, the BC adopts an inhomogeneous linear form with driving term proportional to $1-F/F_{eq}$. This implies that all $<\Delta A_n> \propto (1-F/F_{eq})$, and thus one has $R^B_{rxn}(F) = (1-F/F_{eq})\, R^B_{rxn}(0)$.

Second, the above analysis is useful for understanding the change in initial reactivity (for F=0 where behavior is independent of α) going from irreversible reaction (where $1+K_c^{-1}=1$) to reversible reaction (where $1+K_c^{-1}>1$). Equation (17) indicates that one should have quite similar values of $<\Delta A_1>$ since $k<<h$ (with $<\Delta A_1>$ marginally lower in the reversible case), and (16) indicates that $<\Delta A_n>$ should decay somewhat faster into the pore for the reversible case. Mainly the latter effect produces a slightly lower initial reactivity for the reversible case. In Fig.8, we compare $<\Delta A_n>$ profiles for F=0 and α=1 to confirm this picture.

Third, nonlinear variation of $R^B_{rxn}(F)$ on F when $\alpha \neq 1$ has similar origins to those for the irreversible case. Fourth, our results for the F-dependence of $R^B_{rxn}(F)$ encode complete information about the reaction kinetics as discussed for the irreversible case.

IV. Conclusions

The catalytic activity of nanoporous materials containing multifunctionalized linear nanopores is shown to be strongly dependent on the tunable interaction between reaction products and the interior pore environment. Making the pore interior unfavorable to products not only modifies the reaction equilibrium towards completion, but also reduces pore loading which can significantly enhance diffusivity and thus reactivity especially in the SFD regime. As noted in previous studies, catalytic activity is also strongly dependent on the propensity for passing of reactants and products within the pores [9,14,15,21]. Our generalized hydrodynamic formulation of reaction-diffusion phenomena provides an efficient tool to explore behavior over a broad phase-space of model parameters. This approach can reliably capture the complex interplay between reaction and restricted transport which results in subtle spatial correlations and fluctuations of reactants and products within the pore. These effects are not described by traditional mean-field approaches.

There are numerous possible modifications and extensions of our modeling which could be performed either utilizing refined generalized hydrodynamic RDE or with KMC simulation.

In this contribution, we have considered the benchmark case of equal mobility of reactants and products within the pore, following previous studies of conversion reactions in nanoporous systems [8-14]. However, the basic features of the reaction-diffusion process and the variation for enhanced versus blocked product reentry to the pore will be preserved for unequal mobilities. Some comments pertaining to the required refinement of refined GH formulation are found in Ref. [14]. Another natural extension

of our modeling is to consider different reaction mechanisms, e.g., A+B↔C+D better matching esterification reactions, and to consider the scenario where pore reentry of just one of the two products is enhanced versus blocked. The approximate MF and precise GH formalism described above are readily extended to treat this more complex situation, and preliminary studies reveal analogous behavior to that discussed above for the simpler A↔B conversion reaction mechanism.

Acknowledgements

This work was supported by the U.S. Department of Energy (USDOE), Office of Basic Energy Sciences, Division of Chemical Sciences, Geosciences, and Biosciences through the Ames Laboratory. It was performed at Ames Laboratory which is operated for the USDOE by Iowa State University under Contract No. DE-AC02-07CH11358.

Appendix: Random walk analysis of GH tracer diffusivity $F_{tr}(n)$

The position-dependent tracer diffusion coefficient, $F_{tr}(x=na) = F_{tr}(n)$, for a tagged particle starting at cell n in a pore with a concentration *X* of other particles is central to our generalized hydrodynamic formulation. This quantity is determined by simulations involving a finite concentration of a single type of particle in the pore with dynamics of all particles identical to the tagged particle. This dynamics is naturally selected to match the (equivalent) dynamics A or B particles within the pore: hopping to neighboring empty sites at rate h; exchange with adjacent particles within the pore at rate P_{ex} h; desorption from end sites n=1 and n=L by hopping to empty sites just outside the pore. If the reaction model excludes (includes) exchange in and out of the pore, then this

process is excluded (included) in the simulations to determine F_{tr}. If included with rates described in Sec. II A, then the corresponding single-particle dynamics includes exchange in and out of the pore at rate $e_{ads}P_{ex}h$. This choice recovers the appropriate values for α=1 (where e_{ads} =1) and for F=1 with only B in the fluid (where e_{ads} =α).

Our explicit algorithm to determine $F_{tr}(n)$ is based on a suitably defined "exit time" $t_X(x=na)$ for the tagged particle to exit the pore (where exiting the pore corresponds to reaching a site just outside the pore opening). Given anomalous features of random walks in one-dimension, such as long time-tails in return-time distributions [26], a judicious choice of definition for t_X is appropriate. Rather than simply average exit times over many simulation trials, we define $t_X(x=na)$ as the time when the root-mean-square displacement of the tagged particle reaches the distance to the closest pore opening (i.e., a distance n for n<L/2). Then, we assign $F_{tr}(n) = t_0(n)/t_X(n)$, motivated by the classic result that diffusivity scales like the mean-square displacement divided by time. Here, $t_0(n)$ corresponds to the exit time for an isolated particle in the pore, which can be determined analytically. Thus, one has that $t_X(n) \sim t_0(n)$ and $F_{tr}(n)\rightarrow 1$ for all n, as $X\rightarrow 0$.

For a semi-infinite pore $L\rightarrow\infty$, it is clear that $F_{tr}(n) \rightarrow F_{tr}(DH) = F_{tr}(X, P_{ex})$, as $n\rightarrow\infty$, recalling that $F_{tr}(DH)$ is the standard tracer diffusion coefficient for an infinite system. Thus, one has that $F_{tr}(n) \rightarrow 0$, as $n\rightarrow\infty$ for SFD (P_{ex}=0) when $X > 0$. The anomalous diffusion observed for SFD in infinite systems [20] suggests that $t_X(n) \sim n^4$ [14] versus $t_0(n) \sim n^2$ for classic diffusion. Together, these imply that $F_{tr}(n) \sim 1/n^2$, as $n\rightarrow\infty$, for SFD. Numerical studies show that behavior for SFD is fit well by a more

general form $F_{tr}(n) \propto 1/(n^2 + a\,n + bn^{1/2} + c)$ over a broad range of n [14]. For finite pores $L<\infty$, usually $F_{tr}(n) \rightarrow F_{tr}(DH)$ quickly upon entering the pore interior if $P_{ex} >0$. See Fig. 3(b). For SFD ($P_{ex}=0$), numerical studies reveal that $F_{tr}(na \approx L/2) \sim 1/L$ at the pore center.

To generate optimal numerical data for $F_{tr}(n)$, we sometimes smooth simulation results using a fit $\delta F_{tr}(n) = F_{tr}(n) - F_{tr}(DH) \propto 1/(n^2 + an + c)$, for larger n. Simulations are typically used to generate $F_{tr}(n)$ data for a selected set of values of $X = \langle X_{in} \rangle$. Data for other intermediate *X*-values can be readily and reliably obtained by interpolation.

References

[1] J.A. Melero, R. Van Grieken, and G. Morales, Chem. Rev. 106, 3790 (2006)
[2] E.L. Margelefsky, R.K. Zeiden, and M.E. Davis, Chem. Soc. Rev. 37, 1118 (2008).
[3] J.M. Thomas and R. Raja, Acc. Chem. Res. 41, 708 (2008).
[4] I.K. Mbaraka and B.H. Shanks, J. Catal. 229, 365 (2005).
[5] J.-P. Dacquin, H.E. Cross, D.B. Brown, T. Duren, J.J. Williams, A.F. Lee, and K. Wilson, Green Chem. 12, 1383 (2010).
[6] C.-H. Tsai, H.-T. Chen, S.M. Althaus, K. Mao, T. Kobayashi, M. Pruski, and V.S.-Y. Lin, ACS Cat. 1, 729 (2011).
[7] K. Mao, T. Kobayashi, J.W. Wiench, H.-T. Chen, C.-H. Tsai, V.S.-Y. Lin, and M. Pruski, J. Am. Chem. Soc. 132, 12452 (2010).
[8] J.G. Tsikoyiannis and J.E. Wei, Chem. Eng. Sci. 46, 233 (1991).
[9] J. Kärger, M. Petzold, H.S. Pfieffer, S. Ernst, and J. Weitkamp, J. Catal. 136, 283 (1992).
[10] C. Rodenbeck, J. Kärger, and K. Hahn, J. Catal. 157, 656 (1995).
[11] M.S. Okino, R.Q. Snurr, H.H. Kung, J.E. Ochs, and M.L. Mavrovouniotis, J. Chem. Phys. 111, 2210 (1999).
[12] S.V. Nedea, A.P.J. Jansen, J.J Lukkien, and P.A.J. Hilbers, Phys. Rev. E 65, 066701 (2002); 66, 066705 (2002); 67, 046707 (2003).
[13] D.M. Ackerman, J. Wang, J.H. Wendel, D.-J. Liu, M. Pruski, and J.W. Evans, J. Chem. Phys. 134, 114107 (2011). *(2011 Editors' Choice)*

[14] D.M. Ackerman, J. Wang, and J.W. Evans, Phys. Rev. Lett., 108, 228301 (2012).
[15] J. Wang, D.M. Ackerman, K. Kandel, I.I. Slowing, M. Pruski, and J.W. Evans, MRS Symp. Proc. Vol. 1423 (MRS, Pittsburgh, 2012) DOI: 10.1557/opl.2012.229
[16] R. Kutner, Phys. Lett. 81A, 239 (1981).
[17] J. Quastel, Commun. Pure Appl. Math. 45, 623 (1992).
[18] H. Spohn, *Large Scale Dynamics of Interacting Particles* (Springer, Berlin, 1991).
[19] P.H. Nelson and S.M. Auerbach, Chem. Eng. J. 74, 43 (1999).
[20] T.E. Harris, J. Appl. Probab. 2, 323 (1965).
[21] D.-J. Liu, J. Wang, D.M. Ackerman, K. Kandel, I.I. Slowing, M. Pruski, H.-T. Chen, V.S.-Y. Lin, and J.W. Evans, ACS Cat. 1, 751 (2011).
[22] D.G. Levitt and G. Subramanian, Biochimica et Biophysica Acta 373,132 (1974).
[23] B.J. Alder and W.E. Alley, in Physics Today (January 1984), p.56.
[24] We use the discretization $\nabla J_A \rightarrow \nabla J_A^{n>n+1} = \frac{1}{2}[F_{tr}(n)+F_{tr}(n+1)]\nabla\langle A_n\rangle$.
[25] For irreversible reaction with $\alpha=1$, one can show that net rate of reactant adsorption via hopping at n=1 satisfies $R_A^{ads\text{-}des}(hop) = h\langle X_{out}\rangle\langle E_{out}\rangle(1\text{-}F) - h\langle E_{out}\rangle\langle A_1\rangle$, and via exchange at n=1 satisfies $R_A^{ads\text{-}des}(ex) = P_{ex}h(\langle X_{out}\rangle)^2(1\text{-}F) - P_{ex}h\langle X_{out}\rangle\langle A_1\rangle$. The inhomogeneous BC for species A at cell n=1 come from $R_A^{ads}(hop) - R_A^{des}(hop) + R_A^{ads\text{-}des}(exch) - J_A^{1>2} = 0$. One can also show that $\langle A_1\rangle < (1\text{-}F)\langle X_{out}\rangle$.
[26] S. Redner, *A Guide to First-Passage Processes* (Cambridge University Press, Cambridge, 2001).

Figures

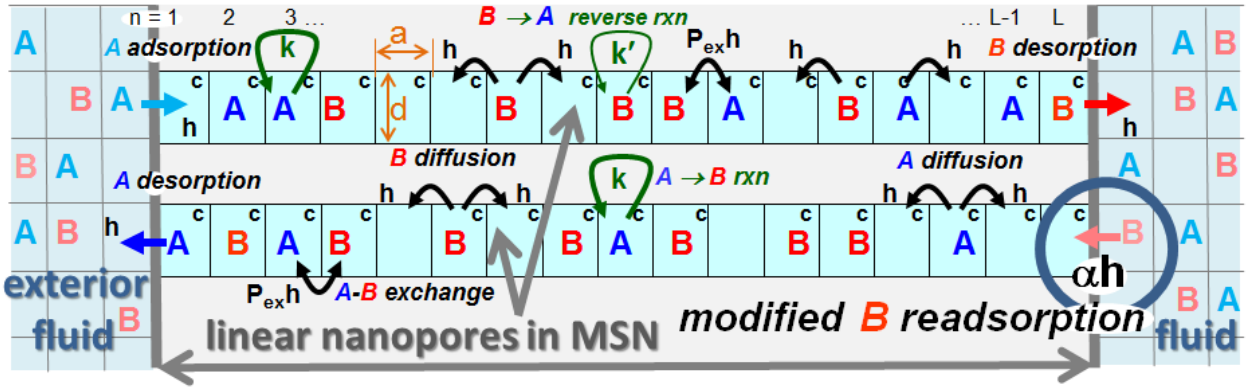

Fig.1. Schematic of the A to B conversion reaction model illustrating processes within pores (shaded light blue), as well as coupling to the surrounding fluid. In-out exchange processes are not shown (but are active in our modeling). ‘c’ denotes catalytic sites.

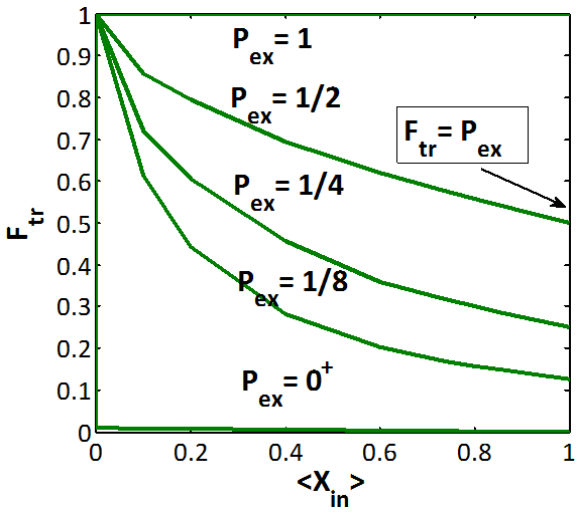

Fig.2. Behavior of the conventional (DH) tracer diffusion coefficient, $F_{tr}(DH)$, for infinite systems as a function of pore loading $\langle X_{in} \rangle$ for various passing probabilities, P_{ex} (shown).

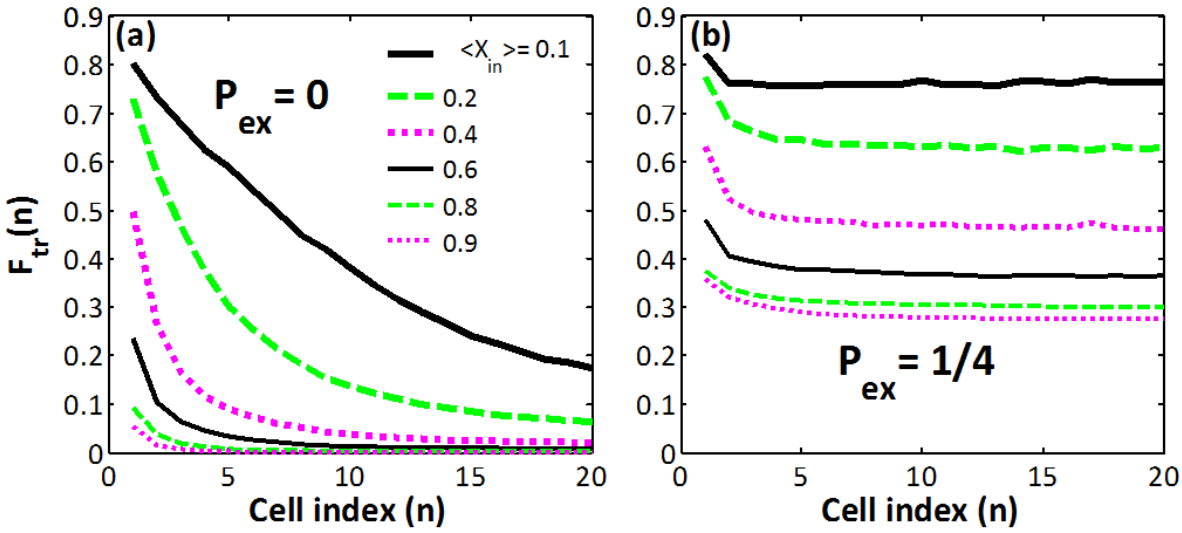

Fig.3. Variation of the generalized hydrodynamic tracer diffusion coefficient, $F_{tr}(n) = D_{tr}(n)/D_0$, with distance x=na into the left end of the pore for a pore on length L=100 a. The plateau value near the pore center corresponds to $F_{tr}(DH)$. Results are shown for fixed $\langle X_{out} \rangle = 0.8$ and varying $\langle X_{in} \rangle$ for: (a) single-file diffusion, $P_{ex} = 0$; and (b) exchange with $P_{ex}=0.25$.

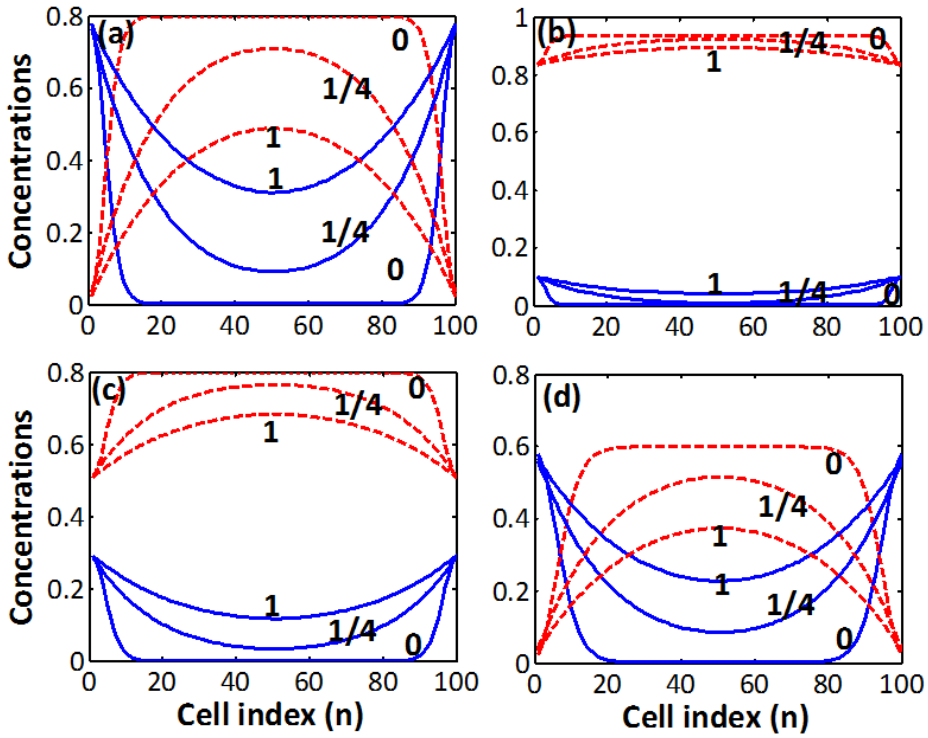

Fig. 4. Local steady-state concentration profiles for irreversible reaction A→B with L=100 a, k = 0.001, h = 1, and $\langle X_{out} \rangle$ = 0.8. A (B) is blue, solid (red, dashed). Behavior for: the onset of the reaction F=0 (a) for all α; and for F = 0.625 with (b) α=5; (c) α=1; (d) α=0.

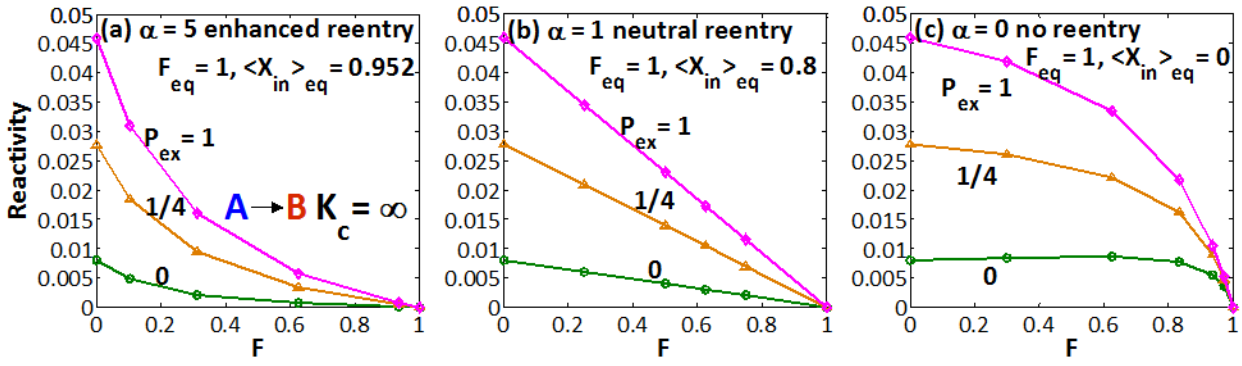

Fig. 5. Net reactivity per pore, R^B_{net}, as a function of the fraction F of reactant converted to product for irreversible reaction A→B with L=100 a, k = 0.001, h = 1, and $\langle X_{out} \rangle$ = 0.8. (a) enhanced product reentry α=5; (b) neutral reentry α=1; (c) blocked reentry α=0.

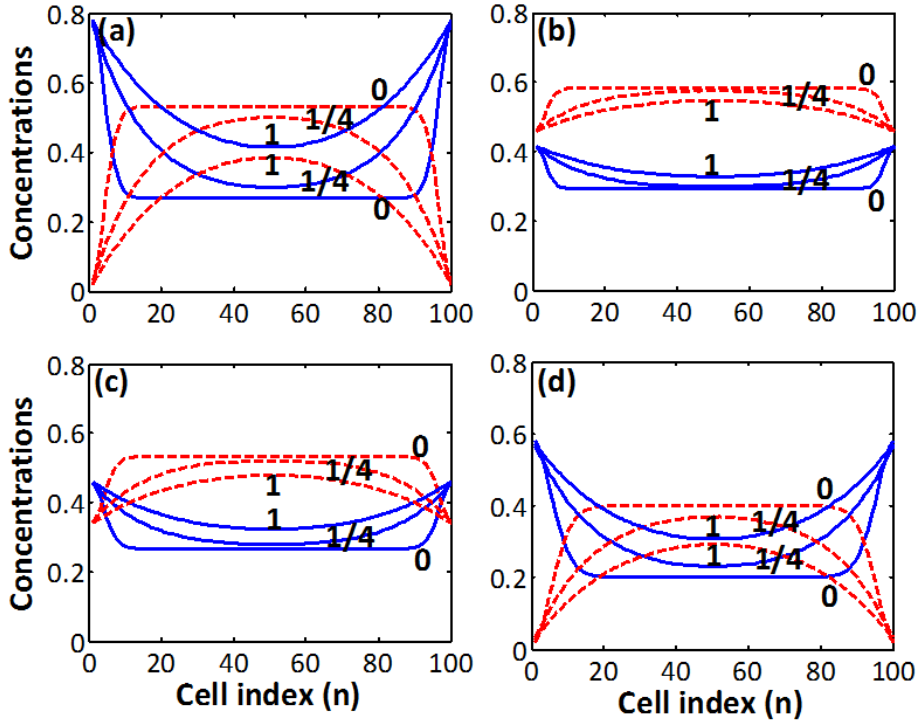

Fig.6. Local steady state concentration profiles for reversible reaction A↔B with L=100 a, k = 0.001, k′=0.0005, h = 1, and $<X_{out}>$ = 0.8. A (B) is blue, solid (red, dashed). Behavior for: the onset of the reaction F=0 (a) for all α; and for F/F_{eq} = 0.625 with (b) α=5; (c) α=1; (d) α=0.

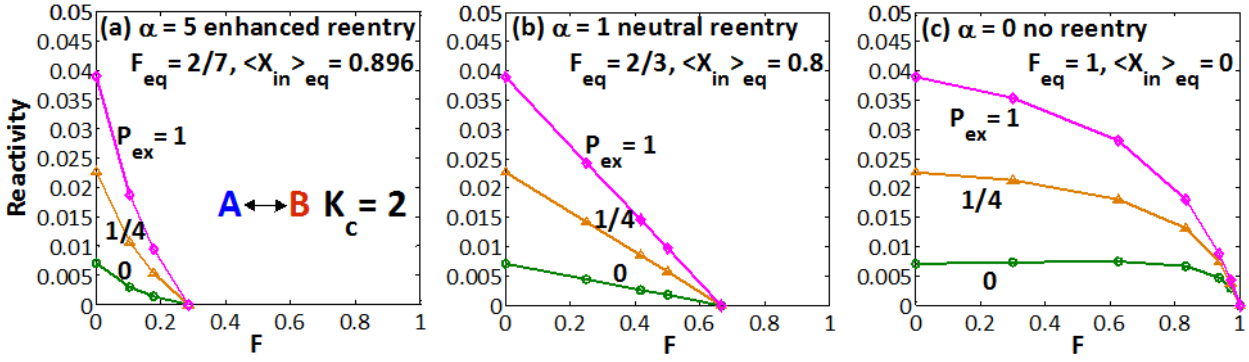

Fig. 7. Net reactivity per pore, R^{B}_{rxn}, as a function of the fraction F of reactant converted to product for reversible reaction A↔B with L=100 a, k = 0.001, k′=0.0005, h = 1, and $<X_{out}>$ = 0.8. (a) enhanced product reentry α=5; (b) neutral reentry α=1; (c) blocked reentry α=0.

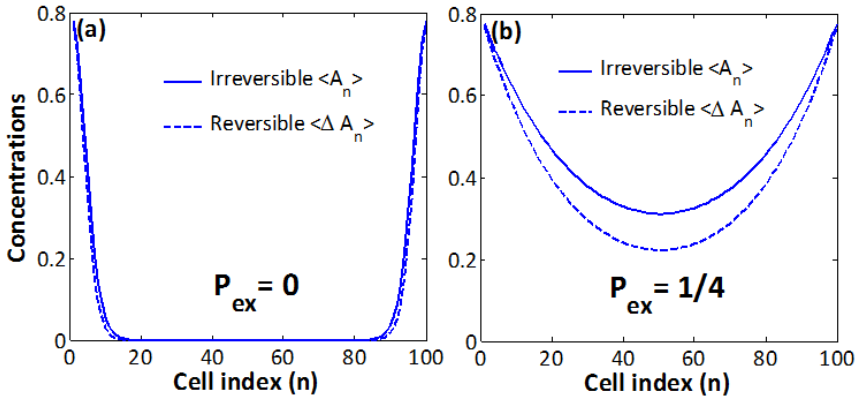

Fig.8. Comparison of excess reactant concentration, $<\Delta A_n>$, for irreversible reaction (where $<A_n> = <\Delta A_n>$) and reversible reaction at the onset of reaction (F=0) with L=100 a, k = 0.001, k′=0.0005, h = 1, α=1, and $<X_{out}> = 0.8$. The net reactivity R^B_{rxn} corresponds to the area under these curves.

CHAPTER 5. HIGHER-ORDER TRUNCATION APPROXIMATIONS TO THE MASTER EQUATIONS FOR SINGLE-FILE REACTION-DIFFUSION PROCESSES: APPLICATION TO TRACER DIFFUSION ANALYSIS

I. Introduction

Traditional mean-field (MF) reaction-diffusion equations (RDE) have been used to model diffusion-mediated reaction processes [1,2]. These RDE include a conventional treatment of chemical kinetics which ignores spatial correlations between reactants. For transport and reaction in single-file systems, the non-trivial nature of diffusion is well-recognized. Such systems are realized by mesoporous or nanoporous materials incorporating arrays of linear pores which are sufficiently narrow that molecules (or particles) cannot pass each other inside the pores. This no-passing feature results in anomalous tracer diffusion [3-5]. There have been several studies of a basic conversion reaction model and its variants [6-12]. In this basic model, the reactant, A, adsorbs at the ends of pore, converts to product, B, at catalytic sites within the pore, and both reactants and products can exit the pore. We are interested in asymptotic decay of reactant concentration as a function of distance into the pore in a semi-infinite SFD system, as well as the related behavior of the tracer diffusion coefficient. These issues are addressed utilizing the traditional mean-field type approximation as well as higher-level approximations.

In Sec. II, we specify in detail the single-file conversion reaction model, the associated hierarchical rate equations and mean-field-type RDE (mf-RDE). Then, in Sec.

III, we analyze the asymptotic decay of the reactant concentration $<A_n>$ at site n for small reaction rate. The associated tracer of diffusion coefficient is also extracted. The conclusions will be presented in Sec.IV.

II. Reaction-diffusion model

In our model for A→B conversion (Fig.1), reactants A enter the pore from the surrounding fluid at rate W_{ads} and are converted to products, B, at catalytic sites (c). Reactants and products within the pore are localized to sites of a 1D linear lattice traversing that pore, and both A and B exit the pore at rate W_{des}. The simplest prescription for diffusion within the pores is that A and B hop to adjacent empty (E) sites at rate **h**. This would correspond to single-file diffusion with a strict no-passing constraint. We also allow positional exchange of adjacent A and B at rate $\mathbf{P_{ex}}$ **h** to relax the strict single-file constraint, noting that exchange of adjacent particles of the same type has no effect. Conversion reaction at catalytic sites (c) occurs at rate **k**.

We consider the development of the master equations for the reaction-diffusion model for the evolution of probabilities of various configurations within the pore [13]. Sites within the pore(s) are labeled by n, and $<A_n>$ ($<B_n>$) denotes the probability that A (B) is at site n, etc. Then, for A→B conversion in the case where all sites are catalytic, one has that

$$d/dt <A_n> = -k<A_n> - \nabla J_A^{n>n+1},\ d/dt <B_n> = +k<A_n> - \nabla J_B^{n>n+1},\ \text{for } 1<n<L. \qquad (1)$$

with separate equations for terminal sites reflecting adsorption-desorption boundary conditions. In (1), the net flux, $J_A^{n>n+1}$, of A from site n to n+1 is given by (E=empty)

$$J_A^{n>n+1} = h\,[\langle A_n E_{n+1}\rangle - \langle E_n A_{n+1}\rangle] + P_{ex}\,h[\langle A_n B_{n+1}\rangle - \langle B_n A_{n+1}\rangle]. \quad (2)$$

where the first half denotes the diffusion and the rest associates the position exchange. Analogous form of flux $J_B^{n>n+1}$can be obtained easily. The key is to find accurate, useable expressions for the fluxes.

These equations (1) are coupled to probabilities for various configurations of pairs of sites. Equations for pair probabilities couple to those for various triples, etc., thus generating a hierarchy. Pair, triplet, etc., probabilities are not trivially related to single-site probabilities due to the presence of spatial correlations. In these models, correlations derive from the interplay of adsorption-desorption and diffusion with reaction. Implementing a simple mean-field (MF) factorization approximation, $\langle K_n E_{n+1}\rangle \approx \langle K_n\rangle\langle E_{n+1}\rangle$, etc., produces a closed set of discrete mf-RDE's for single site concentrations, $\langle A_n\rangle$ and $\langle B_n\rangle$ noting that $\langle A_n\rangle + \langle B_n\rangle + \langle E_n\rangle = 1$.

A more accurate pair approximation retains pair quantities like $\langle K_n E_{n+1}\rangle$, but factorizes triplet quantities, e.g., $\langle K_n M_{n+1} N_{n+2}\rangle \approx \langle K_n M_{n+1}\rangle\langle M_{n+1} N_{n+2}\rangle / \langle M_{n+1}\rangle$, with K, M, N = A, B, or E. This generates a closed set of equations for single site quantities, $\langle A_n\rangle$ and $\langle B_n\rangle$, together with the pair quantities, $\langle A_n A_{n+1}\rangle$, $\langle A_n B_{n+1}\rangle$, $\langle B_n A_{n+1}\rangle$, and $\langle B_n B_{n+1}\rangle$. See, e.g., [6,7,12]. Higher-order approximations are also possible retaining probabilities of configurations of strings of n>2 sites, although the gain in accuracy with increasing order, n, may be slow [13].

It is natural to consider a coarse-grained description of the spatially-discrete reaction-diffusion model which regards the species concentrations per unit length, $C(x=na) \approx a^{-1}\langle C_n\rangle$, as functions of a continuous spatial variable x (leaving the t-

dependence implicit), and denote the total concentration by $X(x) = A(x) + B(x)$. Here "a" denotes the lattice constant (i.e., the distance between sites of cells in the pore.) The continuum RDE for our A to B conversion reaction model with all sites catalytic then have the form

$$\partial/\partial t\, A(x) = -k\, A(x) - \partial/\partial x\, J_A, \text{ and } \partial/\partial t\, B(x) = +k\, A(x) - \partial/\partial x\, J_B. \quad (3)$$

Boundary conditions for (3) at the pore ends reflect the adsorption-desorption dynamics. Description of the diffusion fluxes, J_A and J_B, is non-trivial [13-15]. However, for the special situation applying in the steady-state where X = constant (i.e., independent of x), hydrodynamic theories for diffusion in mixed systems suggest the simple form $J_A = -D_{tr}(X)\, \partial/\partial x\, A$ and $J_B = -D_{tr}(X)\, \partial/\partial x\, B$. Then, if $D_{tr}(X)$ is actually independent of x, simple analysis of (3) in the steady-state reveals that

$$A(x) \sim \exp[-x/L_p] \text{ where } L_p = (D_{tr}/k)^{1/2}. \quad (4)$$

Where L_p is the penetration depth of the reactant A and $D_{tr} = a^2\, h\, F_{tr}$ is the tracer diffusion coefficient.

III. Analysis of asymptotic decay of reactant

As noted in previous studies [13], classic hydrodynamic analysis predicts that in the steady-state, the central region will contain just B and no A, so that $\langle B_n \rangle = W_{ads}/(W_{ads}+W_{des}) \approx X_{eq}$ and $\langle A_n \rangle \approx 0$. Only the end sites have significant A population in our discrete formulation. Thus, the non-zero population of A near the pore ends observed in simulations can be associated with fluctuation effects not included in the hydrodynamic formulation. Since the reactivity of the system is determined by the

population of A within the pore, these fluctuations are entirely responsible for the steady-state reactivity.

This situation motivates more detailed analysis of the dependence of this steady-state $<A_n>$ concentration profile on model parameters. Steady-state profiles appear to have an exponential form,

$$<A_n> \approx c\cdot r^n = c\cdot\exp(-\lambda n) = c\cdot\exp(-n/L_{p1}), \text{ at least for larger } n < L/2. \quad (5)$$

In (5), $\lambda = -\ln r$ is the decay rate, and $L_{p1}=1/\lambda$ is a measure of the penetration depth of A into the pore. Comparison with (5) above indicates that L_{p1} corresponds to L_p if we make the identification of n with x. Thus, we naturally write

$$D_{tr} = k\,(L_{p1})^2 = a^2\, h\, F_{tr}, \text{ where } a = 1 \text{ and } F_{tr} = (k/h)(L_{p1})^2 = k/(h\lambda^2). \quad (6)$$

Analysis below will show that F_{tr} is independent of h and k, depending only on X_{eq}.

Here, we focus on considering the predictions of MF-type analytic treatments regarding the above behavior. The simplest MF approximation exhibits precise exponential decay for long pores. This behavior, noted previously [11], is a result of the feature that $<E_n> = 1-<X_n>$ is constant, which in turn allows reduction of the steady-state form of the first equation in (1) to a linear coupled set of equations. Setting $\varepsilon = k/h$ and $X_{eq} = W_{ads}/(W_{ads}+W_{des})$, then seeking a solution to these linear equations of the form $<A_n> \propto r^n$ yields for r the quadratic equation (cf. [11])

$$(1-X_{eq})(r + r^{-1} -2) = \varepsilon. \quad (7)$$

Consequently, one has that $\delta = 1-r \sim (1-X_{eq})^{-1/2}\,\varepsilon^{1/2}$, for small ε, so that (cf. [11])

$$L_{p1}(MF) \sim \delta^{-1} \sim (1-X_{eq})^{1/2}\,(k)^{-1/2}(h)^{1/2}, \text{ for } k \to 0 \text{ or } h \to \infty. \quad (8)$$

which implies a relation between the tracer diffusion coefficient and the total concentration in the steady-state,

$$F_{tr}(X_{eq}) = (1-X_{eq}) = f(X_{eq})\,(1-X_{eq}) \qquad (9)$$

where $f(X) = 1$.

It is instructive to assess the predictions of the higher-order pair approximation for the behavior of the penetration length, L_p. The complex non-linear form of pair equations [11] excludes exact exponential decay. However, there should be asymptotic exponential decay $\langle A_n \rangle \sim \exp(-n/L_{p1})$ for large $n < L/2$. In the steady-state, one has the relations $\langle A_n \rangle + \langle B_n \rangle = X_{eq}$ and $\langle B_nB_{n+1} \rangle + \langle B_nA_{n+1} \rangle + \langle A_nB_{n+1} \rangle + \langle A_nA_{n+1} \rangle = (X_{eq})^2$. Since one expects that **$\langle A_nA_{n+1} \rangle$ decreases more quickly** than $\langle A_n \rangle$, $\langle A_nB_{n+1} \rangle$, or $\langle B_{n-1}A_n \rangle$ for increasing n, it follows that one can just analyze equations for the latter quantities. Anticipating solutions of the form $\langle A_n \rangle \approx c \cdot r^n$, $\langle A_nB_{n+1} \rangle \approx c \cdot \alpha_1 \cdot r^n$, and $\langle B_{n-1}A_n \rangle \approx c \cdot \alpha_2 \cdot r^n$ and substituting into the rate equations for the pair approximation yields three coupled equations

$$\begin{aligned} &(1-\alpha_2)(r-1) + (1-\alpha_1)(r^{-1}-1) = \varepsilon, \\ &(1-\alpha_1)(\alpha_1^{-1}X_{eq})(r^{-1}+1) - (1-X_{eq}) - (1-\alpha_2) = \varepsilon, \text{ and} \\ &(1-\alpha_2)(\alpha_2^{-1}X_{eq})(r+1) - (1-X_{eq}) - (1-\alpha_1) = \varepsilon. \end{aligned} \qquad (10)$$

Seeking solutions for small ε and $\delta = 1-r$ with $\alpha_1 \approx X_{eq} + B\delta$ and $\alpha_2 \approx X_{eq} + C\delta$ yields

$$L_{p1}(\text{pair}) \sim \delta^{-1} \sim (2-X_{eq})^{1/2}(2+X_{eq})^{-1/2}L_p(\text{MF}) \text{ , for large } L_{p1}. \qquad (11)$$

and

$$F_{tr}(X_{eq}) = (1-X_{eq})\,(2-X_{eq}) / (2+X_{eq}) = f(X_{eq})\,(1-X_{eq}) \qquad (12)$$

where $f(X) = (2-X) / (2+X)$.

Thus, L_{p1}(pair) is smaller than L_{p1}(MF) and closer to the exact L_{p1}, but still has the incorrect asymptotic functional form as $k \to 0$ or $h \to \infty$. The result $C = -B = X_{eq}(1-X_{eq})(2+X_{eq})^{-1}$ obtained in previous study [13] is not necessarily true here.

For even higher-order, say, triplet approximation, in the steady-state, one has the relations $\langle A_n\rangle + \langle B_n\rangle = X_{eq}$, $\langle B_nB_{n+1}\rangle + \langle B_nA_{n+1}\rangle + \langle A_nB_{n+1}\rangle + \langle A_nA_{n+1}\rangle = (X_{eq})^2$ and $\langle B_nB_{n+1}A_{n+2}\rangle + \langle B_nA_{n+1}A_{n+2}\rangle + \langle A_nB_{n+1}A_{n+2}\rangle + \langle A_nA_{n+1}A_{n+2}\rangle + \langle B_nB_{n+1}B_{n+2}\rangle + \langle B_nA_{n+1}B_{n+2}\rangle + \langle A_nA_{n+1}B_{n+2}\rangle + \langle A_nB_{n+1}B_{n+2}\rangle = (X_{eq})^3$. Since one expects that $\langle A_nA_{n+1}\rangle$, $\langle A_nA_{n+1}A_{n+2}\rangle$, $\langle A_nA_{n+1}B_{n+2}\rangle$, $\langle A_nB_{n+1}A_{n+2}\rangle$ and $\langle B_nA_{n+1}A_{n+2}\rangle$ decreases **more quickly** than $\langle A_n\rangle$, $\langle A_nB_{n+1}\rangle$, $\langle B_{n-1}A_n\rangle$, $\langle A_nB_{n+1}B_{n+2}\rangle$, $\langle B_{n-1}A_nB_{n+2}\rangle$, or $\langle B_{n-2}B_{n-1}A_n\rangle$ for increasing n, it follows that one can just analyze equations for the latter quantities. We also add $\langle A_nE_{n+1}B_{n+2}\rangle$ and $\langle B_{n-2}E_{n-1}A_n\rangle$ to the above six quantities, since there is no way to rewrite these two quantities in terms of those six. Anticipating solutions of the form $\langle A_n\rangle \approx c\cdot r^n$, $\langle A_nB_{n+1}\rangle \approx c\cdot\alpha_1\cdot r^n$, $\langle B_{n-1}A_n\rangle \approx c\cdot\alpha_2\cdot r^n$, $\langle A_nB_{n+1}B_{n+2}\rangle \approx c\cdot\beta_1\cdot r^n$, $\langle B_{n-1}A_nB_{n+2}\rangle \approx c\cdot\beta_2\cdot r^n$, $\langle B_{n-2}B_{n-1}A_n\rangle \approx c\cdot\beta_1\cdot r^n$, $\langle A_nE_{n+1}B_{n+2}\rangle \approx c\cdot\gamma_1\cdot r^n$ and $\langle B_{n-2}E_{n-1}A_n\rangle \approx c\cdot\gamma_2\cdot r^n$, and substituting into the rate equations for the triplet approximation yields eight coupled equations

$$
\begin{aligned}
&(1-\alpha_2)(r-1) + (1-\alpha_1)(r^{-1}-1) = \varepsilon,\\
&\gamma_1\alpha_1^{-1}(r^{-1}+1) - (\alpha_1-\beta_1)\alpha_1^{-1} - (\alpha_1-\beta_2)\alpha_1^{-1} = \varepsilon,\\
&\gamma_2\alpha_2^{-1}(r+1) - (\alpha_2-\beta_2)\alpha_2^{-1} - (\alpha_2-\beta_3)\alpha_2^{-1} = \varepsilon,\\
&(\alpha_1-\beta_2)\beta_1^{-1}X_{eq} - (1-X_{eq}) + \gamma_1\beta_1^{-1}r^{-1}X_{eq} - (\alpha_1-\beta_2)\alpha_1^{-1} = \varepsilon, \qquad (13)\\
&(\alpha_2-\beta_2)\gamma_1(1-\alpha_1)^{-1}\beta_2^{-1} - (\alpha_1-\beta_1)\alpha_1^{-1} + (\alpha_1-\beta_1)\gamma_2(1-\alpha_2)^{-1}\beta_2^{-1} - (\alpha_2-\beta_2)\alpha_2^{-1} = \varepsilon,\\
&\gamma_2\beta_3^{-1}r\,X_{eq} - (\alpha_2-\beta_2)\alpha_2^{-1} + (\alpha_2-\beta_3)\beta_3^{-1}X_{eq} - (1-X_{eq}) = \varepsilon,
\end{aligned}
$$

$(\alpha_1 - \beta_1)\gamma_1^{-1} + (\alpha_1 - \beta_2)\gamma_1^{-1} r - 2 + (1 - \alpha_1 - \gamma_1)\gamma_1^{-1}(r^{-1} + 1) X_{eq}$

$$- (1 - X_{eq}) - (1 - \alpha_1 - \alpha_2 + \beta_2)(1 - \alpha_1)^{-1} = \varepsilon, \text{ and}$$

$(\alpha_2 - \beta_2)\gamma_2^{-1} r^{-1} + (\alpha_2 - \beta_3)\gamma_2^{-1} - 2 + (1 - \alpha_2 - \gamma_2)\gamma_2^{-1}(r + 1) X_{eq}$

$$- (1 - X_{eq}) - (1 - \alpha_1 - \alpha_2 + \beta_2)(1 - \alpha_2)^{-1} = \varepsilon.$$

Seeking solutions for small ε and $\delta = 1\text{-}r$ with $\alpha_1 \approx X_{eq} + B_1\delta$, $\alpha_2 \approx X_{eq} + B_2\delta$, $\beta_1 \approx (X_{eq})^2 + C_1\delta$, $\beta_2 \approx (X_{eq})^2 + C_2\delta$, $\beta_3 \approx (X_{eq})^2 + C_3\delta$, $\gamma_1 \approx X_{eq}(1 - X_{eq}) + E_1\delta$, and $\gamma_2 \approx X_{eq}(1 - X_{eq}) + E_2\delta$ yields

$$L_{p1}(\text{triplet}) \sim \delta^{-1} \sim (2\text{-}X_{eq})^{1/2}(4\text{-}3X_{eq}+X_{eq}^2)^{1/2}(8+6X_{eq}\text{-}5X_{eq}^2+X_{eq}^3)^{-1/2} L_p(\text{MF}), \quad (14)$$

for large L_{p1}. And,

$$F_{tr}(X_{eq}) = (1\text{-}X_{eq})(2\text{-}X_{eq})(4\text{-}3X_{eq}+X_{eq}^2) / (8+6X_{eq}\text{-}5X_{eq}^2+X_{eq}^3) = f(X_{eq})(1\text{-}X_{eq}), \quad (15)$$

where $f(X) = (2\text{-}X)(4\text{-}3X+X^2) / (8+6X\text{-}5X^2+X^3)$.

For the quartet approximation additional multisite probabilities are needed to follow the analogous procedure. In the steady-state, we have

$L_{p1}(\text{quartet}) \sim \delta^{-1}$

$$\sim (1600\text{-}1680X_{eq}\text{-}1660X_{eq}^2+3180X_{eq}^3\text{-}1963X_{eq}^4+601X_{eq}^5\text{-}365X_{eq}^6$$

$$+277X_{eq}^7\text{-}88X_{eq}^8+9X_{eq}^9)^{1/2}(1600+3120X_{eq}\text{-}6060X_{eq}^2+4760X_{eq}^3\text{-}2453X_{eq}^4+871X_{eq}^5\text{-}$$

$167X_{eq}^6 - 3X_{eq}^7 + 8X_{eq}^8 - X_{eq}^9)^{-1/2} L_p(\text{MF})$, for large L_{p1}. (16)

And,

$$F_{tr}(X_{eq}) = f(X_{eq})(1\text{-}X_{eq}) = (1\text{-}X_{eq})(1600\text{-}1680X_{eq}\text{-}1660X_{eq}^2+3180X_{eq}^3\text{-}1963X_{eq}^4$$

$$+601X_{eq}^5\text{-}365X_{eq}^6+277X_{eq}^7\text{-}88X_{eq}^8+9X_{eq}^9) / (1600+3120X_{eq}\text{-}6060X_{eq}^2+4760X_{eq}^3$$

$$-2453X_{eq}^4+871X_{eq}^5\text{-}167X_{eq}^6 - 3X_{eq}^7 + 8X_{eq}^8 - X_{eq}^9) \quad (17)$$

where $f(X) = (1600 - 1680X - 1660X^2 + 3180X^3 - 1963X^4 + 601X^5 - 365X^6 + 277X^7 - 88X^8 + 9X^9) / (1600 + 3120X - 6060X^2 + 4760X^3 - 2453X^4 + 871X^5 - 167X^6 - 3X^7 + 8X^8 - X^9)$.

Based on the above calculation, L_{p1}(triplet) is smaller than L_{p1}(MF) and L_{p1}(pair) and L_{p1}(quartet) is smaller than L_{p1}(triplet). To analyze the tracer diffusion coefficient $D_{tr}(X_{eq})$ (or $F_{tr}(X_{eq})$), one can look at $f(X_{eq})$

$$f(X_{eq})_{MF} = 1,$$

$$f(X_{eq})_{pair} = (2-X_{eq})(2+X_{eq})^{-1},$$

$$f(X_{eq})_{triplet} = (2-X_{eq})(4-3X_{eq}+X_{eq}^2)(8+6X_{eq}-5X_{eq}^2+X_{eq}^3)^{-1}, \quad (18)$$

$$f(X_{eq})_{quartet} = (1600-1680X_{eq}-1660X_{eq}^2+3180X_{eq}^3-1963X_{eq}^4+601X_{eq}^5-365X_{eq}^6+277X_{eq}^7-88X_{eq}^8+9X_{eq}^9)(1600+3120X_{eq}-6060X_{eq}^2+4760X_{eq}^3-2453X_{eq}^4+871X_{eq}^5-167X_{eq}^6-3X_{eq}^7+8X_{eq}^8-X_{eq}^9)^{-1}.$$

Assuming that approximations become more accurate with order increasing, we expect the behavior of $f(X_{eq})_{MF\text{-type}}$ converges to the correct limiting behavior $f(X_{eq}) = 0$ for SFD for positive X_{eq}. From Fig.2, we can see that the behavior of the pair and triplet approximations is consistent with this trend; however, the mis-behavior in the tail of quartet (where $f < 0$) seems to break the anticipated tendency of convergence to exact behavior.

IV. Conclusions

The MF-type approximations are traditional and widely used approach in the analysis of discrete RDE. In general, they are expected to converge to the correct

behavior with increasing order, although perhaps slowly. However, the analysis for our model of the forth-order quartet approximation suggests another possibility, specifically that uncontrolled MF-type methods can fail to capture the correct behavior with increasing order.

References

[1] G. Nicolis and I. Prigogine, *Self-organization in Non-equilibrium Systems* (Wiley, New York, 1977).
[2] A.S. Mikhailov, *Foundations of Synergetics I* (Springer, Berlin, 1990)
[3] A.L. Hodgkin and R.D. Keynes, J. Physiol. (London) **128**, 61 (1955).
[4] T.E. Harris, J. Appl. Prob. **2**, 323 (1965).
[5] P.A. Fedders, Phys. Rev. B, **16**, 1393 (1977).
[6] J.G. Tsikoyiannis and J.E. Wei, Chem. Eng. Sci, **46**, 233 (1991).
[7] M.S. Okino, R.Q. Snurr, H.H. Kung, J.E. Ochs, and M.L. Mavrovouniotis, J. Chem. Phys. **111**, 2210 (1999).
[8] J. Kärger, M. Petzold, H. Pfieffer, S. Ernst, and J. Weitkamp, J. Catal. **136**, 283 (1992).
[9] C. Rodenbeck, J. Kärger, and K. Hahn, J. Catal. **157**, 656 (1995).
[10] C. Rodenbeck, J. Kärger, and K. Hahn, Phys. Rev. E **55**, 5697 (1997).
[11] S.V Nedea, A.P.J. Jansen, J.J. Lukkien, and P.A.J. Hilbers, Phys. Rev. E **65**, 066701 (2002); **66**, 066705 (2002).
[12] S.V Nedea, A.P.J. Jansen, J.J. Lukkien, and P.A.J. Hilbers, Phys. Rev. E **67**, 046707 (2003).
[13] D.M. Ackerman, J. Wang, J.H. Wendel, D.-J. Liu, M. Pruski, and J.W. Evans, J. Chem. Phys. 134, 114107 (2011).
[14] J. Quastel, Commun. Pure Appl. Math. **45**, 623 (1992).
[15] D.M. Ackerman, J. Wang, and J.W. Evans, Phys. Rev. Lett. 108, 228301 (2012).

Figures

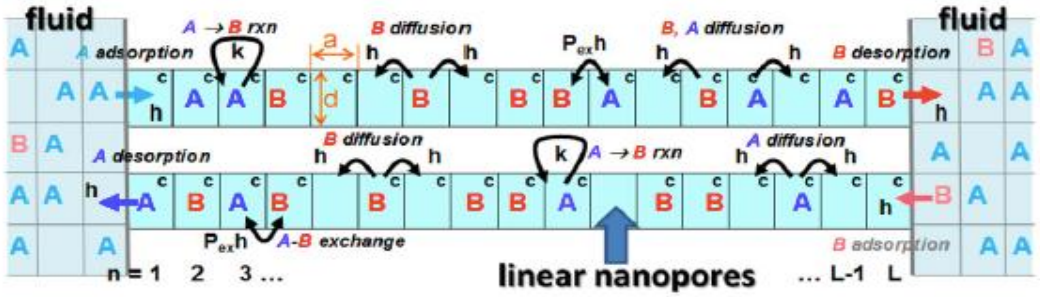

Fig 1. Schematic of the A→B conversion reaction model illustrating processes within a single pore (shaded blue), as well as the surrounding fluid. 'c' denotes catalytic sites.

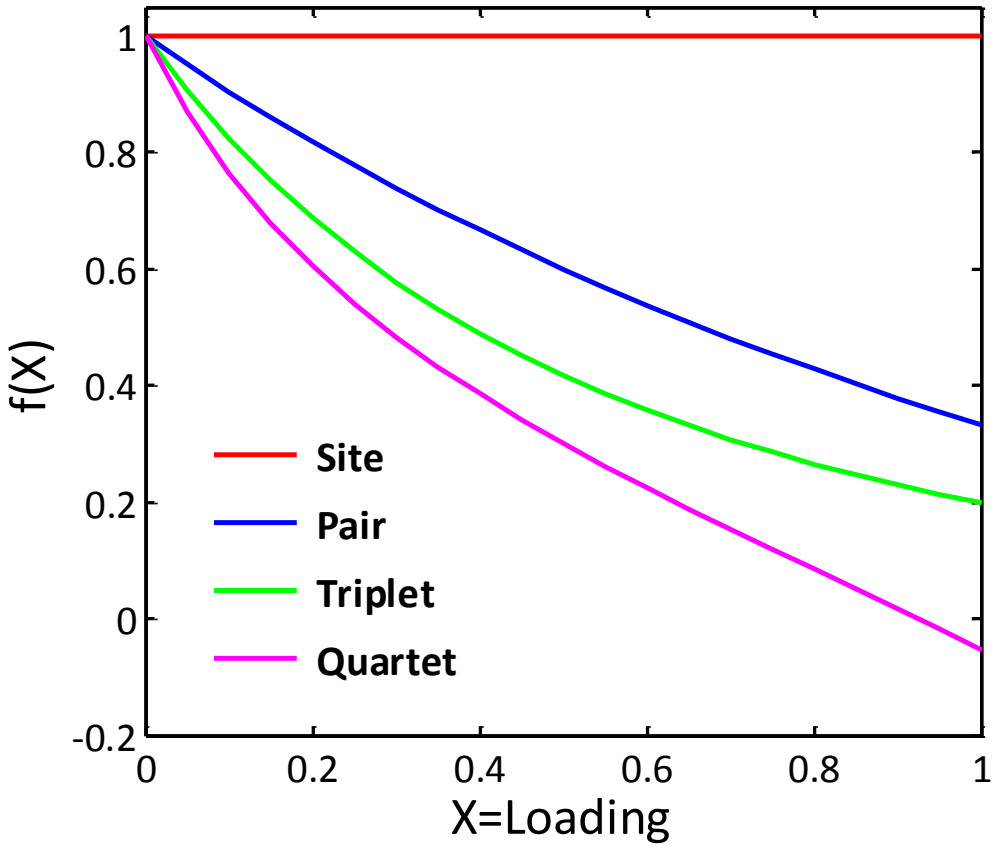

Fig 2. $f(X_{eq})_{\text{MF-type}}$ behavior for MF (Site), pair, triplet and quartet approximation.

CHAPTER 6. TAYLOR EXPANSION ANALYSIS OF A GENERALIZED POSITION-DEPENDENT TRACER DIFFUSION COEFFICIENT FOR TRASNPORT IN SEMI-INFINITE PORES

I. Introduction

Anomalous tracer diffusion of a "tagged" particle in a single-file diffusion (SFD) system, where particles within narrow pores cannot pass each other, was proven in the 1960's for hard-core interactions [1] and later for general interactions [2]. Numerous studies have considered single-file tracer diffusion in finite open [3], periodic [4,5], or closed [6] "pores", and in other systems [7]. For the reaction-diffusion phenomena with functionalized nanoporous materials which are of broad interest in the catalysis community, it is actually chemical diffusion [8] which controls behavior [9]. However, there is a connection between chemical and tracer diffusion (although this connection is not well recognized). It is also the case here that analysis of tracer diffusion in finite length systems is of importance (in contrast to the traditional analysis for infinite systems). Thus, for these important applications there is considerable motivation to provide a more detail understanding and characterization of tracer diffusion for transport in finite systems (noting that tracer diffusion is independent of the details of the reaction model).

The traditional mean-field approximation in a SFD system implies that the tracer diffusion coefficient $D_{tr} = 1 - \chi$ [9,10] where χ is the total concentration of particles within the pore in the steady state. This choice overestimates chemical diffusion fluxes

for SFD. A standard SFD-analysis for a system of length L indicates that $D_{tr} \sim 1/L \to 0$, as $L \to \infty$ [3,4]. This recovers the familiar exact result that $D_{tr} = 0$ in infinite systems due to the SFD constraint. The associated "hydrodynamic" reaction-diffusion equations (RDE) with constant $D_{tr} \sim 1/L$ can describe, e.g., the evolution of slowly varying profiles during filling of long pores [12]. However, this formulation neglects fluctuations near pore openings, and thus underestimates associated effective chemical diffusion fluxes. These observations prompt our development of a more general formulation of position-dependent tracer diffusion in finite or semi-infinite systems.

In Sec. II, we generalize a standard definition of the tracer diffusion coefficient D_{tr} for infinite systems to finite or semi-infinite systems (pores) motivated by the expectation that tracer diffusion is effectively enhanced near pore openings. These D_{tr} are determined from analysis of a complex many-particle transport problem for which exact analytic solution is not viable. One possible strategy for their determination is kinetic Monte Carlo simulation. However, here we develop and alternative Taylor expansion analysis which can be effectively applied to assess the D_{tr} at least close to the pore openings and for low loading χ.

II. Taylor expansion for tracer diffusion coefficient $D_{tr}(n)$

As a natural generalization of tracer diffusion for infinite systems, we determine $D_{tr}(n)$ at site n for a pore with uniform loading $<X_n>=\chi$. Our definition and determination of $D_{tr}(n)$ is based analysis of the time, $t_n(\chi)$, for a tagged particle starting at this cell to "reach a pore opening" in the sense that its suitably defined root-mean-

square (rms) displacement grows to match the distance from the nearest pore opening (See Fig.1). For a finite pore of length L, this distance is the smaller of n or L – n. For a semi-infinite pore of interest here, this distance is always n. Specifically, we set $D_{tr}(n) = D_0\, t_n(0+)/t_n(\chi) = t_n(0+)/t_n(\chi)$ as $D_0=1$ since diffusivity is inversely proportional to the time for the rms displacement to reach a certain value. This recovers the correct limiting value $D_{tr}(n)\to 1$ as $\chi\to 0+$.

In our model, particles in a finite or semi-infinite pore hop to adjacent empty site at rate $W_{hop} =1$. A single tagged particle starting at site n has the same hopping dynamics within the pore as all the other particles. To maintain a pore with uniform concentration $<X_n>=\chi$, we allow the untagged particles to hop into the pore at rate W_{ads} and the tagged and all untagged particles to hop out of the pore at rate W_{des} which follows $<X_n> = \chi = W_{ads} / (W_{ads} + W_{des})$. (The tagged particle cannot hop back in to the pore.) Without loss of generality, assume $W_{ads} + W_{des} = 1$ resulting in $W_{ads} = \chi$ and $W_{des} = 1 - \chi$. Let P_j denote the probability that the tagged particle is at site j, $P(x_j\, o_{j+1})$ that the tagged particle x is at site j and that site j+1 is empty (o), etc. Also, P_0 denotes the probability that the tagged particle has hopped out of the pore. Then we can determine the mean position, $<j>$, the mean-squared position, $<j^2>$, etc. for the tagged particle as moments of P_j via $<j^n> = \sum_j (j^n P_j)$.

Since the average position of the tagged particle inside the pore may “drift” for $\chi > 0$, there is more than one reasonable way to define mean-square displacement. One could consider the mean-square (ms) displacement about the average (time-varying)

position, although we do not do so here. Instead, one could consider the mean-square displacement from the initial position $j_0 = n$ via

$$\text{ms displacement} = \langle (j-j_0)^2 \rangle = \langle j^2 \rangle - 2j_0 \langle j \rangle + (j_0)^2. \quad (1)$$

This definition was used in our previous simulation studies [11,12]. An alternative, which neglects drift in the mean position, is to use

$$\text{ms type displacement} = \langle j^2 \rangle - \langle j^2 \rangle_0 = \langle j^2 \rangle - (j_0)^2. \quad (2)$$

The exact Taylor expansion for these quantities expansions for $\langle j \rangle$ and $\langle j^2 \rangle$, e.g.,

$\langle j^2 \rangle =$

$$\langle j^2 \rangle_0 + d/dt \langle j^2 \rangle_0 t + d^2/dt^2 \langle j^2 \rangle_0 t^2/2! + d^3/dt^3 \langle j^2 \rangle_0 t^3/3! + d^4/dt^4 \langle j^2 \rangle_0 t^4/4! + \ldots \quad (3)$$

for analysis of which determination of the initial values of $d/dt \langle j^2 \rangle$, $d^2/dt^2 \langle j^2 \rangle$, $d^3/dt^3 \langle j^2 \rangle$, etc. is required.

This analysis proceeds from the exact master equations for this many-particle system with a single tagged particle which have the form

$$\begin{aligned}
d/dt\, P_0 &= W_{des}\, P_1, \\
d/dt\, P_1 &= -W_{des}\, P_1 - P(x_1\, o_2) + P(o_1\, x_2), \\
d/dt\, P_2 &= P(x_1\, o_2) - P(o_1\, x_2) - P(x_2\, o_3) + P(o_2\, x_3), \\
d/dt\, P_3 &= P(x_2\, o_3) - P(o_2\, x_3) - P(x_3\, o_4) + P(o_3\, x_4), \\
d/dt\, P_4 &= P(x_3\, o_4) - P(o_3\, x_4) - P(x_4\, o_5) + P(o_4\, x_5), \\
&\ldots \\
d/dt\, P_j &= P(x_{j-1}\, o_j) - P(o_{j-1}\, x_j) - P(x_j\, o_{j+1}) + P(o_j\, x_{j+1}), \\
&\ldots
\end{aligned} \quad (4)$$

Examples of the next higher-order equations for pair quantities are

$$d/dt\ P(x_1\ o_2) = -\ W_{des}\ P(x_1\ o_2) - P(x_1\ o_2) + P(o_1\ x_2)$$
$$- P(x_1\ o_2\ \blacklozenge_3) + P(x_1\ \blacklozenge_2\ o_3) \quad (5a)$$

…

$$d/dt\ P(x_j\ o_{j+1}) = -\ P(x_j\ o_{j+1}) + P(o_j\ x_{j+1}) - P(o_{j-1}\ x_j\ o_{j+1}) + P(x_{j-1}\ o_j\ o_{j+1})$$
$$- P(x_j\ o_{j+1}\ \blacklozenge_{j+2}) + P(x_j\ \blacklozenge_{j+1}\ o_{j+2}) \quad (5b)$$

where $P(x_j\ o_{j+1}\ \blacklozenge_{j+2})$ denotes the probability that the tagged particle (x) is at site j, site j+1 is empty (o) and another particle ($\blacklozenge$) is at site j+2.

Note that from these equations, it immediately follows that

$$d/dt\ \sum_j (P_j) = 0 \quad (6)$$

so it follows that $\sum_j (P_j) = 1$ (consistent with the initial conditions). More generally, one can generate rate equations for the moments $\langle j^n \rangle = \sum_j (j^n\ P_j)$. As noted above, of particular importance here is the behavior of $\langle j \rangle$ and $\langle j^2 \rangle$ as this is used to determine $D_{tr}(n)$.

In (4), if the equation of P_j is multiplied by j, the master equations become

$$0\ d/dt\ P_0 = 0\ W_{des}\ P_1$$
$$1\ d/dt\ P_1 = 1\ [-\ W_{des}\ P_1 - P(x_1\ o_2) + P(o_1\ x_2)]$$
$$2\ d/dt\ P_2 = 2\ [P(x_1\ o_2) - P(o_1\ x_2) - P(x_2\ o_3) + P(o_2\ x_3)]$$
$$3\ d/dt\ P_3 = 3\ [P(x_2\ o_3) - P(o_2\ x_3) - P(x_3\ o_4) + P(o_3\ x_4)] \quad (7)$$
$$4\ d/dt\ P_4 = 4\ [P(x_3\ o_4) - P(o_3\ x_4) - P(x_4\ o_5) + P(o_4\ x_5)]$$

…

$$j\ d/dt\ P_j = j\ [P(x_{j-1}\ o_j) - P(o_{j-1}\ x_j) - P(x_j\ o_{j+1}) + P(o_j\ x_{j+1})]$$

...

Summing over equations in (7), one has

$$d/dt \langle j \rangle = d/dt \sum_j (j P_j) = - W_{des} P_1 + P(x_1 o_2)$$
$$+ P(x_2 o_3) - P(o_1 x_2)$$
$$+ P(x_3 o_4) - P(o_2 x_3) + \ldots$$
$$+ P(x_j o_{j+1}) - P(o_{j-1} x_j) + \ldots \quad (8)$$

Similarly multiplying the jth equation in (4) by j^2 yields

$$0^2 \, d/dt \, P_0 = 0^2 \, W_{des} \, P_1$$
$$1^2 \, d/dt \, P_1 = 1^2 \, [- W_{des} \, P_1 - P(x_1 o_2) + P(o_1 x_2)]$$
$$2^2 \, d/dt \, P_2 = 2^2 \, [P(x_1 o_2) - P(o_1 x_2) - P(x_2 o_3) + P(o_2 x_3)]$$
$$3^2 \, d/dt \, P_3 = 3^2 \, [P(x_2 o_3) - P(o_2 x_3) - P(x_3 o_4) + P(o_3 x_4)] \quad (9)$$
$$4^2 \, d/dt \, P_4 = 4^2 \, [P(x_3 o_4) - P(o_3 x_4) - P(x_4 o_5) + P(o_4 x_5)]$$
$$\ldots$$
$$j^2 \, d/dt \, P_j = j^2 \, [P(x_{j-1} o_j) - P(o_{j-1} x_j) - P(x_j o_{j+1}) + P(o_j x_{j+1})]$$
$$\ldots$$

Taking the summation of equations in (9), one has,

$$d/dt \langle j^2 \rangle = d/dt \sum_j (j^2 P_j) = 3 P(x_1 o_2) - W_{des} P_1$$
$$+ 5 P(x_2 o_3) - 3 P(o_1 x_2)$$
$$+ 7 P(x_3 o_4) - 5 P(o_2 x_3) + \ldots$$
$$+ (2j + 1) P(x_j o_{j+1}) - (2j - 1) P(o_{j-1} x_j) + \ldots \quad (10)$$

Clearly one can continue this procedure to obtain an equation for $d/dt \langle j^n \rangle$.

Determination of a Taylor expansion for $\langle j \rangle$ motivates the differentiation

$$d^2/dt^2 \langle j \rangle = d/dt \, (d/dt \langle j \rangle)$$

$$= - W_{des}\, d/dt\, P_1 + d/dt\, P(x_1 o_2) + d/dt\, P(x_2 o_3) - d/dt\, P(o_1 x_2)$$
$$+ d/dt\, P(x_3 o_4) - d/dt\, P(o_2 x_3) + \ldots + d/dt\, P(x_j o_{j+1}) - d/dt\, P(o_{j-1} x_j) + \ldots$$
$$= - 2\, P(x_1 o_2) + W_{des}^2\, P_1 + (3 - 2W_{des})\, P(o_1 x_2) - P(x_1 o_2 \blacklozenge_3)$$
$$+ P(x_1 \blacklozenge_2 o_3) + P(x_1 o_2 o_3) - P(o_1 o_2 x_3) - 2\, P(x_2 o_3) + 2\, P(o_2 x_3)$$
$$- P(x_2 o_3 \blacklozenge_4) + P(x_2 \blacklozenge_3 o_4) - W_{des}\, P(\blacklozenge_1 x_2) + P(x_2 o_3 o_4) - P(x_3 o_4)$$
$$+ P(o_3 x_4) - P(x_3 o_4 \blacklozenge_5) + P(x_3 \blacklozenge_4 o_5) + \ldots \qquad (11)$$

where we use (5b) for $d/dt\, P(x_j o_{j+1})$, etc. Further differentiation yields equations for $d^3/dt^3 \langle j \rangle$, $d^4/dt^4 \langle j \rangle$ and higher order terms.

Determination of a Taylor expansion for $\langle j^2 \rangle$ motivates the differentiation

$d^2/dt^2 \langle j^2 \rangle = d/dt\, (d/dt \langle j^2 \rangle)$

$$= 3\, d/dt\, P(x_1 o_2) - W_{des}\, d/dt\, P_1 + 5\, d/dt\, P(x_2 o_3) - 3\, d/dt\, P(o_1 x_2)$$
$$+ 7\, d/dt\, P(x_3 o_4) - 5\, d/dt\, P(o_2 x_3) + \ldots$$
$$+ (2j + 1)\, d/dt\, P(x_j o_{j+1}) - (2j - 1)\, d/dt\, P(o_{j-1} x_j) + \ldots$$
$$= (- 2W_{des} - 6)\, P(x_1 o_2) + W_{des}^2\, P_1 + (9 - 4W_{des})\, P(o_1 x_2)$$
$$- 3\, P(x_1 o_2 \blacklozenge_3) + 3\, P(x_1 \blacklozenge_2 o_3) + 5\, P(x_1 o_2 o_3) - 2\, P(o_1 x_2 o_3) - 3\, P(o_1 o_2 x_3)$$
$$- 10\, P(x_2 o_3) + 10\, P(o_2 x_3) - 5\, P(x_2 o_3 \blacklozenge_4) + 5\, P(x_2 \blacklozenge_3 o_4)$$
$$- 3W_{des}\, P(\blacklozenge_1 x_2) + 7\, P(x_2 o_3 o_4) - 2\, P(o_2 x_3 o_4) - 14\, P(x_3 o_4) + 14\, P(o_3 x_4)$$
$$- 7\, P(x_3 o_4 \blacklozenge_5) + 7\, P(x_3 \blacklozenge_4 o_5) + 9\, P(x_3 o_4 o_5) + \ldots \qquad (12)$$

where we use (5b) for $d/dt\, P(x_j o_{j+1})$, etc. Further differentiation yields equations for $d^3/dt^3 \langle j^2 \rangle$, $d^4/dt^4 \langle j^2 \rangle$ and higher order terms.

Suppose that the tagged particle is initially located at site 1, and then the corresponding derivatives of $\langle j \rangle$ and $\langle j^2 \rangle$ are as below:

$$d/dt \langle j \rangle_0 = 0,$$

$$d^2/dt^2 \langle j \rangle_0 = 2W_{des}^2 - 2W_{des} = -2\chi\,(1-\chi),$$

$$d^3/dt^3 \langle j \rangle_0 = -2W_{des}^3 - 4W_{des}^2 + 6W_{des}$$

$$= 2\chi\,(1-\chi)\,(4-\chi),$$

$$d^4/dt^4 \langle j \rangle_0 = 4W_{des}^4 + 3W_{des}^3 + 12W_{des}^2 - 19W_{des}$$

$$= \chi\,(1-\chi)\,(-30 + 15\chi - 4\chi^2),$$

$$d^5/dt^5 \langle j \rangle_0 = -4W_{des}^5 - 13W_{des}^4 - 24W_{des}^3 - 21W_{des}^2 + 62W_{des}$$

$$= \chi\,(1-\chi)\,(124 - 87\chi + 29\chi^2 - 4\chi^3), \qquad (13)$$

and

$$d/dt \langle j^2 \rangle_0 = 2W_{des} = 2(1-\chi),$$

$$d^2/dt^2 \langle j^2 \rangle_0 = 4W_{des}^2 - 6W_{des} = 2(1-\chi)\,(-1-2\chi),$$

$$d^3/dt^3 \langle j^2 \rangle_0 = 2W_{des}^3 - 16W_{des}^2 + 18W_{des}$$

$$= 2(1-\chi)\,(2 + 6\chi + \chi^2),$$

$$d^4/dt^4 \langle j^2 \rangle_0 = 8W_{des}^4 - 15W_{des}^3 + 44W_{des}^2 - 47W_{des}$$

$$= (1-\chi)\,(-10 - 38\chi + 9\chi^2 - 8\chi^3),$$

$$d^5/dt^5 \langle j^2 \rangle_0 = 2W_{des}^5 - 40W_{des}^4 + 52W_{des}^3 - 135W_{des}^2 + 186W_{des}$$

$$= (1-\chi)\,(65 + 143\chi - 56\chi^2 + 32\chi^3 + 2\chi^4). \qquad (14)$$

Next, we describe the estimation of $t_1(\chi)$ for various total concentrations χ. Here we focus on three cases: (i) low loading χ=0.2 with W_{des} = 0.8, (ii) high lowing χ=0.8 with W_{des} = 0.2, and (iii) χ = 0+ as there is no other particles within the pore. In Fig. 2

and Fig. 3, illustrate our approach to obtaining $t_1(\chi)$ values with $\chi = 0+$ and $\chi = 0.2$ respectively by solving the fifth-order polynomial equations

$$\text{ms displacement} = \langle (j-j_0)^2 \rangle = \langle j^2 \rangle - 2j_0 \langle j \rangle + (j_0)^2$$

$$= \langle j^2 \rangle - \langle j^2 \rangle_0 - 2j_0 (\langle j \rangle - j_0) = 1. \qquad (15)$$

and

$$\text{ms type displacement} = \langle j^2 \rangle - \langle j^2 \rangle_0$$

$$\approx d/dt \langle j^2 \rangle_0 t + d^2/dt^2 \langle j^2 \rangle_0 t^2/2! + d^3/dt^3 \langle j^2 \rangle_0 t^3/3!$$

$$+ d^4/dt^4 \langle j^2 \rangle_0 t^4/4! + d^5/dt^5 \langle j^2 \rangle_0 t^5/5! = 1. \qquad (16)$$

Moreover, comparison of the results obtained from (15) with the $t_1(\chi)$ values obtained by Kinetic Monte Carlo (KMC) simulation in a semi-infinite pore is appropriate and is provided in Table 1. The procedure to obtain estimates of $t_2(\chi)$, $t_3(\chi)$, etc. is analogous, although estimates will be less accurate due to the longer times involved.

III. Conclusions

The Taylor expansion analysis of $t_n(\chi)$ offers a way to estimate the generalized position-dependent tracer diffusion coefficient effectively at least for sites close to the pore opening. The shortcoming of the truncated Taylor expansion analysis is that it is never exact and must give artificial behavior for long times. However, it is a way, probably the only way, to estimate tracer diffusion analytically. It is reasonably good for low loading, e.g. χ=0.2, and not too good for high loading, e.g. χ=0.8. An appropriate rearrangement of Taylor expansion may boost the convergence.

References

[1] T.E. Harris, J. Appl. Prob. 2, 323 (1965).
[2] M. Kollman Phys. Rev. Lett. 90, 180602 (2003).
[3] J.E. Santos and G.M. Schutz, Phys. Rev. E 64, 036107 (2001).
[4] H. van Beijeren, K.W. Kehr, and R. Kutner, Phys. Rev. B 28, 5711 (1983).
[5] A. Taloni and F. Marchesoni, Phys. Rev. E 74, 051119 (2006).
[6] L. Lizana and T. Ambjornsson, Phys. Rev. Lett. 100, 200601 (2008).
[7] E. Barkai and R. Silbey, Phys. Rev. Lett. 102, 050602 (2009).
[8] R. Krishna, J. Phys. Chem. C 113, 19765 (2009).
[9] D.M. Ackerman, J. Wang, J.H. Wendel, D.-J. Liu, M. Pruski, and J.W. Evans, J. Chem. Phys. 134, 114107 (2011).
[10] S.V. Nedea, A.P.J. Jansen, J.J. Lukkien, and P.A.J. Hilbers, Phys. Rev. E 65, 066701 (2002)
[11] D. Ackerman, J. Wang, and J.W. Evans, Phys. Rev. Lett. 108, 228301 (2012).
[12] J. Wang, D.M. Ackerman, V.S.-Y. Lin, M. Pruski, and J.W. Evans, J. Chem. Phys. 138, 134705 (2013).

Tables

Table 1. D_{tr} (1) = $t_1(0+)/t_1(\chi)$ comparison of KMC simulation and Taylor Expansion Analysis (TEA) for both lowing loading $\chi = 0.2$, high loading $\chi = 0.8$ and $\chi = 0+$.

	KMC	TEA with 1st term	TEA with first 3rd terms	TEA with first 5th terms
$t_1(0.2)$	0.798407	0.625	0.7976	0.78513
$t_1(0.8)$	6.96930	2.5	1.8217	1.48871
$t_1(0+)$	0.64673	0.5	0.6105	0.61834
$D_{tr}(1) = t_1(0+)/ t_1(0.2)$	0.810025	0.8	0.7654	0.78756
$D_{tr}(1) = t_1(0+)/ t_1(0.8)$	0.092797	0.2	0.3351	0.41535

Figures

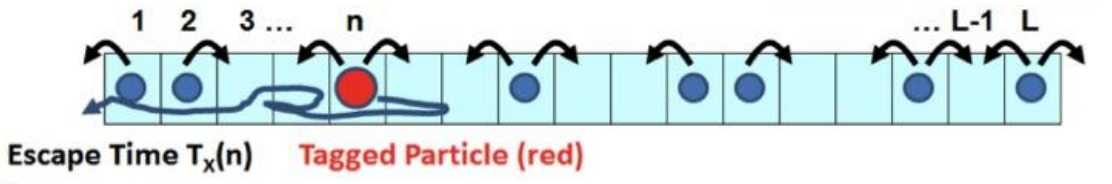

Fig.1. Schematic of a tagged particle to escape the pore with a finite density χ of other particles.

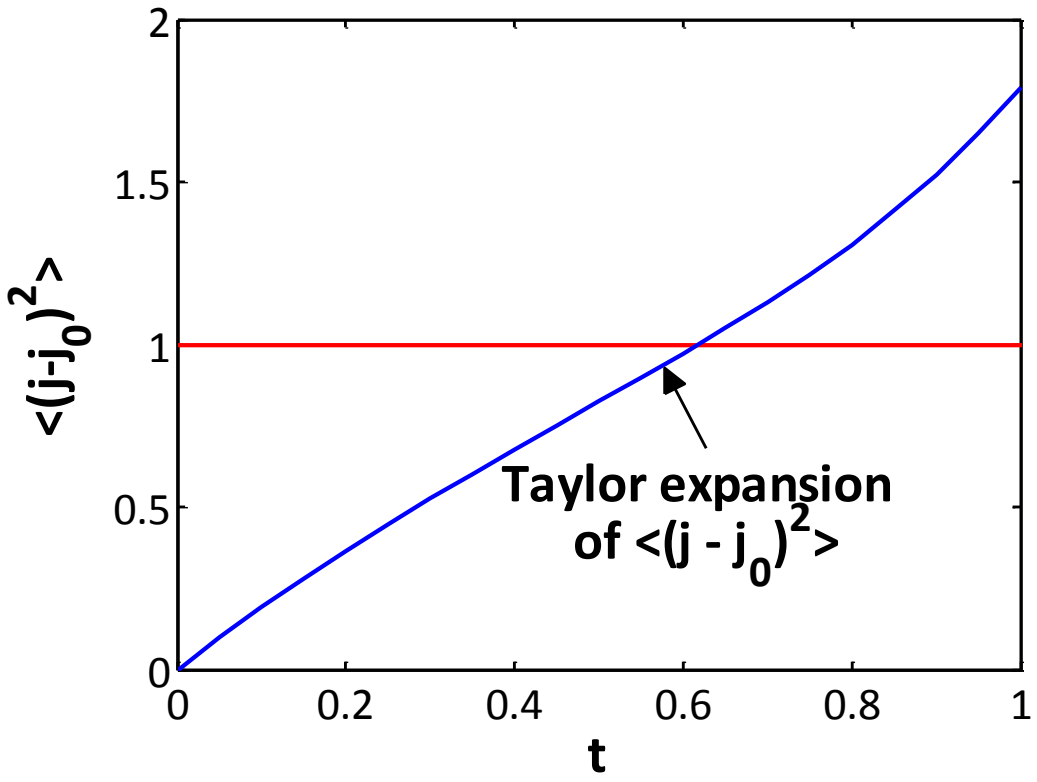

Fig.2. The point of intersection gives the time $t_1(\chi)$ in the case χ=0+ with a truncation error in order $o(t^6)$.

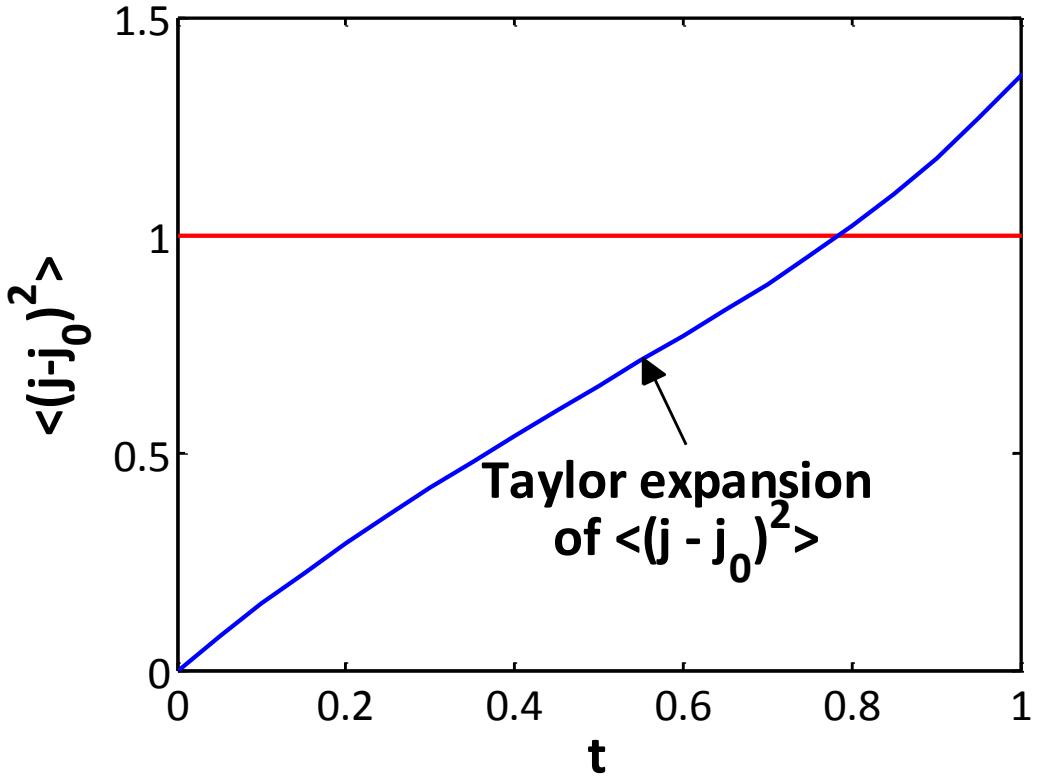

Fig.3. The point of intersection gives the time $t_1(\chi)$ in the case χ=0.2 with a truncation error in order $o(t^6)$.

CHAPTER 7. ANALYSIS OF THE STEADY-STATE CONTINUUM REACTION-DIFFUSION EQUATIONS FOR CATALYTIC CONVERSION REACTIONS IN 1D PORES WITH SINGLE-FILE DIFFUSION

I. Introduction

The nontrivial nature of diffusion is well recognized in single-file systems, and there is appreciation that this will impact reaction-diffusion processes in nanoporous systems. The no-passing feature results in anomalous tracer diffusion [1-4]. There have been extensive studies often motivated by studies of transport and catalytic reaction in zeolites [5] and other functionalized nanoporous materials, emphasizing the anomalous nature of tracer- or self-diffusion [5,6]. This anomaly is reflected in a sub-linear increase with time in the mean-square displacement of a specific "tagged" particle [2,7]. Our interest is in the interplay between this type of anomalous transport and the catalytic reaction kinetics. Such behavior is traditionally described by reaction-diffusion equations (RDE). However, characterization of chemical diffusion (rather than tracer diffusion), which provides key input to these equations, has received relatively little attention for quasi-single-file systems. Its correct description is a non-trivial statistical mechanical challenge.

Our specific focus is on simple first-order conversion reactions, A –> B (see Fig.1), occurring inside a parallel array of linear nanopores of a catalytically functionalized material such as mesoporous silica. Reactants, A, enter the pore openings, diffuse to adjacent empty cells of a 1D linear lattice at rate h, convert to a product at

catalytic cells (c), B, with microscopic rate k, and both reactants and products can diffuse out of the pore [8-14]. The cell width "a" is chosen as 1 nm comparable to species size. This would correspond to single-file diffusion (SFD) with a strict no-passing constraint.

In Sec. II, we first describe our continuum model for conversion reaction in linear nanopores, and the associated reaction-diffusion equations (RDE). Then, we present the results for improved analysis of the steady-state continuum RDE. Our conclusions are presented in Sec. III.

II. Analysis of the steady-state continuum reaction-diffusion equations

A. Continuum reaction-diffusion equations

The exact master equations for stochastic lattice-gas (LG) reaction-diffusion model for the evolution of probabilities of various configurations within the pore have been developed [12, 14] where we used $\langle C_n \rangle$ to denote the probability or ensemble averaged concentration for species C = A or B at site n (or for this site to be empty when C = E). For smoothly varying concentrations within the pore, it is natural to consider a coarse-grained description of the spatially-discrete reaction-diffusion model which regards the species concentrations per unit length, $C(x=na) \approx a^{-1} \langle C_n \rangle$, as functions of a continuous spatial variable x (leaving the t-dependence implicit), and denote the total concentration by $X(x) = A(x) + B(x)$. The continuum RDE for our A to B conversion reaction model with all sites catalytic then have the form

$$\partial/\partial t\, A(x) = -k\, A(x) - \partial/\partial x\, J_A, \text{ and } \partial/\partial t\, B(x) = +k\, A(x) - \partial/\partial x\, J_B. \quad (1)$$

Boundary conditions for (1) at the pore ends reflect the adsorption-desorption dynamics. Description of the diffusion fluxes, J_A and J_B, is non-trivial, actually critical.

Analysis from the theory of interacting particle systems [16, 22] for the hydrodynamic regime of slowly varying concentrations suggests the general form [16]

$$J_A = - D_0 (A/X)\partial X/\partial x - D_{tr}[(B/X)\partial A/\partial x - (A/X)\partial B/\partial x]. \quad (2)$$

Here $D_0 = a^2 h$ is the chemical diffusion coefficient for particles X, and $D_{tr} = D_0 F_{tr}$ is a tracer diffusion coefficient. Here, it suffices to consider the local steady-state regime with uniform total concentration, $X = a^{-1}\chi$, corresponding to a counter-diffusion mode [17] where $\partial A/\partial x = - \partial B/\partial x$. Then, (2) and the analogous expression for J_B simply reduce to [12,17]

$$J_A = - D_{tr}\, \partial A/\partial x \text{ and } J_B = - D_{tr}\, \partial B/\partial x. \quad (3)$$

Given the shortcomings of the mean-field (MF) approximation [12, 14] and the classic "hydrodynamic" approach [14] for D_{tr} or $F_{tr,}$ we have developed a "generalized hydrodynamic" treatment [14] which incorporates a position-dependent $F_{tr}(x=na)$. This F_{tr} is enhanced near pore openings and decays to a value ~1/L in the pore center for pores of length L. Thus, for semi-infinite pores of interest here, $F_{tr}(x) \to 0$, as $x \to 0$. Further discussion of $F_{tr}(x)$ appears in the following section.

B. Lowest-order analysis of A(x) in the steady state

Insight into the consequences of decay of $F_{tr}(x)$ comes from analysis of the steady-state solutions of the continuum RDE for a semi-infinite pore $x \geq 0$ using (3) with

the form $F_{tr}(x) \sim 1/x^p$. Assume $A(x) \sim \exp[-(x/L_p)^q] = \exp(-\alpha x^q)$ where L_p denotes the penetration depth of reactant A, then in the steady-state one finds,

$$0 = \partial/\partial t\, A(x) = -\, k\, A(x) - \partial/\partial x\, (-\, D_{tr}\, \partial A/\partial x) \qquad (4)$$

which implies

$$k/D_0 \exp[-(x/L_p)^q] = \partial/\partial x\, \{1/x^p\, \partial/\partial x\, (\exp[-(x/L_p)^q])\} \qquad (5)$$

After differentiating and dropping of non-dominant part, one obtains

$$k/D_0 = q^2\, (x^{2q-p-2})/\, L_p{}^{2q} \qquad (6)$$

It follows that

$$2q - p - 2 = 0, \text{ and } L_p = (k/D_0/q^2)^{-1/(2q)} \sim (k/D_0)^{-1/(2q)} \qquad (7)$$

Hence, for small reaction rate k and large penetration depth L_p, we have the dominant form

$$A(x) \sim \exp[-(x/L_p)^q] \text{ where } q=(2+p)/2, \text{ and } L_p \sim (k/D_0)^{\zeta} \text{ with } \zeta = -1/(2+p). \qquad (8)$$

The true asymptotic scaling exponent for L_p is $\zeta = -1/4$ corresponding to the true asymptotic exponent for decay of F_{tr} of $p = 2$. However, behavior mimicking $\zeta = -1/3$ for non-asymptotic effective exponent $p = 1$ might be seen for lower *X*. Both contrast MF behavior $\zeta = -1/2$ corresponding to $p = 0$ (i.e., constant F_{tr}) [11,12]. These predictions are confirmed by numerical analysis of discrete generalized hydrodynamic RDE's exploiting the capability of this deterministic treatment to obtain much more precise ζ-values than possible by KMC simulation [14].

C. Improved analysis of A(x) in the steady state

Success in the lowest-order analysis motivates an attempt to develop the next order correction to $A(x)$. We continue using (3) with the form $F_{tr}(x) = f\,x^{-p} \sim 1/x^{p}$. Assume $A(x) \sim (1+c\,x^{-s})\exp[-(x/L_p)^q] = (1+c\,x^{-s})\exp(-\alpha x^q)$, then we have,

$$\partial A/\partial x = [-cs\,x^{-s-1} - \alpha q\,x^{q-1}(1+c\,x^{-s})]\exp(-\alpha x^q),$$

$$F_{tr}\,\partial A/\partial x = [-fcs\,x^{-s-p-1} - f\alpha q\,x^{q-p-1}(1+c\,x^{-s})]\exp(-\alpha x^q), \text{ and}$$

$$\begin{aligned}\partial/\partial x\,(F_{tr}\,\partial A/\partial x) &= [fcs(s+p+1)\,x^{-s-p-2} - f\alpha q\,(q-p-1)\,x^{q-p-2}(1+c\,x^{-s}) \\ &\quad + f\alpha qcs\,x^{q-p-s-2}]\exp(-\alpha x^q) \\ &\quad - \alpha q\,x^{q-1}[-fcs\,x^{-s-p-1} - f\alpha q\,x^{q-p-1}(1+c\,x^{-s})]\exp(-\alpha x^q) \\ &= [fcs(s+p+1)\,x^{-s-p-2} - f\alpha q\,(q-p-1)\,x^{q-p-2} - f\alpha qc\,(q-p+2s-1)\,x^{q-p-s-2} \\ &\quad + f\alpha^2 q^2\,x^{2q-p-2} + cf\alpha^2 q^2\,x^{2q-p-s-2}]\exp(-\alpha x^q) \qquad (9)\end{aligned}$$

In the steady-state,

$$(k/D_0)\;A(x) = \partial/\partial x\,(F_{tr}\,\partial A/\partial x) \qquad (10)$$

Hence, after substituting the above results into both sides, one obtains

$$\begin{aligned}(k/D_0)(1+c\,x^{-s})\exp(-\alpha x^q) &= [fcs(s+p+1)\,x^{-s-p-2} - f\alpha q\,(q-p-1)\,x^{q-p-2} \\ &\quad - f\alpha qc\,(q-p+2s-1)\,x^{q-p-s-2} + f\alpha^2 q^2\,x^{2q-p-2} + cf\alpha^2 q^2\,x^{2q-p-s-2}]\exp(-\alpha x^q) \qquad (11)\end{aligned}$$

which implies the dominant relationship for large x of

$$k/D_0\,x^0 = f\alpha^2 q^2\,x^{2q-p-2} \qquad (12)$$

Therefore, $k/D_0 = f\alpha^2 q^2$ and $q = (p+2)/2$, and (11) becomes

$$cx^{-s}(k/D_0) = fcs(s+2q-1)\,x^{-s-2q} - f\alpha q\,(-q+1)\,x^{-q} - f\alpha qc\,(-q+2s+1)\,x^{-q-s} + cf\alpha^2 q^2\,x^{-s} \qquad (13)$$

For $s>0$, it is natural to choose $s=q$ to balance dominant terms for large x. But then, using the identity $k/D_0 = f\alpha^2 q^2$ yields

$$c\,f\alpha^2 q^2 = -f\alpha q\,(-q+1) + cf\alpha^2 q^2, \text{ (for } s=q) \qquad (14)$$

which can only be satisfied setting q=1 (p=0) which contradicts the assumption of *A*(x). This failure prompts alternative strategies to determine higher-order behavior.

An alternative more general approach to assess higher-order behavior starts by assuming the form $A(x) = G(x) \exp[-(x/L_p)^q] = G(x) \exp(-\alpha x^q)$, with $F_{tr}(x) = f\, x^{-p}$. From (10), we obtain a relation involving G(x),

$$(k/D_0)\, G(x) = f\, G''(x) x^{-p} - f\, G'(x)\, (p\, x^{-p-1} + 2\alpha q\, x^{q-p-1}) - f\, G(x)\, [\alpha q(q-p-1)\, x^{q-p-2} - \alpha^2\, q^2\, x^{2q-p-2}], \quad (15)$$

from which follows a second order differential equation of G(x)

$$G''(x) - G'(x)\, (p\, x^{-1} + 2\alpha q\, x^{q-1}) - G(x)\, [\alpha q(q-p-1)\, x^{q-2} - \alpha^2\, q^2\, x^{2q-2} + (k/D_0/f)\, x^p] = 0 \quad (16)$$

In principle, numerical solution of this equation with an appropriate choice of parameters and initial values can provide more detailed insight into behavior of A(x).

D. Removal of singularity of A(x) in the steady state

Returning to analysis at the lowest-order as in Subsection B, in order to avoid singularity, we assume that $F_{tr}(x) = f\,(1+x/x_d)^{-p} = f\, u^{-p}$ with a nonzero number x_d and $A(x) \sim \exp[-(u/L_p)^q] = \exp(-\alpha\, u^q)$, then $du = dx/x_d$ and in the steady-state,

$$k/D_0 \exp[-(u/L_p)^q] = \partial/\partial x\, \{f u^{-p}\, \partial/\partial x\, (\exp[-(u/L_p)^q])\} \quad (17)$$

Differentiating we have,

$$k/D_0 \exp[-(u/L_p)^q] = x_d^{-2}\, f\, q^2\, (u^{2q-p-2})/\, L_p^{2q} \exp[-(u/L_p)^q] + \text{lower order terms} \quad (18)$$

Hence the dominant form is

$$q = (p+2)/2\,,\ \alpha = (k/f/D_0)^{1/2}\, x_d/q \text{ and } L_p = (k\, x_d^2/f/D_0/q^2)^{-1/(2q)} \sim (k/D_0)^{-1/(p+2)} \quad (19)$$

This recovers the same exponents as obtained in the singular case. Here, the value of x_d is critical in changing variables. F_{tr} for a semi-infinite pore can be obtained by KMC simulation and the parameter x_d therefore can be determined. As in Fig.2, $p \approx 2$ and $x_d = 1$.

III. Conclusions

An analysis is provided of the decay of the reactant concentration A(x) in the steady-state with utilizing the relevant continuum RDE incorporating a location-dependent of tracer diffusion coefficient. The lowest-order analysis is quite effective at elucidating the non-exponential decay and scaling of the penetration depth with key model parameters. However, extension to higher-order of this analysis is problematic.

References

[1] A. L. Hodgkin and R. D. Keynes, J. Physiol. (London) 128, 61 (1955).
[2] T. E. Harris, J. Appl. Probab. 2, 323 (1965).
[3] P. A. Fedders, Phys. Rev. B 16, 1393 (1977).
[4] J. G. Tsikoyiannis and J. E. Wei, Chem. Eng. Sci. 46, 233 (1990).
[5] J. Karger and D. Freude, Chem. Eng. Technol. 25, 769 (2002).
[6] Reikert, L. In Advances in catalysis; Eley, D. D., Pines, H., Weisz, P. B., Eds.; Academic Press: New York, Vol.21, p281 (1970).
[7] Fedders, P. A. Phys. Rev. B 17, 4046 (1978).
[8] J. G. Tsikoyiannis and J. E. Wei, Chem. Eng. Sci. 46, 233 (1991).
[9] C. Rodenbeck, J. Karger, and K. Hahn, J. Catal. 157, 656 (1995).
[10] M. S. Okino, R. Q. Snurr, H.H. Kung, J. E. Ochs, and M. L. Mavrovouniotis, J. Chem. Phys. 111, 2210 (1999).
[11] S.V. Nedea, A. P. J. Jansen, J. J. Lukkien, and P. A. J. Hilbers, Phys. Rev. E 65, 066701 (2002).
[12] D. M.Ackerman, J.Wang, J. H.Wendel,D.-J. Liu,M.Pruski, and J.W. Evans, J. Chem. Phys. 134, 114107 (2011).
[13] D.-J. Liu, J. Wang, D. Ackerman, I.I. Slowing, M. Pruski, H.-T. Chen, V.S.-Y. Lin, and J.W. Evans, ACS Catalysis 1, 751-763 (2011).

[14] D. Ackerman, J. Wang, and J.W. Evans, Phys. Rev. Lett. 108, 228301 (2012).
[16] J. Quastel, J. Commun. Pure Appl. Math. 45 (1992).
[17] P.H. Nelson and S.M. Auerbach, Chem. Eng. J. 74, 43 (1999).
[18] A.L. Hodgkin and R.D. Keynes, J. Physiol. 128, 61 (1955).
[19] E.J. Harris, "Transport and accumulation in biological systems" (AP, New York, 1960).
[20] H. van Beijeren, K.W. Kehr, and R. Kutner, Phys. Rev. B 28, 5711 (1983).
[21] A. Taloni and F. Marchesoni, Phys. Rev. E 74, 051119 (2006).
[22] H. Spohn, Large scale dynamics of interacting particles (Springer, Berlin, 1991).

Figures

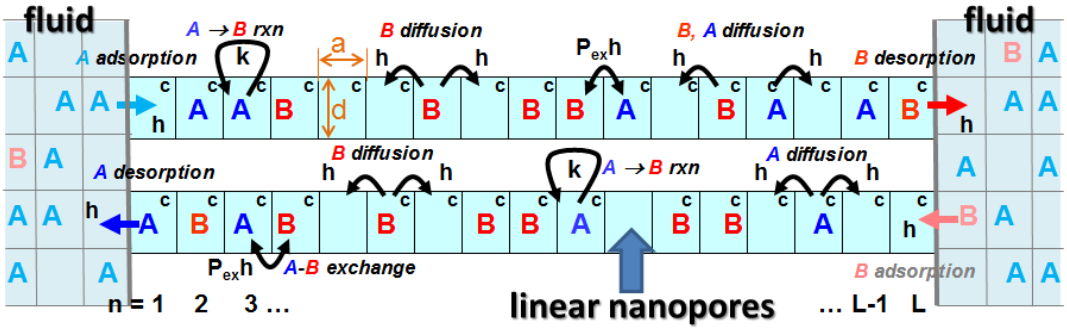

Fig.1. Schematic of the key steps in our A→B catalytic conversion reaction model. "c" denote catalytic cells where reaction occurs at rate k. Behavior is shown in two adjacent pores which should be regarded as part of a larger array of pores.

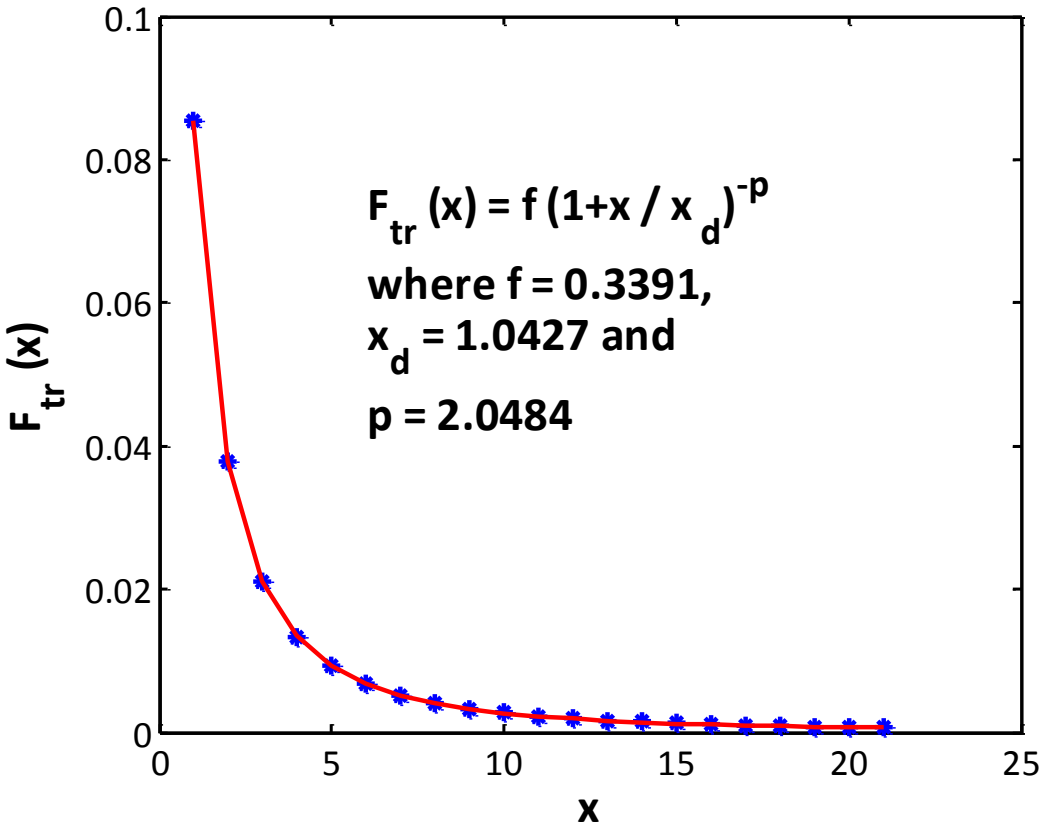

Fig.2. Blue stars are the F_{tr} values from KMC simulation when the total concentration is X=0.8 in the steady-state in a semi-infinite pore with a = h = 1 and red curve is the least square fitting curve in form $F_{tr}(x) = 0.3391\ (1 + x/1.0427)^{-2.0484}$.

CHAPTER 8. GENERAL CONCLUSION

The studies in this thesis focus on analysis of interplay between single-file diffusion and conversion reaction in mesoprous systems (or nanopores). The transient and steady-state behavior of single-file conversion reaction systems displays some general features. Transient evolution of concentration profiles is effectively described by hydrodynamic RDE which properly incorporate the single-file nature of diffusion. However, steady-state reactivity is controlled by fluctuation effects not incorporated in the hydrodynamic treatment. MF-type treatments can capture some aspects of this steady-state behavior, but not scaling properties for extreme choices of reaction and diffusion rates. Then we turn to the so-called generalized hydrodynamic formulation. The location dependence of tracer diffusion near the openings of narrow pores is shown to control non-MF scaling of reactant penetration depth and thus reactivity for conversion reactions. Generalized hydrodynamic RDE's provide a powerful tool with which to analyze this behavior. Taking account of strong dependence of catalytic activity on the tunable interaction between reaction products and the interior pore environment. Making the pore interior unfavorable to products not only modifies the reaction equilibrium towards completion, but also reduces pore loading which can significantly enhance diffusivity and thus reactivity especially in the SFD regime. Our generalized hydrodynamic formulation of reaction-diffusion phenomena provides an efficient tool to explore behavior over a broad phase-space of model parameters. This approach can reliably capture the complex interplay between reaction and restricted transport which

results in subtle spatial correlations and fluctuations of reactants and products within the pore. These effects are not described by traditional mean-field approaches.

There are numerous possible modifications and extensions of our modeling which could be performed either utilizing refined generalized hydrodynamic RDE or with KMC simulation. Another natural extension of our modeling is to consider different reaction mechanisms, e.g., A+B↔C+D better matching esterification reactions, and to consider the scenario where pore reentry of just one of the two products is enhanced versus blocked. The approximate MF and precise GH formalism are readily extended to treat this more complex situation, and preliminary studies reveal analogous behavior to that discussed above for the simpler A↔B conversion reaction mechanism.

Furthermore, the tracer diffusion plays an important role in our model. Tracer diffusion coefficients associated with MF-type approximation have been studied and thus show the uncontrolled behavior of MF-type treatment. Taylor expansion has been applied to the study of tracer diffusion coefficient that is independent of reactions but dependent on transport. Improved analysis of the steady-state continuum RDE are offered but can be further developed.